Chapter 4

Influence of Y_2BaCuO_5 particles

4.1 Introduction

Melt Textured Growth has enabled the obtention of large monocrystalline samples (up to $\Phi \sim 10cm$ [49]) much bigger than single crystals and therefore, suitable for power applications involving large currents circulating through the sample. The preparation of these large samples, however, requires the presence of a secondary phase embedded in the matrix, Y_2BaCuO_5, which may lead to a strong modification of the superconducting properties as shown in section 1.4.2. Thus, Y_2BaCuO_5 particles themselves (and the $YBa_2Cu_3O_{7-\delta}/Y_2BaCuO_5$ interface in particular) are expected to be the main source of modifications in the superconducting properties when the content of Y_2BaCuO_5 particles is modified. However, it has been demonstrated that these particles strongly modify the microstructural characteristics of the sample [88].

As seen in figure 4.1, these particles embedded into the $YBa_2Cu_3O_{7-\delta}$ matrix, have a large radius ($d \sim 1\mu m$), which is much larger than the vortex coherence length ($\xi_{ab} \sim 15$Å). As it has been pointed out in section 1.2, vortex pinning is optimized when the considered microstructural defect has dimensions similar to that of the coherence length, and therefore, one should not expect a dramatic influence of Y_2BaCuO_5 particles by themselves. The strong influence of the addition of particles on superconducting properties, attributed to their interface is shown in figure 4.2, where the temperature dependence of the inductive critical current density for different $YBa_2Cu_3O_{7-\delta}$ samples is represented. Different hypothesis have been developed in order to explain this enhancement of the critical currents with the content of Y_2BaCuO_5. In particular, it has been proposed that the decay of the order parameter near the superconducting/isolating interface ($YBa_2Cu_3O_{7-\delta}/Y_2BaCuO_5$) should promote vortex pinning [47]. These interfaces are then acting as a linear-like pinning center for lengths of the order of the size of the particles: $l \sim 1\mu m$. Critical currents have been shown to increase mainly at high temperatures, following the temperature dependence predicted by Nelson and Vinokur [17] for correlated disorder. However, the exact deformation and distribution of supercurrents around the particle remains as an important drawback. In fact, it has been

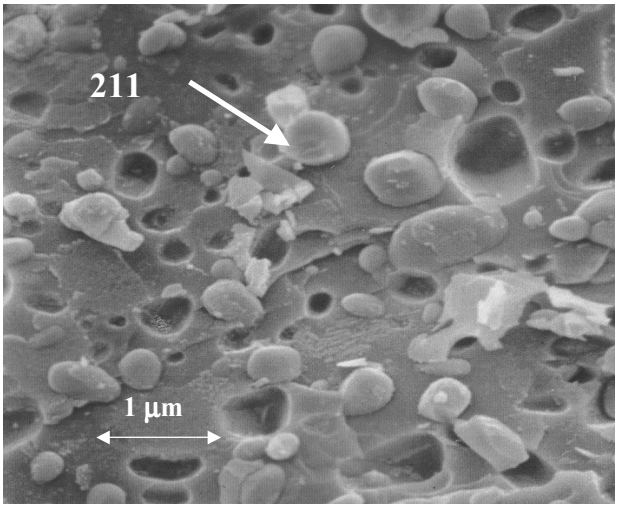

Figure 4.1: Scanning Electron Microscopic image of a MTG-$YBa_2Cu_3O_{7-\delta}$ sample. Shown are the Y_2BaCuO_5 particles.

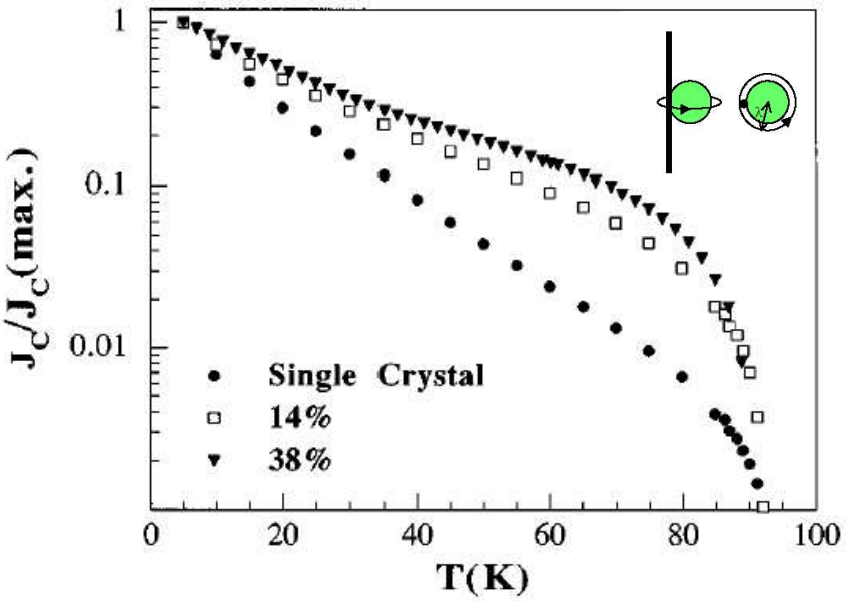

Figure 4.2: Temperature dependence of the inductive critical currents for samples with different content of Y_2BaCuO_5 particles. Also shown is an scheme of the distribution of supercurrents around a Y_2BaCuO_5 particle.

suggested [51] that only the interfaces of Y_2BaCuO_5 particles with diameters lower than 2λ may act as effective pinning centers.

The main goal of this chapter is to study and extend the analysis of the influence of the $YBa_2Cu_3O_{7-\delta}/Y_2BaCuO_5$ interface to the vortex liquid vortex state. In particular, we want to analyze the influence of these particles on vortex dynamics in the vortex liquid state. The angular dependence of the superconducting properties with the direction of the magnetic field is a key issue due to the quasisperical morphology of these particles, they are expected to modify them for all the directions of the magnetic field.

Previously, the analysis of the influence of Y_2BaCuO_5 particles in vortex motion had been studied in a sample with a fixed concentration of Y_2BaCuO_5 [89–91]. This study, however, was not able to determine whether vortex dynamics in MTG-$YBa_2Cu_3O_{7-\delta}$ samples with strong pinning centers were related to plastic motion of dislocations [92] or cutting and recombination processes [93] enhanced by the presence of Y_2BaCuO_5 particles. In order to distinguish between these two possibilities, three different samples with markedly different Y_2BaCuO_5 contents have been studied and analyzed. These samples have been grown by the methods described previously in section 2.

Measurements of the paramagnetic signal of the Y_2BaCuO_5 phase determined that the final content of the three analyzed samples are 0% wt, 18%wt and 31%wt. Scanning Electron Microscopy analysis of the samples enabled us to obtain the mean diameter of these samples is $\langle d \rangle \approx 0.95 \mu m$, thus leading to a interface density $\frac{V}{d} \sim 0\ cm^{-1}$, 2000 cm^{-1} and 3300 cm^{-1}.

4.2 Phase diagram

Pieces of these MTG-$YBa_2Cu_3O_{7-\delta}$ samples with different Y_2BaCuO_5 contents ranging from 0% wt to 31% wt were cut down in dimensions of $0.1x0.5x1mm^3$. In figure 4.3, the temperature dependence of the resistivity for the different samples is shown for H||c at different intensities of the magnetic field. In order to compare the resistive measurements for the different samples taking into account the slight difference in T_c and the normal state resistivity, these curves have been normalized by the critical temperature and the normal state resistivity.

In this figure, it is observed that the normalized resistivity decreases as the density of Y_2BaCuO_5 particles is enhanced, thus demonstrating that, similarly to that observed in the solid state, a strong influence of Y_2BaCuO_5 particles exist in the vortex liquid state. Moreover, it is shown that a certain influence of Y_2BaCuO_5 particles on enhancing vortex viscosity exists up to very high resistivities ($\frac{\rho}{\rho_n} \approx 0.9$ at H=1T) and temperatures (T^{onset}) close to T_c. The region of influence of Y_2BaCuO_5 particles in the liquid state is found to be wider than that obtained when ion tracks ($\frac{\rho^{onset}}{\rho_n} \sim 0.7$) [94] or twin boundaries are considered, acting as linear pinning centers. Furthermore, it is even higher than the one obtained for splayed defects ($\frac{\rho^{onset}}{\rho_n} \sim 0.55$ at H=3T) [95], where the reduction of vortex motion has been attributed to an enhancement of vortex entanglement due to the particular geometry of these defects.

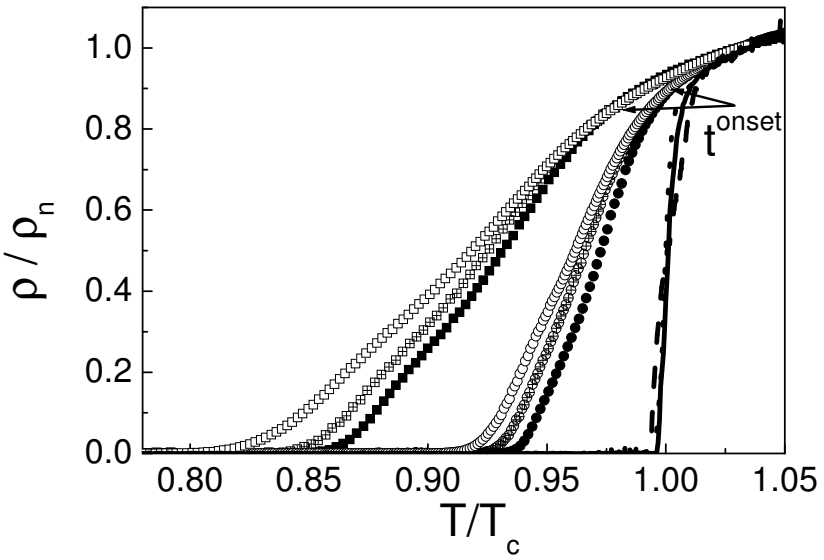

Figure 4.3: Temperature dependence of the resistivity for H=3T (•, ⊕ and ∘ for the samples with 31%, 18% and 0% wt of Y_2BaCuO_5, respectively) and H=9T (■(31%), ⊞ (18%) and □(0%)) for H||c. Shown in the figures is t^{onset}.

These measurements also allows us to define the irreversibility temperature for the three samples (using the criteria $\rho(T_{irr}) = \frac{1}{1000}\rho_n$), and the limit of influence of these particles on vortex motion, as the temperature (T^{onset}) above which the normalized resistivities are equal within a 5%. The dependence of T^{onset} with the applied magnetic field, together with the obtained irreversibility lines for the samples with different content of Y_2BaCuO_5 particles are represented in the magnetic phase diagram (figure 4.4). It is demonstrated that the $YBa_2Cu_3O_{7-\delta}/Y_2BaCuO_5$ interface have a strong influence on the phase diagram for H||c.

Although we have shown the influence of Y_2BaCuO_5 particles for H||c, these particles, due to their spherical geometry should promote a reduction of vortex motion for all the directions of the magnetic field. Therefore, it is worth to explore the whole angular dependent phase diagram in order to determine and quantify the upwards shift of the irreversibility line due to Y_2BaCuO_5 particles and deconvolute it from the shift of the irreversibility line due to twin boundaries that exists for H||c. To determine the angular dependent magnetic phase diagram and whether Y_2BaCuO_5 particles promotes a reduction of vortex motion for all the directions of the magnetic field, we proceeded by obtaining a set of R-T measurements for different directions of the magnetic fields, rotating it from the c-axis to the ab-plane. These measurements, are shown in figure 4.5, where it is observed that there is a reduction of dissipation as one increases the content of Y_2BaCuO_5 from 0% to 31%. This reduction of vortex motion is found for all the directions of the magnetic field, in agreement with the expectations and presents a similar behavior with that observed for H||c: an upwards shift of the irreversibility line as increasing the density of Y_2BaCuO_5 particles for all the directions

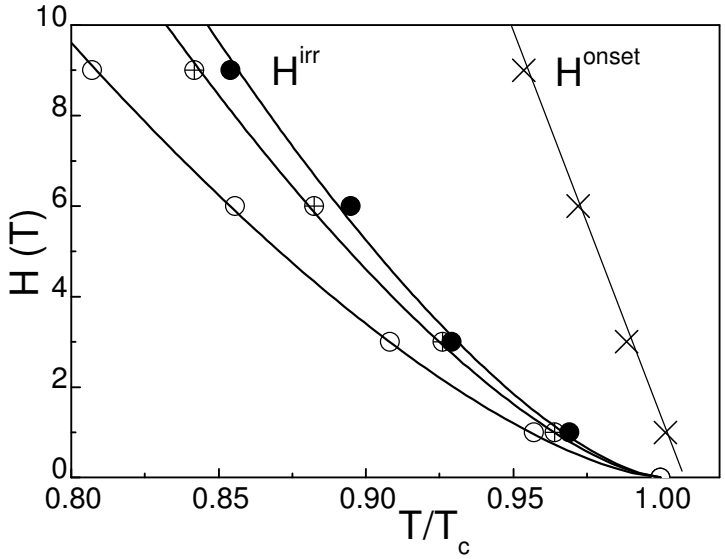

Figure 4.4: Magnetic Phase diagram for H||c for three different MTG-$YBa_2Cu_3O_{7-\delta}$ samples with 0% wt (○), 18% wt (⊕) and 31% wt (●). Shown are the irreversibility lines and the limit of influence of Y_2BaCuO_5 particles, H^{onset}.

of the magnetic field. In addition, the study of the angular dependence of these measurements also enables to study the region with influence of twin boundaries (θ_{acc}) by measuring at a fixed temperature, the angular dependence of the resistivity (see figure 4.6). Similarly to figure 3.11 (page 61), the enhancement of pinning for directions close to H||c is related to the influence of twin boundaries. The limits of this influence are therefore determined at each measured temperature and by varying the temperature, the whole region of the phase diagram influenced by twin boundaries is obtained. Certainly, these measurements also allows us to determine the angular dependent irreversibility line, and lead to the same results (within the experimental error) than those obtained by measuring the temperature dependence of the resistivity for different directions of the magnetic field.

Thus, the different regions of the angular dependent magnetic field have been obtained for these samples, and are represented in figure 4.7. It is demonstrated that there exists an upwards shift of the irreversibility line as increasing the content of Y_2BaCuO_5 particles for all the directions of the magnetic fields. It is also observed that the upper limit of influence of Y_2BaCuO_5 particles, T^{onset} increases as one approaches the ab-plane, following the anisotropy of the sample.

In this angular dependent phase diagram it is also observed a similar structure of the region influenced by twin boundaries, although it is shown to be slightly wider (around H||c) for the samples with a certain content of Y_2BaCuO_5 particles. Although this region will be further studied in chapter 7, where the analysis of the influence of twin boundaries will

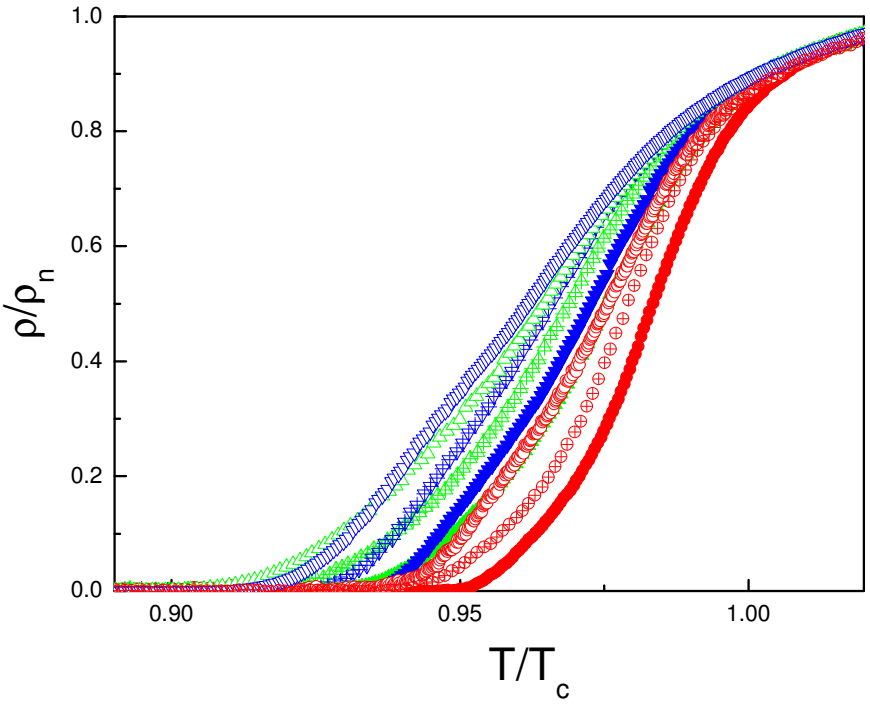

Figure 4.5: Temperature dependence of the resistivity at H=3T for $\theta = 60$ (○, ⊕ and ●), $\theta = 30$ (△, ⟑ and ▲) and $\theta = 0$ (▽,⟒ and ▼) for samples with different densities of Y_2BaCuO_5 particles: 0%wt (empty symbols), 18%wt (crossed symbols) and 31% wt (solid symbols).

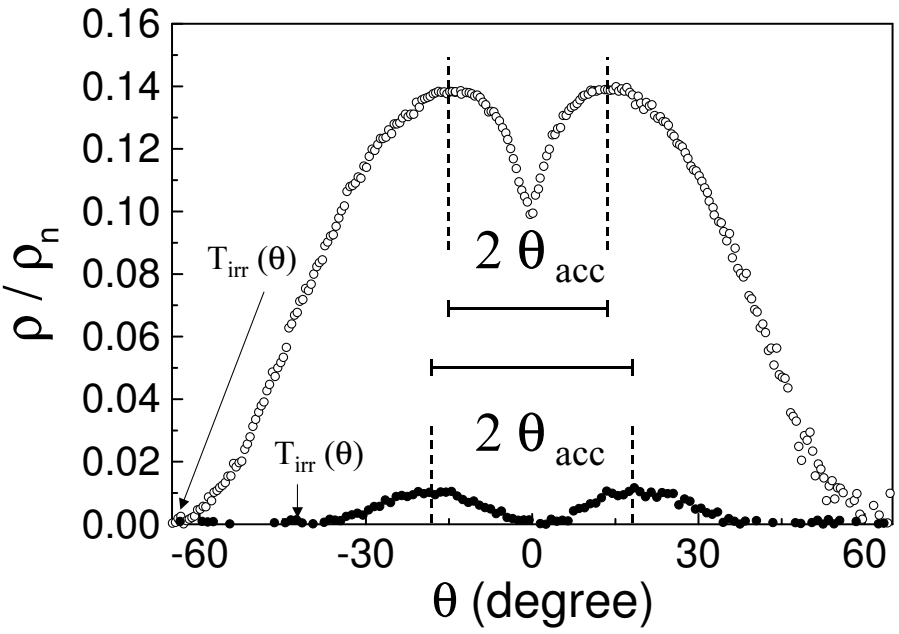

Figure 4.6: Angular dependence of the resistivity for the samples with 0% (○) and 31 %wt (●) of Y_2BaCuO_5 particles at H=3T and T/T_c=0.932. Shown are the irreversibility temperature and the limit of influence of twin boundaries.

be performed, it is worth to note that, in spite of the difference in the actual value of the accommodation angle, the temperature at which this accommodation angle vanishes (T^*) is very similar for all the samples.

Therefore, the angular dependent phase diagram enables us to extract several features concerning the magnetic phase diagram for H||c: the irreversibility line without the influence of twin boundaries, by using equation 3.4 and the limit of influence of twin boundaries (T^*). The extended H-T phase diagram for these samples is shown in figure 4.8.

This figure enables to observe that the magnetic field dependence of the limit of effectivity of twin boundaries (T^*) is the same, within the experimental resolution, for these samples. Furthermore, the fit of the irreversibility lines to equation 3.6 enables to quantify the obtained shift as a function of the content of Y_2BaCuO_5 present in the sample.

Therefore, we are able to determine the dependence of the fitting parameter H_0^i (i=TB,bg) with the interface density of Y_2BaCuO_5 particles, which is shown in figure 4.9. Here, it is observed a linear dependence of the enhancement of H_0 with the content of the area of Y_2BaCuO_5 particles, further demonstrating the strong influence of Y_2BaCuO_5 particles in the irreversibility line.

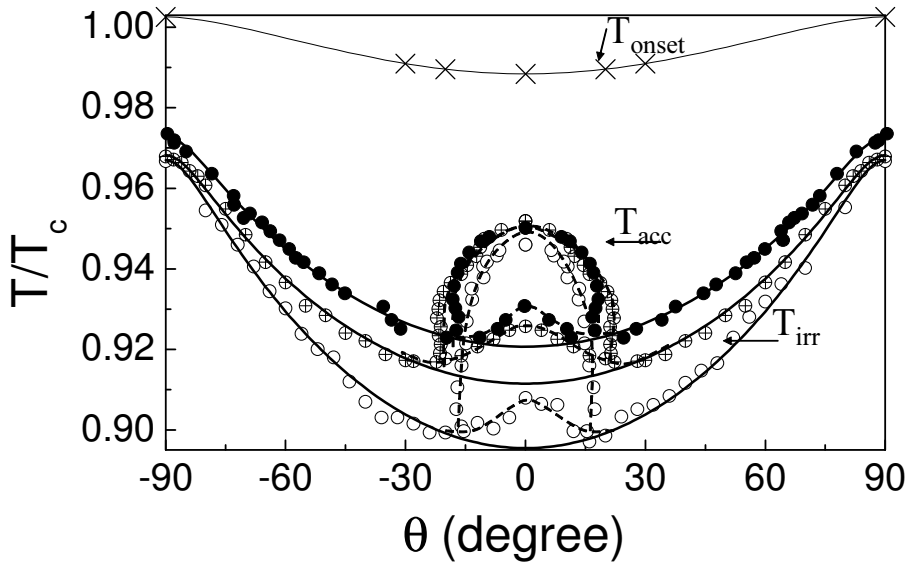

Figure 4.7: Angular dependent phase diagram for the sample with 0% wt (○), 18% wt (⊕) and 31% wt (●). Shown are the irreversibility line, the region of influence of twin boundaries and the accommodation angle (×).

4.3 Vortex Dynamics

Y_2BaCuO_5 particles, however, may also have an important influence on vortex dynamics, since it should strongly modify the characteristics of vortices. The determination of the vortex activation energy at temperatures just above the irreversibility line may enable to quantify the influence of microstructure over vortex pinning energy. At these temperatures (slightly above the irreversibility line) the barriers to vortex motion still have a strong influence over their dynamics, reduces their motion and dissipation is governed by thermally activated processes.

Therefore, we proceed by determining the angular dependence of the vortex activation energy for these samples, U(θ)=$U_0(\theta)\cdot(1-\frac{T}{T_c})$, from the fit of the experimental data to the Arrhenius expression, given by equation 1.5. In figure 4.10, the angular dependence of $U_0(\theta)$ in samples with different densities of pinning centers is represented. It is observed that $U_0(\theta)$ increases with V/d but this enhancement is not linear. This behavior is different to that observed with the irreversibility line, where a linear upwards shift was observed with the density of pinning centers (namely, the overall area of Y_2BaCuO_5 particles).

The angular dependence of the vortex activation energy at different magnetic fields, enables to determine the dependance of this vortex activation energy related to non-aligned defects (i.e., where the influence of twin bondaries has been extracted). In figure 4.11, it is observed a decay of the vortex activation energy for both samples as:

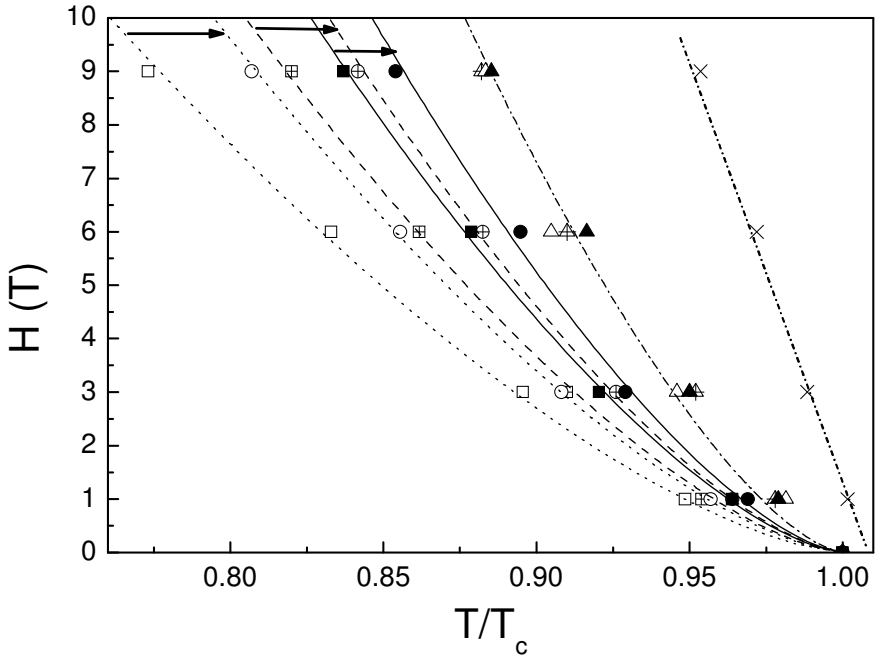

Figure 4.8: Magnetic phase diagram for H$\|$c for the samples with different content of Y_2BaCuO_5 particles: 0%wt (empty symbols), 18%wt (crossed symbols) and 31% wt (solid symbols) at H=3T. Shown are the background irreversibility line (■, ⊞ and □) the experimental irreversibility line (●,⊕ and ○) and the limit of influence of twin boundaries (▲,◭ and △) and Y_2BaCuO_5 particles (×).

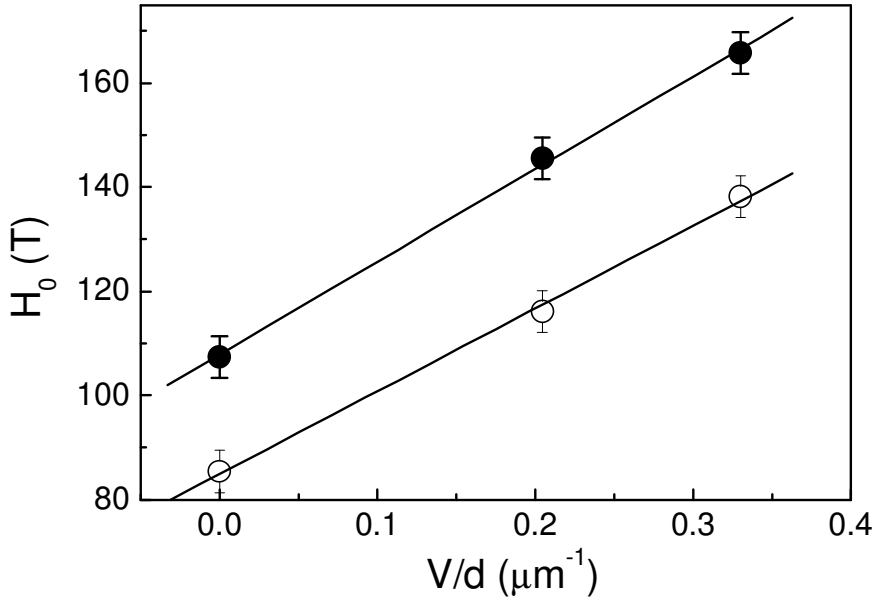

Figure 4.9: Dependence of the fitting parameter H_0^{bg} (○) and H_0^{TB} (●) with the area of Y_2BaCuO_5 particles in the sample. Shown is the linear dependence of H_0 with $\frac{V}{d}$.

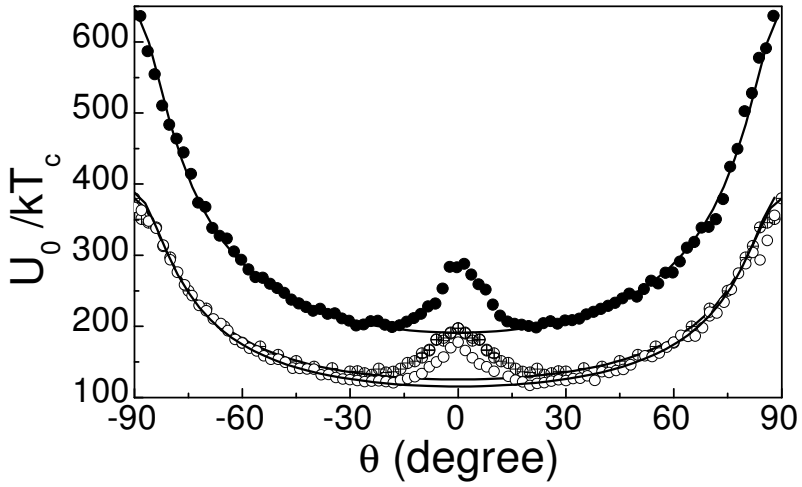

Figure 4.10: Angular dependence of the vortex activation energy for the samples with 0% wt (○), 18% (⊕) and 31%wt (●) of Y_2BaCuO_5 particles, for H=3T.

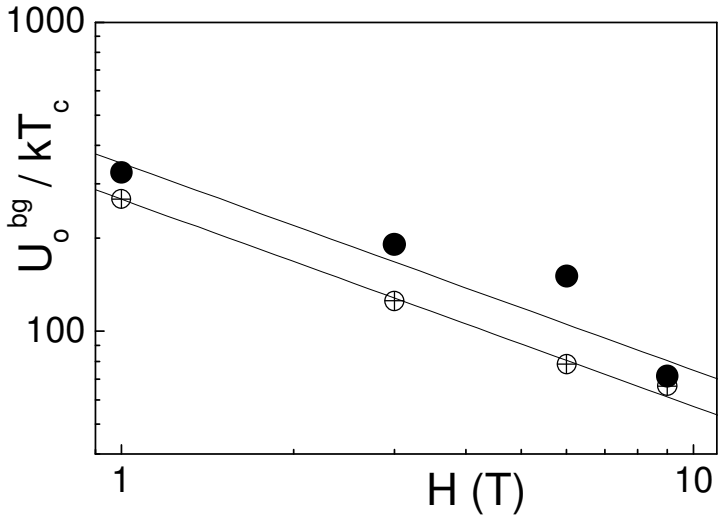

Figure 4.11: Magnetic field dependence of the vortex activation energy for the sample with V/d=2000 cm^{-1} ($\oplus$) and 3300 cm^{-1}($\bullet$).

$$U_0 \propto H^{-0.7} \tag{4.1}$$

Both, plastic motion and cutting and recombination processes, however were expected to lead to $U_0 \propto H^{-0.5}$, thus obtaining a decay of the vortex activation energy lower than our experimental results. However, experimental studies of plastic vortex creep in $YBa_2Cu_3O_{7-\delta}$ single crystals also lead to $U_0 \propto H^{-0.7}$ [96]. Furthermore, recent theoretical investigations [97] on systems with strong disorder (which is likely to occur in MTG-$YBa_2Cu_3O_{7-\delta}$ samples) capable to promote an amorphous vortex glass have shown that plastic motion on these systems should promote an enhancement on this coefficient. Therefore, our experimental results are shown to be consistent with plastic motion of dislocations in strongly disordered systems. Within this model, vortex motion is related to the motion of dislocations in a system where vortices are pinned.

Further insight into vortex dynamics in these samples can be reached by comparing the ratio between the thermal energy (kT) and the vortex activation energy (the barrier to be overcame, U(T)) at the solid-liquid transition.

The angular dependence of this ratio, shown in figure 4.12 for the different samples studied in this chapter, provides a quantitative estimation of the thermal energy required to overcome the barrier potential. In this figure, it is observed that, for all of these samples, the relative thermal energies required are independent of the direction of the magnetic field, except for directions of the magnetic field influenced by twin boundaries, where it decreases. The origin of this decrease will be discussed in chapter 7. The isotropic behavior of $\frac{kT_{irr}}{U_0(T_{irr})}$ (for $\theta \geq 30^o$) suggest, on the other hand, that the same microscopic mechanism rules out

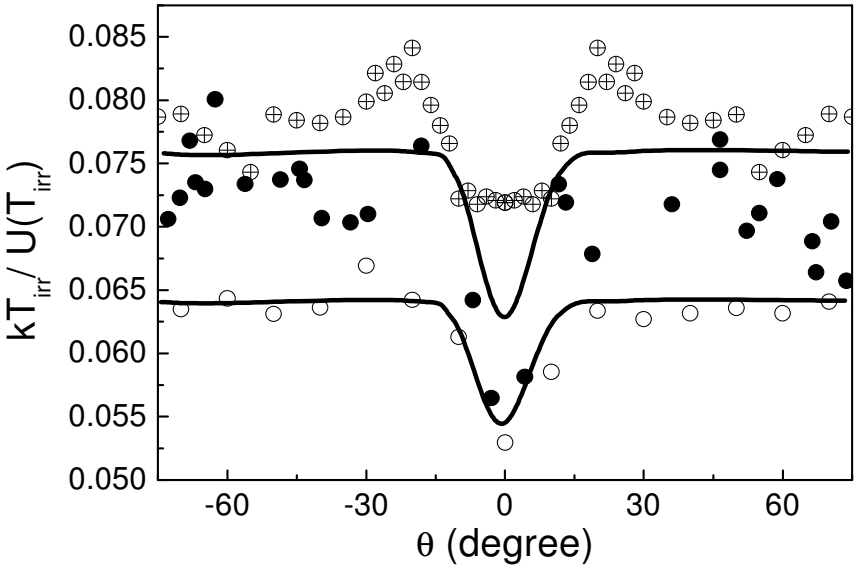

Figure 4.12: Angular dependent ratio between the thermal energy and the vortex activation energy for the samples with 0% wt (○), 18% (⊕) and 31%wt (●) of Y_2BaCuO_5 particles, at H=1T.

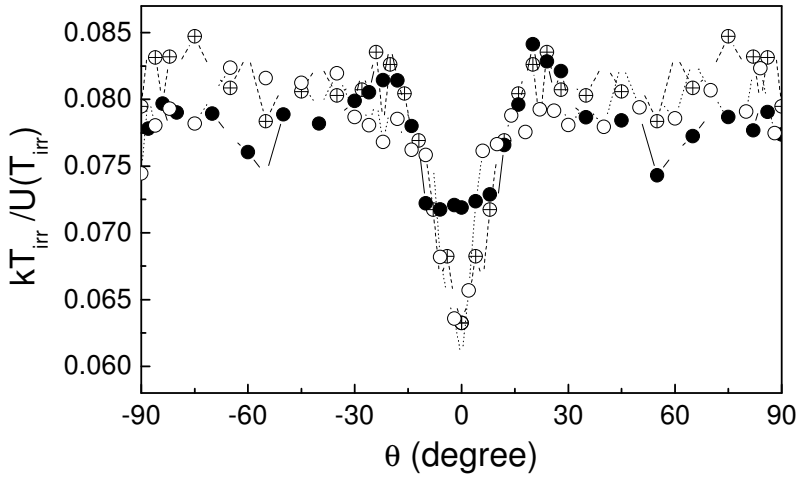

Figure 4.13: Angular dependent ratio between the thermal energy and the vortex pinning energy at the solid-liquid transition for the sample with 18% of Y_2BaCuO_5 particles at H=1T (•), 3T (⊕) and 6T (○).

the vortex dynamics in the whole angular range where Y_2BaCuO_5 are the dominant pinning centers. Furthermore, for each sample, it is observed that the value of this ratio is field independent, within the experimental error, as shown in figure 4.13.

This relation, therefore, appears to be controlled by the microstructure of the sample and independent of the magnetic field and its direction. In what concerns the influence of microstructure on vortex dynamics, there appears to be two different regimes: the sample with small pinning strength (MTG-$YBa_2Cu_3O_{7-\delta}$ sample with a vanishingly small content of Y_2BaCuO_5 particles), has a smaller $\frac{kT_{irr}}{U(T_{irr})}$ than that obtained in samples with strong pinning centers.

This enhancement (as Y_2BaCuO_5 particles are introduced) of the thermal energy required, actually means that to overcome the energy barrier is easier for samples with a lower degree of disorder: a thermal energy corresponding to $\sim$6.5% of the vortex activation energy is enough to promote the solid-liquid transition, while for samples with Y_2BaCuO_5 particles, the relative thermal energy required is bigger $\sim$ 8%, and therefore, the onset of vortex motion is delayed.

The origin of these differences must be related to the strong influence of Y_2BaCuO_5 particles over vortices. The interface $YBa_2Cu_3O_{7-\delta}/Y_2BaCuO_5$ is a strong pinning center, while, due to their distribution, they should promote vortex wandering, and therefore, vortex entanglement. This vortex entanglement, thus could harden the solid and delay the solid-liquid transition. In this sense, the influence of these particles may be similar to the behavior observed in clean $YBa_2Cu_3O_{7-\delta}$ samples where a high density of splayed defects have been introduced through irradiation with heavy ions. In these samples, it has been reported that the

peculiar structure of splayed defects promotes a strong reduction of vortex motion, even at very high temperatures. This strong influence has also been related to vortex entanglement, making harder to obtain vortex motion. From a theoretical point of view the hardening of the vortex solid as the density of $Y_2BaCuO_5/YBa_2Cu_3O_{7-\delta}$ interfaces is enhanced, acting as strong pinning centers, is consistent with the plastic motion of dislocations. In this system, as the density of strong, disordered pinning centers increases, it promotes an enhancement of vortex pinning, as shown in figure 4.10. However, the microscopic mechanism promoting vortex motion in this system (related to the relative thermal energy required to promote the solid-liquid transition) is not modified once Y_2BaCuO_5 particles are introduced.

4.4 Conclusions

In this chapter, the influence of randomly oriented $YBa_2Cu_3O_{7-\delta}/Y_2BaCuO_5$ interfaces in the vortex liquid phase diagram of MTG-$YBa_2Cu_3O_{7-\delta}$ has been investigated. It has been shown, firstly, that MTG-$YBa_2Cu_3O_{7-\delta}$ samples with different contents of Y_2BaCuO_5 follow the same angular behaviour than the samples analyzed in chapter 3, i.e., a peak for H||c related to twin boundaries superimposed over an anisotropic background given by the intrinsic anisotropy of the sample. For the present samples, it has been observed that the intrinsic anisotropy is not modified by the presence of Y_2BaCuO_5 particles.

It has been observed that the presence of this interface leads to an upwards shift of the irreversibility line for all the directions of the magnetic field. This upwards shift of the irreversibility line has been shown to be linear with the interface density of Y_2BaCuO_5 particles. The regions of influence of twin boundaries and Y_2BaCuO_5 particles has been determined by means of angular dependent measurements and comparison between the temperature dependence of the resistivity for the different samples. It has been shown that, although the region of influence of twin boundaries (θ_{acc} (T)) of the different samples is slightly different, the limit of this region for H||c, T^*, is independent of the interface density. On the other hand, the limit of influence of Y_2BaCuO_5 particles on the resistivity reaches temperatures higher than that of columnar tracks or even splayed defects.

We have also investigated the influence of the $Y_2BaCuO_5/YBa_2Cu_3O_{7-\delta}$ interface on the vortex activation energy. We have observed that, at low contents of Y_2BaCuO_5 particles, there is not a significant enhancement of the vortex activation energy, while at higher content, it increases. To further investigate this non-linear behavior, the ratio between the thermal energy and the vortex activation energy at the irreversibility line for the different samples has been determined. It is observed that this ratio, related to how difficult is to promote the solid-liquid transition, is independent of the magnetic field and its direction (outside the influence of twin boundaries, where a dip is obtained). It is also observed that the value of this ratio is slightly smaller for the sample without Y_2BaCuO_5 particles than that for the samples with a certain content of Y_2BaCuO_5 particles, thus suggesting that Y_2BaCuO_5 particles modify the mechanism controlling vortex dynamics. This upwards shift of the relative thermal energy

required, showing a hardening of the vortex solid state, could be related to the enhanced wandering of vortices that leads to a higher entanglement or to an increase of the plastic energy barrier controlling the movement of dislocation lines in a landscape of pinned vortices.

Chapter 5

In-plane dislocations

5.1 Introduction

In MTG-$YBa_2Cu_3O_{7-\delta}$ samples, the presence of Y_2BaCuO_5 particles destroys the first order solid-liquid transition that appears in clean single crystals (see section 3.2), where the destruction of the first order transition has been extensively investigated through the introduction of artificial defects in the sample, created by irradiation with electrons, or protons [26, 98–100] which create point defects or with heavy ions [27, 30, 31, 95, 101] that introduce columnar defects. These artificially created defects lead to an increase of vortex pinning for certain directions of the magnetic fields, and enable to study the influence of these defects on vortex motion, and compare the results with the existing theories for the solid-liquid transition: a vortex-glass transition [16] for samples with point disorder and a Bose-glass transition [17] when columnar defects are present.

In MTG-$YBa_2Cu_3O_{7-\delta}$ samples, the interest is to generate natural defects in a controlled and scalable way and thus, it has originated an intensive research on different post-processes or treatments in order to modify the microstructure and create defects with similar characteristics. The influence of different post-processing treatments on the microstructure and vortex pinning has been studied [102, 103]. In particular, two different treatments have been used at the Institut de Ciència de Materials de Barcelona to study vortex dynamics and improve vortex pinning: Cold Isostatic Pressing (CIP) [58] and a High Oxygen Pressure (HOP) [52, 60]:

CIP: MTG-$YBa_2Cu_3O_{7-\delta}$ samples are submitted to an isostatic pressure at 2kbar Ar atmosphere for 12h at 300^oC. The application of this isotropic pressure to an anisotropic material leads to a plastic deformation of the sample which promotes a reorientation of the stacking faults already existing in the sample. These stacking faults, which are locally a new superconducting phase, $YBa_2Cu_4O_8$, with $T_c \sim 82K$, are surrounded by partial dislocations, which may act as good pinning centers. The stacking faults, while preserving its surface during the treatment, develop a fingertype structure, as

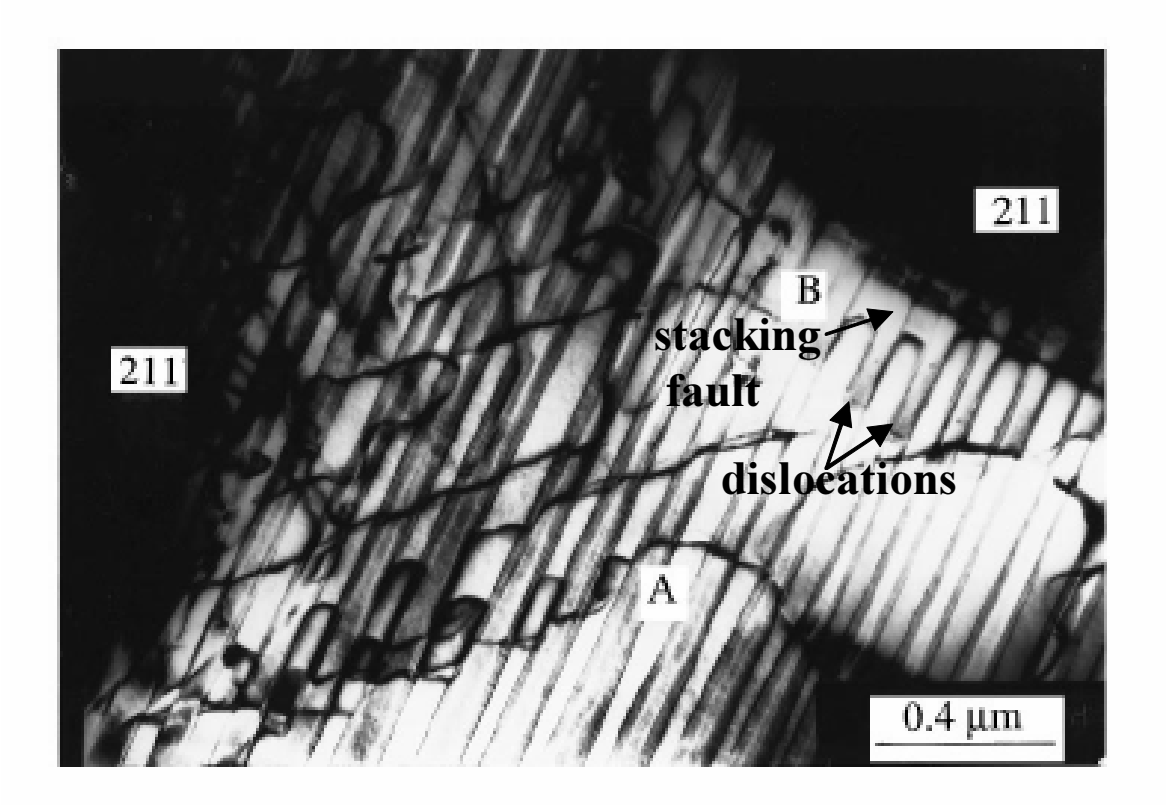

Figure 5.1: Transmission Electron Microscopy of a sample submitted to a cold isostatic pressing for 12h at 300^{o}C.

seen in figure 5.1. This structure has a larger perimeter and, then, an important increase in the length of the dislocations is obtained (the initial density of dislocations $\sigma \sim 10^9 cm^{-2}$, has been observed to peak up to $\sigma \sim 10^{11} cm^{-2}$)[58]. The generated dislocations lay parallel to the ab-plane, as the stacking faults, and are parallel to the directions [110] and [1$\bar{1}$0], coinciding with the direction of twin boundaries in the ab-plane. A mechanism, based on the different stacking fault energy in each twin variant, has been proposed [58] to explain the direction of dislocations obtained (parallel to twin boundaries). This coincidence between both directions, strongly difficulties to distinguish the contribution of dislocations as linear defects when the magnetic field is applied within the ab-plane since the contribution of twin boundaries should be first extracted.

In the solid state of vortex, measurements of the inductive critical current for H$\|$c, in which case dislocations act as point disorder have demonstrated (see figure 5.2) that the existence of a higher density of dislocations promotes an enhancement of the critical current [58]. The observed increase of the critical currents is produced, mainly,

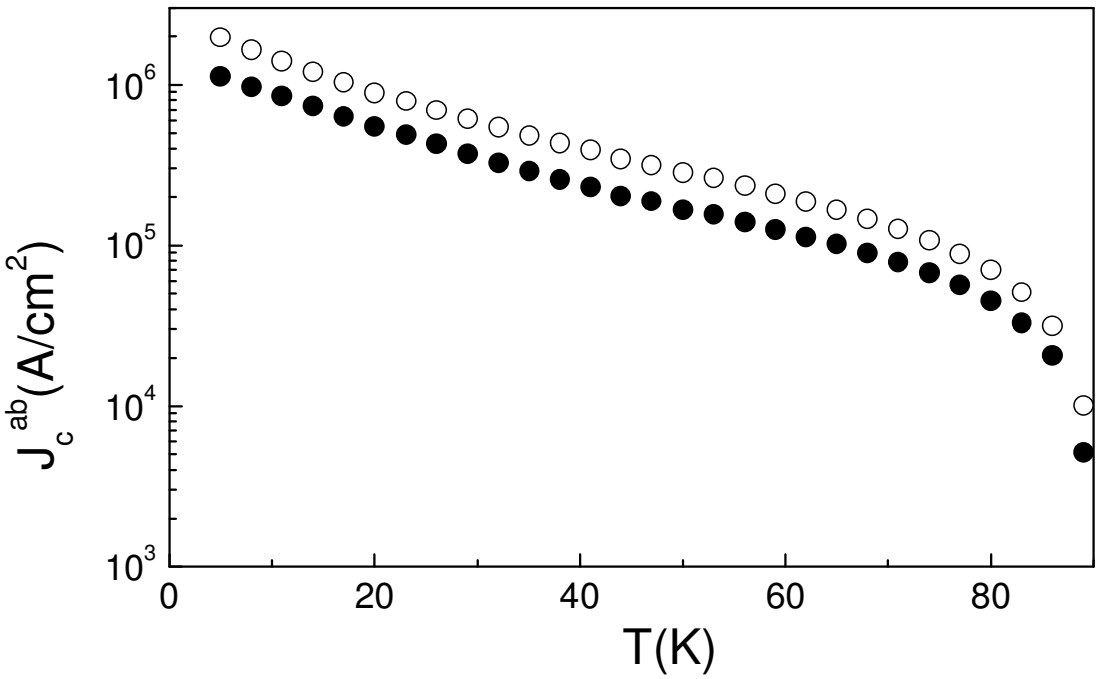

Figure 5.2: Temperature dependence of the critical current for MTG-$YBa_2Cu_3O_{7-\delta}$ samples: as-grown(•) and after CIP (○).

at low temperatures, as expected for weak pinning centers.

HOP: MTG-$YBa_2Cu_3O_{7-\delta}$ samples are submitted to a high pressure of oxygen (P=100bar). The mechanism giving rise to the enhancement of the density of dislocations has been described in [51]. Basically, the external pressure of oxygen, induces the diffusion of oxygen into the sample in an amount determined by the temperature and the time of the process. The oxygen incorporated reacts with the Cu present in the interface $YBa_2Cu_3O_{7-\delta}/Y_2BaCuO_5$, forming Cu-O. Since at these conditions the $YBa_2Cu_3O_{7-\delta}$ +Cu-O is unstable against the formation of $YBa_2Cu_4O_8$, locally, this new phase will appear in the sample in the form of stacking faults, surrounded by partial dislocations, as observed by Transmission Electron Microscopy (see figure 5.3). The creation of these different defects, as mentioned in section 2.2, has been shown to lead to the existence of two competing effects: at early stages of this process, the contribution of point-like pinning centers increases due to the enhancement of the density of dislocations (up to $\sigma \sim 2 \cdot 10^{10} cm^{-2}$ near Y_2BaCuO_5 particles). At latter stages, however, a decrease of the critical current is found, which has been related to the appearance of a much higher density of stacking faults (see figure 5.4).

Since the diffusion of the Cu is easier along the [100] and [010] axis, the stacking faults

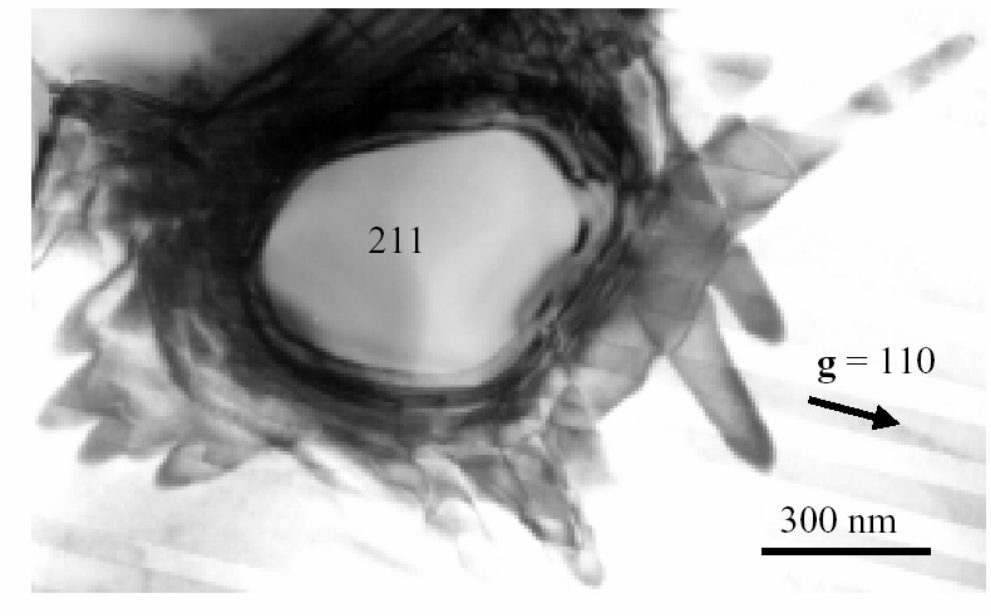

Figure 5.3: Image obtained by Transmission Electron Microscopy of an ab-plane of a MTG-$YBa_2Cu_3O_{7-\delta}$ sample submitted to a HOP treatment at 100bar, 450^{o}C for 12h [52].

and the dislocations extend parallel to these axis, at 45 degrees from twin boundaries. Therefore, a treatment at a high oxygen pressure provides a unique tool in order to study the influence of aligned defects in the ab-plane.

It has to be noted that the dislocations created either by CIP and HOP will have different behaviors depending on the direction of the magnetic field. For magnetic fields rotating from the c-axis to the ab-plane, dislocations will act as point like pinning centers, while for magnetic fields rotating within the ab-plane, it will eventually coincide with the direction of dislocations, and they will act as linear defects with a length $\sim 1\mu m$. Thus, depending on the direction of the magnetic field and therefore the configuration of the experiment, in-plane dislocations will show a strongly different behavior. In the following, the capability of these treatments to enhance the density of dislocations has been used to explore the influence of dislocations. Their influence on the solid-liquid transition and in the liquid state will be studied, both, acting as point like (with out-of-plane measurements) and linear like pinning centers (with in-plane measurements). In chapter 6, the influence of the stacking faults created by HOP will be explored.

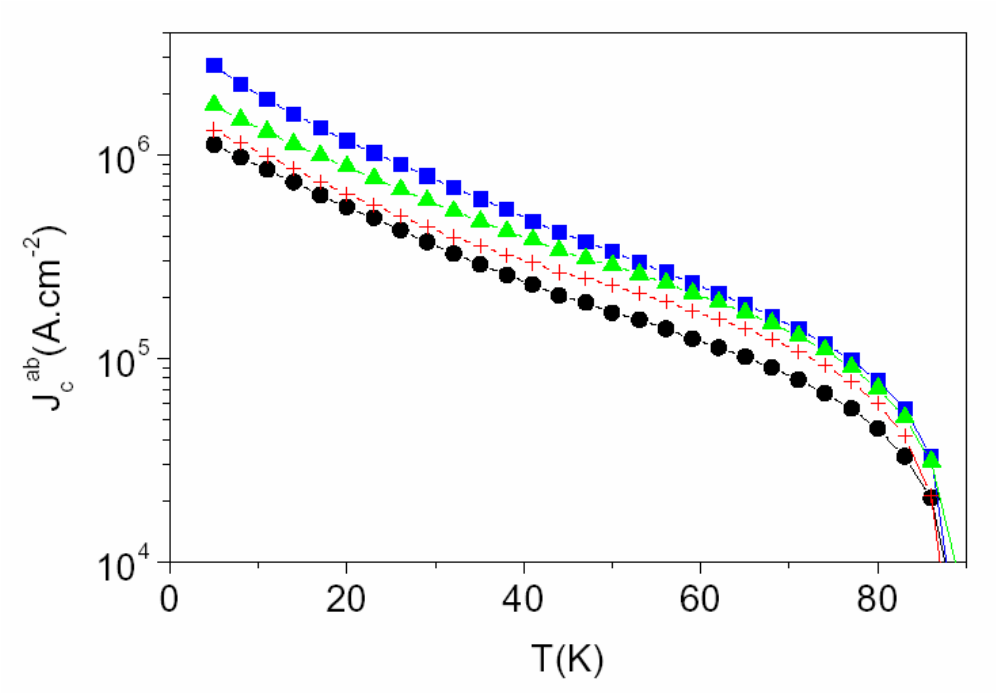

Figure 5.4: Temperature dependence of the critical current for the as grown sample (•), after HOP at 600°C,12h (+), 600°, 2h (▲) and 450°C, 12h (■).

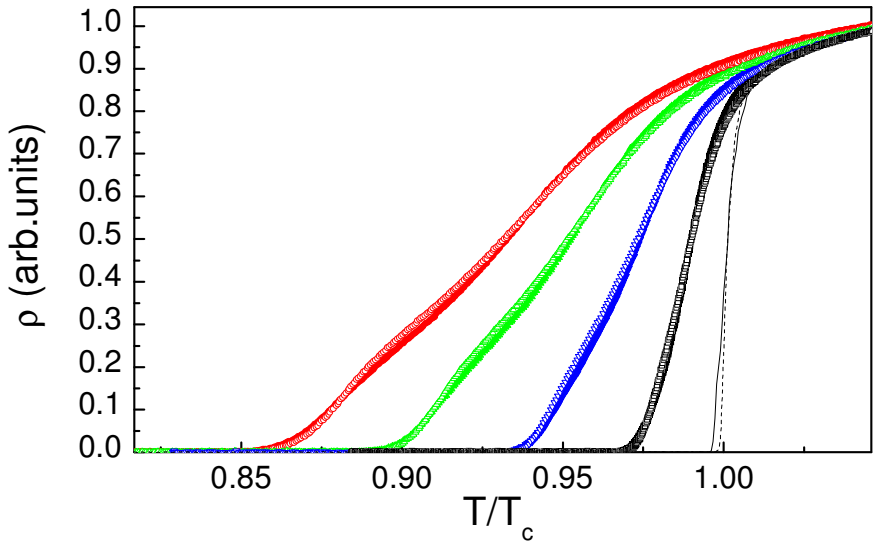

Figure 5.5: Temperature dependence of the resistivity for the as grown sample (solid symbols) and the sample submitted to CIP(open symbols) at H=1,3,6 and 9T, normalized by the critical temperature and the normal state resistance.

5.2 Out of plane measurements: Comparison between an as-grown and a CIP sample

In order to study the influence of dislocations when acting as point-like defects, a MTG-$YBa_2Cu_3O_{7-\delta}$ sample has been cut in two small pieces. One of them was kept virgin and measured. The results of these measurements have already been detailed in chapter 4. The other piece of the sample has been submitted to a Cold Isostatic Pressing at 300^{o}C and 2kbar Ar, in order to generate a high density of in-plane dislocations oriented in the direction $\langle 110 \rangle$, and measured in the same geometry. It has to be noted that these samples have been cut with the twin boundaries (and dislocations) laying at 45 degrees from the edges of the sample. Since the applied magnetic field is perpendicular to the current (which is parallel to the sample edges), even when the magnetic field is applied parallel to the ab-plane it is applied also at 45 degrees of the dislocations and therefore, they are expected to act as point like defects.

The resistivity of both samples at zero field have been measured, displaying a critical temperature $T_c = 90.30K$ for the as-grown sample and $T_c = 90.80K$ for the sample submitted to CIP. In figure 5.5, there are shown the resistivity curves for these two samples at H$\|$c. It is observed that the post-process applied to the sample does not clearly modify the behavior of the temperature dependence of the resistivity.

We may wonder, however, if this similarity in the behavior of the temperature dependence

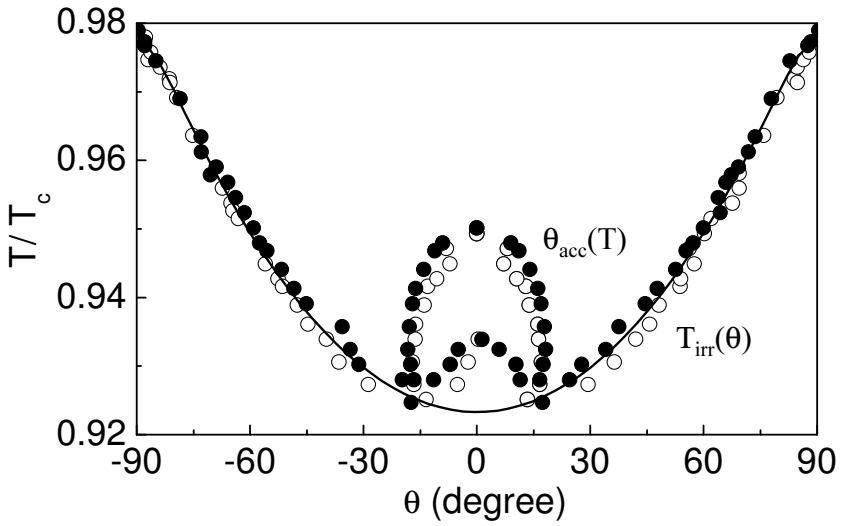

Figure 5.6: Angular dependent phase diagram (for H=3T) for the virgin sample (solid symbols) and the sample submitted to the cold isostatic pressing (open symbols). Shown are the angular dependent irreversibility line (black) and the limit of influence of twin boundaries (red).

of the resistivity is translated into an invariance of the irreversibility line. In figure 5.6, it is observed that, in spite of the strong enhancement of the density of dislocations (from $\sigma \sim 10^9 cm^{-2}$ to a peak up to $\sigma \sim 10^{11} cm^{-2}$), there is not a noticeable modification of the angular dependent irreversibility line. This lack of influence of dislocations, when acting as point-like pinning centers, is certainly in good agreement with the results that one would expect in a system where pinning is already dominated by strong, correlated pinning centers such as twin boundaries or the interfaces $YBa_2Cu_3O_{7-\delta}/Y_2BaCuO_5$. It has to be pointed out, however, that the accommodation angle (θ_{acc}(T)) for the sample submitted to the CIP is slightly reduced respect to that of the virgin sample (see figure 5.6), thus suggesting a small decrease of the efficiency of twin boundaries on pinning vortices. A deformation of the twin boundaries along the c-axis of the sample observed in TEM images in samples submitted to HOP [51] could be the responsible of this decrease of the pinning efficiency. However, and similarly to that observed in the samples with different Y_2BaCuO_5 content, the temperature above which twin boundaries are no longer effective to reduce vortex motion T^* is not changed.

Obtaining the angular dependent phase diagram at different intensities of the magnetic

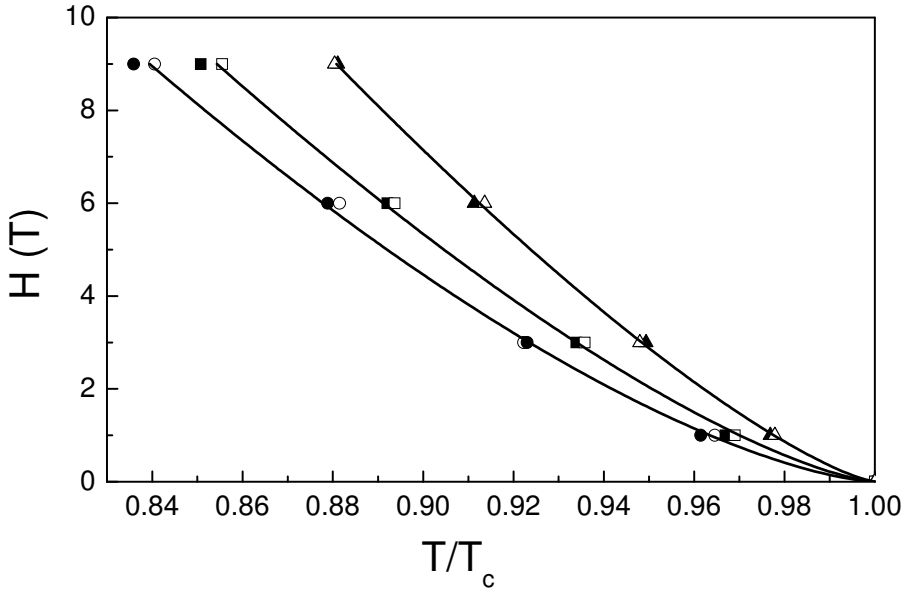

Figure 5.7: Magnetic Phase diagram for the sample before (○, △, □) and after (●, ▲, ■) the cold isostatic pressing. Shown are the irreversibility line related to the background (○, ●), the irreversibility line related to twin boundaries (□, ■) and the limit of influence of twin boundaries (▲, △).

field enables us to determine the magnetic phase diagram for H$\|$c, where the lack of influence of point-like defects in MTG-$YBa_2Cu_3O_{7-\delta}$ samples is further demonstrated. This independence contrasts with its strong influence in the critical currents, although it has been demonstrated [58] that the influence of point-like defects on the critical current strongly decreases with temperature and high magnetic fields where thermally activated flux creep could be very relevant. Therefore, a vanishingly small contribution of point pinning centers at the irreversibility line would be actually expected. Moreover, from the theoretical point of view, this is actually to be anticipated in samples having a Bose-glass transition, since at these temperatures, the correlation volume is large enough to ensure that the average of the random potential vanishes[17]. If the existence of strong pinning centers, such as Y211 particles acting for all the orientations of the magnetic field, lead to a similar increase of the correlation volume near the solid-liquid transition, the introduction of a certain amount of disorder should not modify the T_{irr}, as we have observed.

We have demonstrated so far that the position of the solid-liquid transition has not been modified by the presence of a high density of dislocations acting as point like defects. However, the possible modification of the vortex activation energy has certainly to be considered in order to further study the influence of dislocations on the vortex liquid state. Figure 5.8 shows the vortex activation energy for these two samples, from where it appears clearly that,

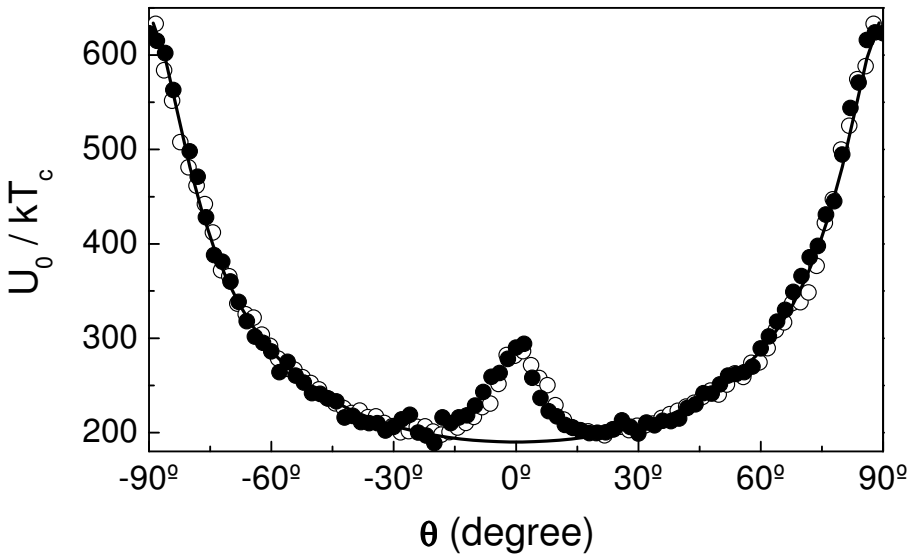

Figure 5.8: Angular dependent vortex activation energy for the virgin sample (open symbols) and the sample submitted to CIP (solid symbols) at H=3T.

similarly to that observed in the magnetic phase diagram, there is no significant influence of the dislocations.

The above presented results, therefore, strongly suggest that dislocations aligned within the ab-plane, and therefore point like disorder does not modify the properties of the liquid vortex state. Following the arguments arising from a Bose-glass transition, and considering the strong influence of the interface $YBa_2Cu_3O_{7-\delta}/Y_2BaCuO_5$ in the liquid state demonstrated in the previous chapter, this further suggests that the strong influence of correlated vortex pinning for all the directions of the magnetic field is capable to overcome vortex pinning by point-like disorder. In addition, the smearing of the influence of point like pinning centers as approaching the irreversibility line further difficults the dislocation pinning to be effective. A determination of whether a Bose-glass transition occurs in this system (by means of a scaling analysis of the I-V curves) or not would help to clarify this point.

5.3 In-plane Measurements: Comparison between an as-grown sample and a HOP sample

5.3.1 In-plane measurements for an as-grown sample

A MTG-$YBa_2Cu_3O_{7-\delta}$ piece with a long dimension along the c-axis (l$\sim$ 1 mm) has been obtained for the same sample that has been already analyzed in chapter 4 (although in a

different configuration). The results obtained for H||ab (and I||c) and those obtained for H||c (and I||ab), will be compared in chapter 8 in order to further investigate the influence of the anisotropy in magnetoresistive measurements.

Following the procedure explained in section 2.4.2, the temperature dependence of the resistivity for different directions of the applied magnetic field within the ab plane have been obtained, where φ is the angle between the magnetic field and the direction of one family of twin boundaries. Results are shown in figure 5.9 for H=1.5T. In this figure we observe that, at low temperatures, the resistivity of the sample is lower for the direction of twin boundaries ($\varphi = 0$). This behavior is in agreement with that observed previously, where an enhancement of vortex pinning leads to a decrease of vortex motion even in the liquid vortex state.

This result, however, contrasts with that observed by D.Bourgault et al. [104],where no effect of twin boundaries was observed at temperatures slightly below the irreversibility line, while rotating the magnetic field within the ab-plane. Those results have been found by analyzing the angular dependence of the transport critical current and it has been observed that at high enough temperatures, there is no influence of the twin boundaries to J_c. This lack of influence has been attributed to a delocalization of vortex as the temperature is increased. Firstly, it has to be noted that direct comparison between these results may not be performed due to the different sensitivity between resistivity measurements and measurements of the transport critical currents. However, this discrepancy about the influence of twin boundaries near the irreversibility line could be related to the range of the magnetic field used. In their measurements, much lower magnetic fields have been used and, since the amplitude of thermal fluctuations increases as reducing the magnetic field, this may enhance the influence of delocalization and lead to the lack of influence of twin boundaries that they observed.

The results obtained from angular dependent resistivity measurements in the present work, actually suggest that there is a strong influence of twin boundaries even at temperatures much higher than the irreversibility line. Similarly to what has been done in the previous sections, the limit of effectivity of twin boundaries for H||c on reducing vortex motion has been defined (T*). From these measurements, and using the same criteria used previously, the angular dependent irreversibility line is determined. It has been also obtained, for each temperature the accommodation angle of the vortex around the twin boundaries which completes the angular dependent phase diagram for in-plane measurements. These data are represented in figure 5.10, where it is observed that the angular dependence of the irreversibility line has a flat background (T_{irr}^{bg}) and an increase of the irreversibility temperature for directions of the magnetic field close to twin boundaries (T_{irr}^{TB}). The flat background shows that the possible existence of a (small) a-b anisotropy observed in untwinned single crystals[105] is smeared out in the present case by the twinned structure. On the other hand, the temperature dependence of φ_{acc} shows a monotonic decrease as increasing temperature. At T*, twin boundaries are no longer effective to reduce vortex motion.

Also from the temperature dependence of the resistivity, the angular dependence of the vortex activation energy may be obtained, by fitting the experimental data to equation 1.5. We observe in figure 5.11 that there is an increase of vortex activation energy when the mag-

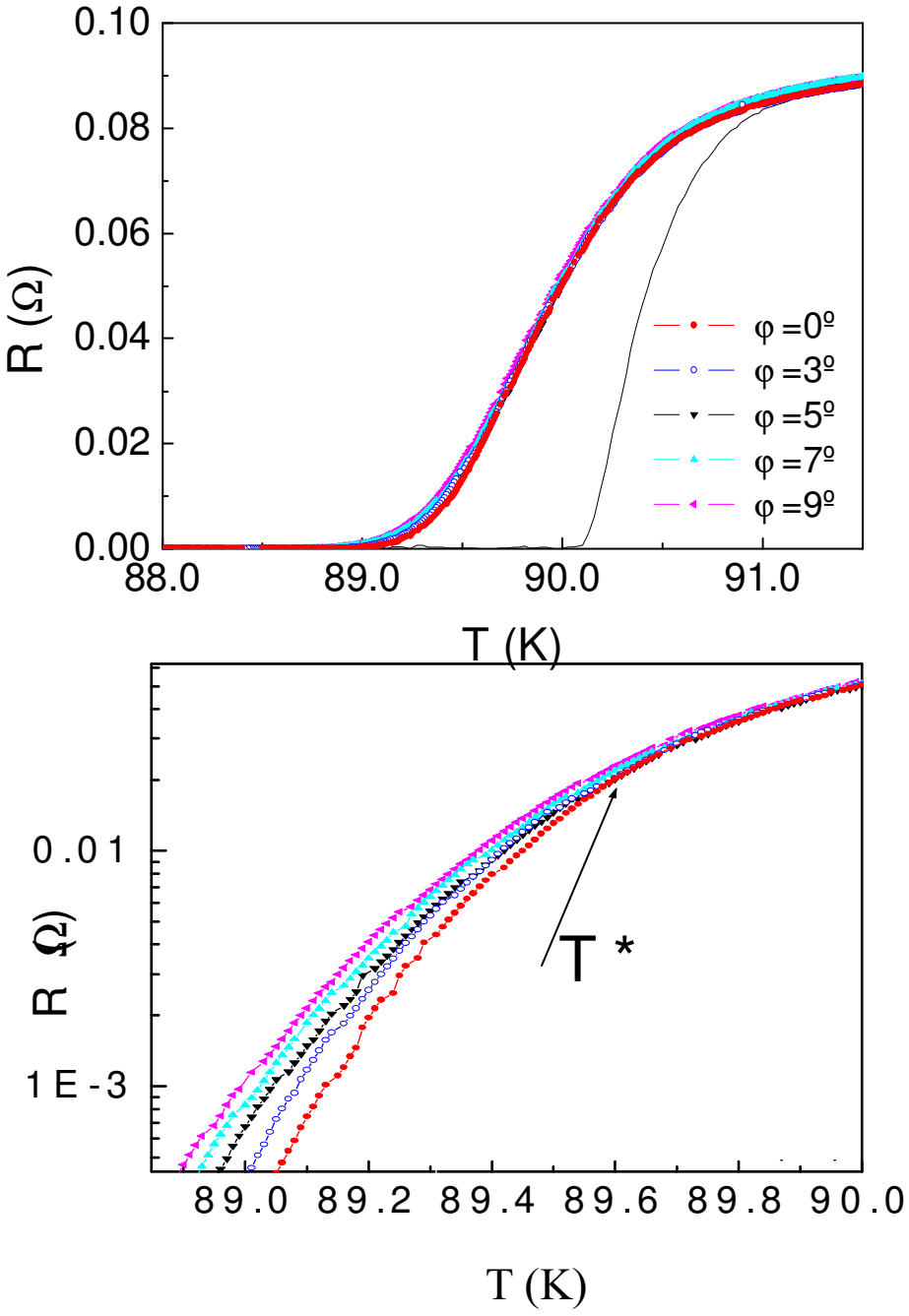

Figure 5.9: Up:Temperature dependence of the resistivity for different directions of the magnetic field (H=1.5T). Also shown is the zero field transition. Down: Temperature dependence of the same curves in a log-linear scale.

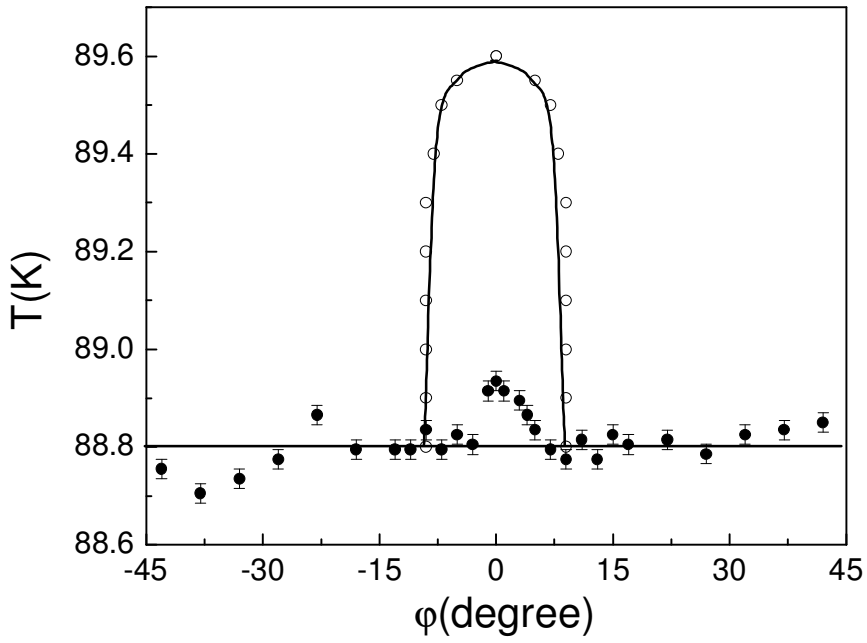

Figure 5.10: Angular dependent phase diagram for an as-grown sample while rotating the magnetic field (H=1.5T) within the ab-plane. Shown is the irreversibility line, $T_{irr}(\varphi)$ (•) and the limit of effectivity of twin boundaries, $T_{acc}(\varphi)$ (○).

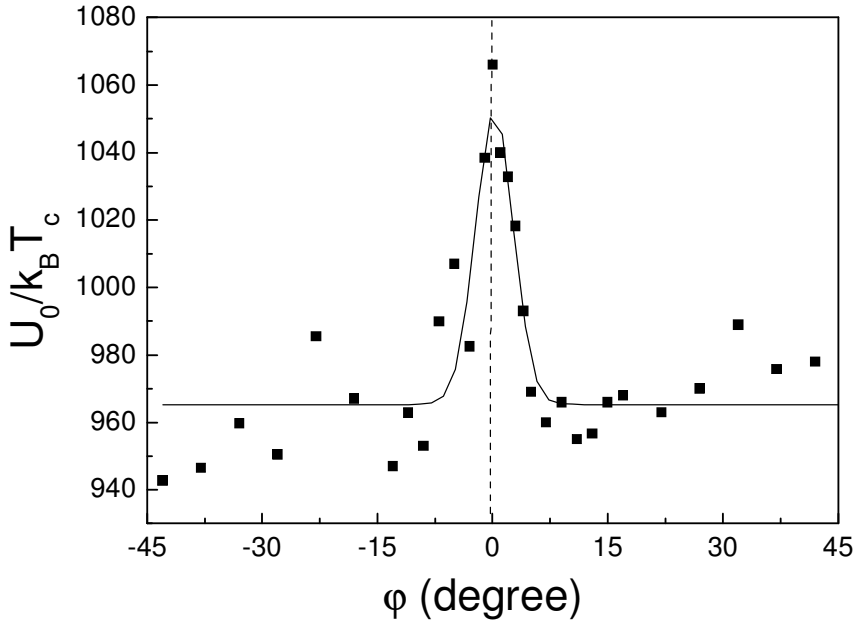

Figure 5.11: Angular dependence of the vortex activation energy for an as grown MTG-sample at H=1.5T.

netic field is applied parallel to twin boundaries, consistently with the upwards shift of the irreversibility line for this particular direction of the magnetic field. Therefore, the angular dependence of both, the irreversibility line and the vortex activation energy demonstrates that vortex motion behaves isotropically when H||ab and F_L ||ab, except for the direction of twin boundaries where an increase of pinning is found.

5.3.2 In-plane results for an HOP sample

In order to study the influence of dislocations acting as linear pinning centers, a MTG-$YBa_2Cu_3O_{7-\delta}$ sample has been submitted to a high oxygen pressure to strongly increase the density of in plane dislocations (from $\sigma \sim 10^9 cm^{-2}$ to $\sigma \sim 2 \cdot 10^{10} cm^{-2}$), which, as we have mentioned before are mainly directed along <100> axis.

The temperature dependence of the resistivity has been obtained for several orientations of the in-plane magnetic field. In figure 5.12 it is shown the temperature dependence of the resistivity for magnetic fields parallel to twin boundaries ($\varphi = 0^o$), dislocations ($\varphi = 45^o$) and an intermediate direction ($\varphi = 22^o$). It appears that at low temperatures, the resistivity for fields parallel to twin boundaries is lower than that for the intermediate direction. This behavior is similar to that observed in the as-grown sample and confirms vortex-pinning by

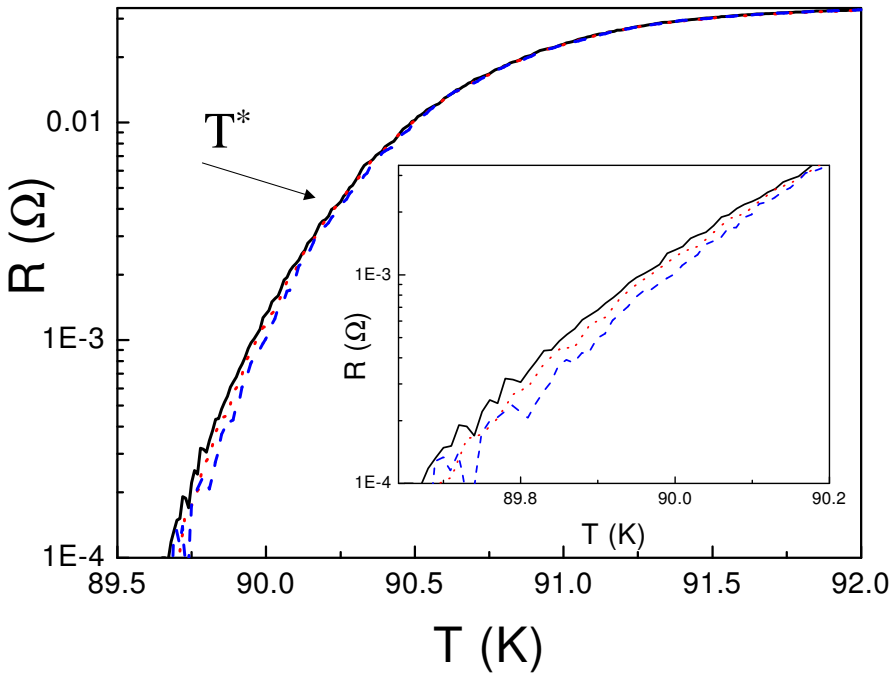

Figure 5.12: Temperature dependence of the resistivity for the sample submitted to a HOP at H=1.5T, for φ=0 (dashed), 22 (continuous) and 45 (dotted) degree. Inset: Detail of the same curves below T^*.

twin boundaries also in this sample.

However, and contrasting with that observed in the as-grown sample, it is also observed a decrease of the resistivity when $\varphi = 45^o$.This direction coincides with the direction of the dislocations created during the HOP, thus demonstrating that the aligned dislocations generated by the HOP are effective linear pinning centers (for H||<100>), in a similar manner to columnar defects created by heavy ion irradiation and twin boundaries. The observed decrease of the resistivity, however, is lower for dislocations than for twin boundaries.

These measurements of the temperature dependence of the resistivity enables us to determine, once more, the angular dependence of the phase diagram, is shown in figure 5.13. In this figure, the angular dependence of the irreversibility line clearly shows the presence of a flat background, where two peaks appear. The increase of the irreversibility line for magnetic fields parallel to the linearly correlated defects, is in good agreement with the behavior expected from two Bose-glass transitions at two different orientations of the magnetic field generated by twin boundaries and in-plane dislocations. To our knowledge, this is the first time that a double Bose-glass transition is observed simultaneously in the same sample for two different magnetic field orientations.

Two main ideas surge when the influence on the magnetic phase diagram of twin bound-

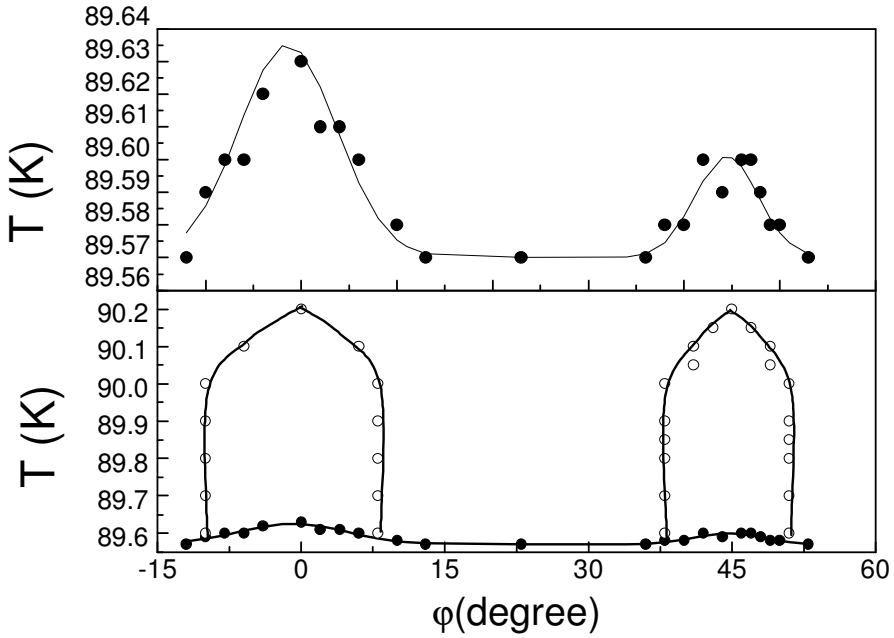

Figure 5.13: Up:Angular dependence of the irreversibility line for the sample submitted to a HOP at H=1.5T. Down: Angular dependent phase diagram. Shown is the angular dependence of the irreversibility line, $T_{irr}(\varphi)$, (•), and the limit of the regions with influence, $T_{acc}(\varphi)$, of twin boundaries ($\varphi = 0$) and dislocations ($\varphi = 45$) (○).

aries and dislocations is compared:

- Firstly, the upwards shift of the irreversibility line is slightly higher for twin boundaries than for dislocations. As it will be shown in chapter 7, the upwards shift of the irreversibility line due to the presence of twin boundaries is directly related to its concentration. The observation of a lower enhancement of the irreversibility temperature by dislocations could be simply explained by considering the different dimensionality of the defects (dislocations are 1-D defects and therefore, enable only to pin 1 vortex, while twin boundaries, being 2-D defects enable the presence of several vortex, separated by a distance of the order of a_0 along the c-axis). However, an additional influence of the shorter length of dislocations could also exist.

- Secondly, although $\varphi_{acc}(T)$ is slightly smaller for dislocations than for twin boundaries ($\varphi_{acc}^{disl} \approx 6^o$ and $\varphi_{acc}^{TB} \approx 9^o$), the end-point of the influence of twin boundaries and dislocations (T^*) is not modified within our experimental resolution. This coincidence, strongly suggests that the limit of effectivity of linear defects is an intrinsic property of the material, independent of the size of the defect or its density or even its dimensionality. This feature will be studied in detail in chapter 8.

After exploring the phase diagram and considering the differences between twin boundaries and dislocations on the enhancement of the irreversibility line, one may wonder whether these differences are also present in the angular dependence of the vortex activation energy. In figure 5.14, the angular dependent vortex activation energy is shown for H=1.5T. There, it is observed a similar qualitative behavior to that of the angular dependent irreversibility line: a flat background with two peaks, related to the enhanced pinning due to twin boundaries and dislocations respectively. In the present figure, however, we note that both defects lead to a similar increase of the vortex activation energy, although they produce a different shift of the irreversibility line. This different behavior could suggest that, either, the vortex pinning energy or the enhancement of the irreversibility temperature are not unambiguously related to the density of pinning centers present in the sample. Actually, and taking into account that the density of dislocations is lower than the density of twin boundaries, we may suggest that the vortex activation energy is not simply related to the density of defects. It is also very likely that the coexistence of strong pinning centers such as Y_2BaCuO_5 particles and the linearly correlated defects smears out its influence on the activation energy.

Both, the angular dependence of the phase diagram and the vortex activation energy, have demonstrated the reduction of vortex motion due to the presence of in-plane, linearly correlated pinning centers such as twin boundaries and dislocations. Therefore, for this particular direction of the magnetic field, dislocations have been demonstrated to act as strong, linearly correlated vortex pinning centers. Thus, dislocations generated by the High Oxygen Pressure become, up to our knowledge, the first linear defect aligned within the ab-plane which has been shown to behave as linear pinning centers. Since the influence of these in-plane generated dislocations is very similar to that widely reported in the literature for

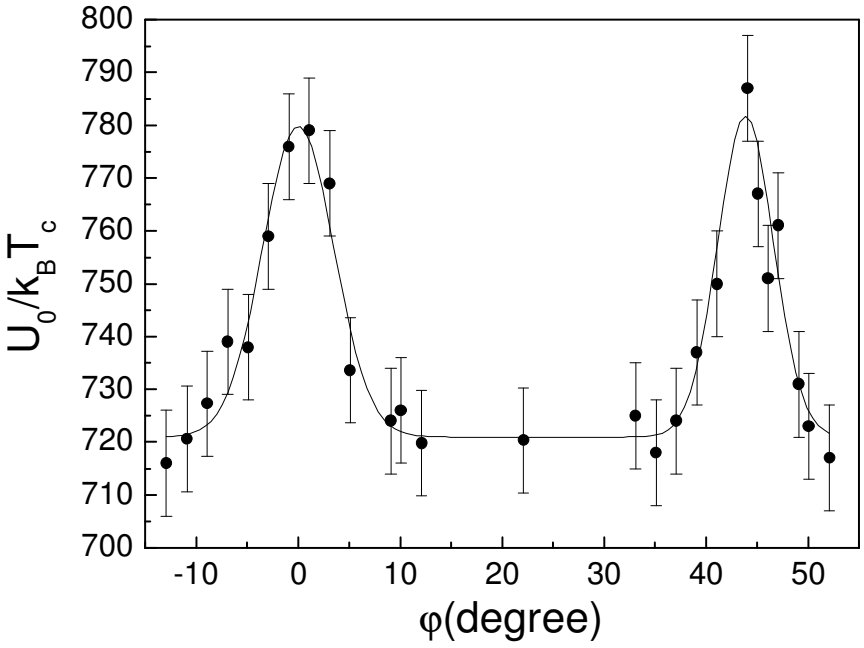

Figure 5.14: Angular dependence of the vortex activation energy at H=1.5T.

Bose-glass transitions, we suggest that a Bose-glass transition is also present for in-plane magnetic fields parallel to linearly correlated pinning centers. Furthermore, the modification of the superconducting properties in the liquid state due to the presence of dislocations for this particular configuration contrasts with their lack of influence when acting as point-like pinning centers, and remarks the importance of the relative direction vortex/defect and the defects dimensionality.

5.4 Conclusions

In this chapter we have investigated the influence of in-plane aligned dislocations generated by different treatments. Two completely different behaviors have been observed:

- For magnetic field rotating from the c-axis to the ab-plane, no influence of the in-plane dislocations is observed, nor in the irreversibility line or in the vortex activation energy. This lack of influence of dislocations acting as point-like pinning centers in the vortex liquid state is actually what should be at high temperatures expected in a system with strong pinning centers such as $YBa_2Cu_3O_{7-\delta}/Y_2BaCuO_5$ interface and twin boundaries.

- In order to analyze the influence of dislocations as linear-like pinning centers, in-plane

measurements had to be performed. These measurement were done using a cryostat with two degrees of freedom, at the Materials Science Division in the Argonne National Laboratory, USA. Firstly, a virgin sample has been studied where we have observed a flat background (corresponding to the isotropy of the ab-plane) for both the irreversibility line and the vortex activation energy with one peak corresponding to twin boundaries. For the sample submitted to HOP, together with the flat background, two peaks have been observed, related to the influence of twin boundaries and dislocations, is found in the irreversibility line. Furthermore, the region of influence of both defects has been determined. Although a slight difference is found between the values of φ_{acc} for twin boundaries and dislocations, the temperature at which it vanishes, T^* coincides. The origin of this coincidence will be further studied in chapter 8. To summarize, a strong influence of in-plane dislocations as linear-like pinning centers in the vortex liquid state has been demonstrated.

Chapter 6

Vortex Breaking defects

6.1 Introduction

Up to now, the influence of different defects on the liquid vortex state has been studied. The influence of these microstructural defects on the superconducting properties has been analyzed in terms of their action as pinning centers (either point-like or linear-like). Microstructural defects, however, may also have a detrimental influence on the superconducting properties due to the loss of coherence around these defects. This detrimental influence of certain microstructural defects has been unambiguously demonstrated for grain boundaries[19]. Planar defects may also lead to a partial suppression of the superconducting properties. These planar defects (due to its non-superconducting nature) may act as a boundary capable of enhancing the decoupling of the vortex. Thus, the possible reduction of the vortex length should play a role on vortex motion.

This role of the finite-size of the vortex has been widely studied both, theoretically by means of simulations. However, the experimental results on this issue are restricted to short lengths (up to tens of nanometers) by considering multilayers or thin films, due to the limited thickness of $YBa_2Cu_3O_{7-\delta}$ thin films. In this sense, L.Civale [106] showed that, at small thickness (below 100 nm), the irreversibility line is shifted upwards as the thickness of the thin film increases, while, at higher thickness, the position of the irreversibility line is almost thickness independent. A similar upwards shift of the irreversibility line has been observed in $YBa_2Cu_3O_{7-\delta}$/$PrBa_2Cu_3O_{7-\delta}$ multilayers [107] and NbN/AlN multilayers [108], and it has been related to the modification of the 2-D character of the strongly layered cuprates. On the other hand, flux transformer measurements for twinned $YBa_2Cu_3O_{7-\delta}$ samples with different thickness have been performed [41]. It has been observed that as the thickness of the sample increases, the temperature where full vortex correlation is lost decreases, thus demonstrating the strong influence of finite-size effects on vortex dynamics. In spite of the extensive work performed on this subject, a clear picture concerning the influence of the separation between the planar defects on vortex motion is still missing.

In order to study the influence of the vortex length in MTG-$YBa_2Cu_3O_{7-\delta}$ samples and

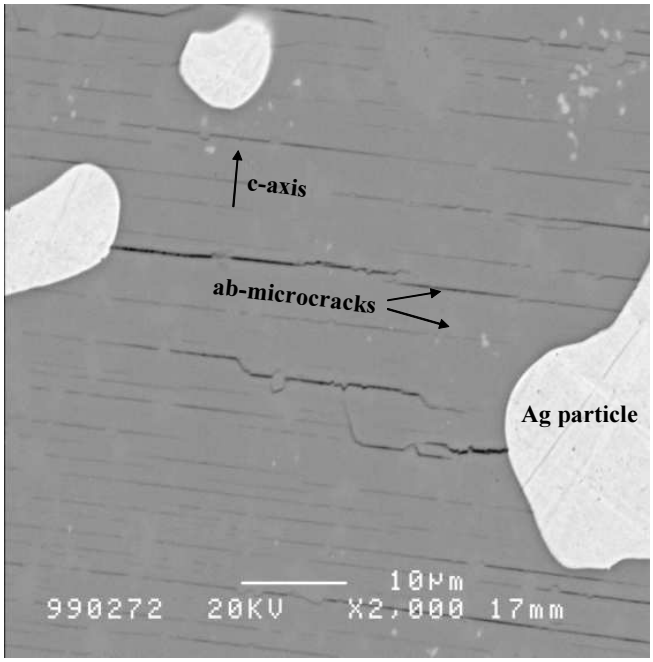

Figure 6.1: SEM Image of an ac-plane of MTG-$YBa_2Cu_3O_{7-\delta}$ sample with 20%wt of silver obtained by Scanning Electron Microscopy. Silver particles and microcracks are shown in the image.

expand this analysis to larger lengths, two different defects have been considered in this chapter, covering a wide range on the distance (d_{planar}) between the defects: microcracks and stacking faults. In order to strongly modify the distance between these defects, two different processing methods have been used: silver additions and a high oxygen pressure process.

Silver Addition: In order to study the influence of microcracks as a defect breaking the correlation of the vortex along the c-axis, MTG-$YBa_2Cu_3O_{7-\delta}$ samples with different contents of Ag precipitates have been studied. In order to maintain the influence of Y_2BaCuO_5 particles constant, the same ratio between the content of $YBa_2Cu_3O_{7-\delta}$ and Y_2BaCuO_5 has been employed in all the samples studied (18%wt of Y_2BaCuO_5 prior to the incorporation of silver). The addition of silver particles from 0% to 20% wt has been shown to strongly modify the distance between microcracks from $1.7\mu m$ to $6.7\mu m$.[61]

The study of the inductive critical currents in the solid state reported an increase of J_c as the content of Ag is enhanced. The large dimensions of the silver particles (up to $50\mu m$), even compared with those of Y_2BaCuO_5 particles, impeded a noticeable effect of silver particles on the critical current, and therefore, the increase of the critical current was attributed to the reduction of the density of microcracks.[61] However, a

careful, quantitative characterization of the microstructure of samples with different densities of silver particles reported an strong enhancement of the density of dislocations [51] and twin boundaries. These results, together with the analysis of the temperature dependence of the critical temperature demonstrated that the increase in the density of defects explain the observed enhancement of the critical currents, leaving no observable effect of microcracks on critical currents.

In spite of the independence of critical currents in the vortex solid state with the density of microcracks, a certain influence of the distance between microcracks could exist in the vortex liquid state, since thermal activation may be favored, enhancing vortex motion. It has to be noted that any possible contribution of the modification of the density of twin boundaries and dislocations on vortex motion may be successfully extracted by the use of angular dependent measurements of the magnetoresistance enabling to study the influence of microcracks without misleading influences.

High Oxygenation Process: The oxygenation at P=100 bar is an interesting tool to generate partial dislocations, and thus increasing vortex pinning as it was reported in chapter 5. At a latter stage, however, an excessive oxygen promotes a massive creation of stacking faults in the whole sample, with distances between stacking faults of the order of 40nm along the c-axis. In figure 6.2, it is shown an image obtained by Transmission Electronic Microscopy of an ac-plane showing the high density of stacking faults generated by long stages of oxygenation.

Measurements of the inductive critical currents in samples with a high density of stacking faults, have revealed a strong decrease of the critical currents, demonstrating the detrimental effects of stacking faults even deeply in the vortex solid state. This contrasts with the lack of influence of microcracks in vortex motion in the vortex solid state.

This behavior of the critical currents at large densities of stacking faults pushed us to study its influence on the angular dependent phase diagram. Furthermore, comparison between the influence of stacking faults and microcracks may enable us to study the influence of planar defects separated apart up to 2 orders of magnitude.

It has to be noted, however, that microcracks and stacking faults are planar defects but have a finite size. The finite size of these defects may promote that vortices are simply distorted by the presence of microcracks or stacking faults. Therefore, the particular influence of these defects over vortices depends on the concrete energy cost for cutting or elongating the vortex. Consequently, both actions of microcracks and stacking faults may be found simultaneously, depending on the particular position of the vortex considered.

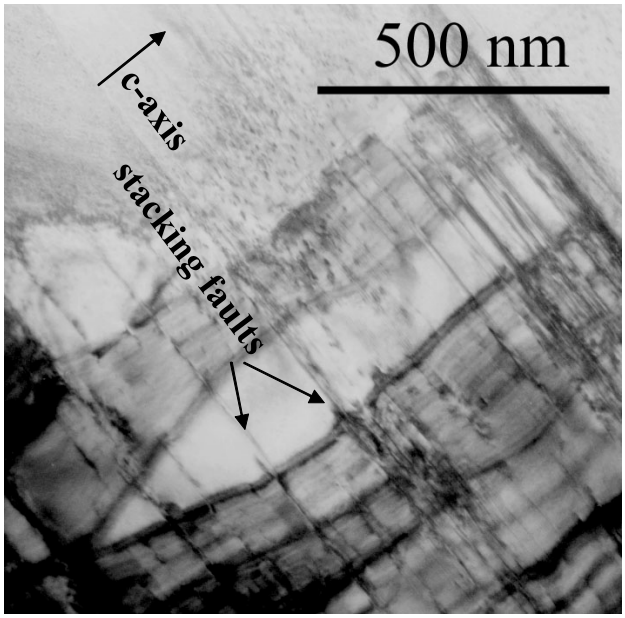

Figure 6.2: TEM image of a MTG-$YBa_2Cu_3O_{7-\delta}$ sample submitted to a high oxygen pressure at 600^{o}C for 24h.

6.2 Influence of microcracks

6.2.1 Magnetic phase diagram

Three MTG-$YBa_2Cu_3O_{7-\delta}$ samples with different initial content of Ag_2O particles, ranging from 0% to 20% wt have been studied. The initial composition of Y_2BaCuO_5 has been chosen in order to ensure a sample independent ratio between the content of Y_2BaCuO_5 and $YBa_2Cu_3O_{7-\delta}$. The independence of this ratio has been verified by determining the paramagnetic signal of Y_2BaCuO_5 at temperatures above T_c.

In order to study the influence of microcracks in the vortex liquid state, these $YBa_2Cu_3O_{7-\delta}$ samples have been analyzed by determining their angular dependent magnetoresistance. Figure 6.3 shows the resistive transition of these samples together with the temperature dependence of the resistance for different magnetic fields and H$\|$c, normalized by the normal state resistance and the critical temperature. It is observed that at high temperatures, there is a strong similarity between the normalized resistivity of these three samples, while at lower temperatures, the temperature dependence of the resistivity for these three samples starts to deviate from each other and reaches zero resistance at different points. Appears clearly from the figure, that as increasing the distance between microcracks, vortex motion starts at higher temperatures. This modification in the onset of dissipation is trans-

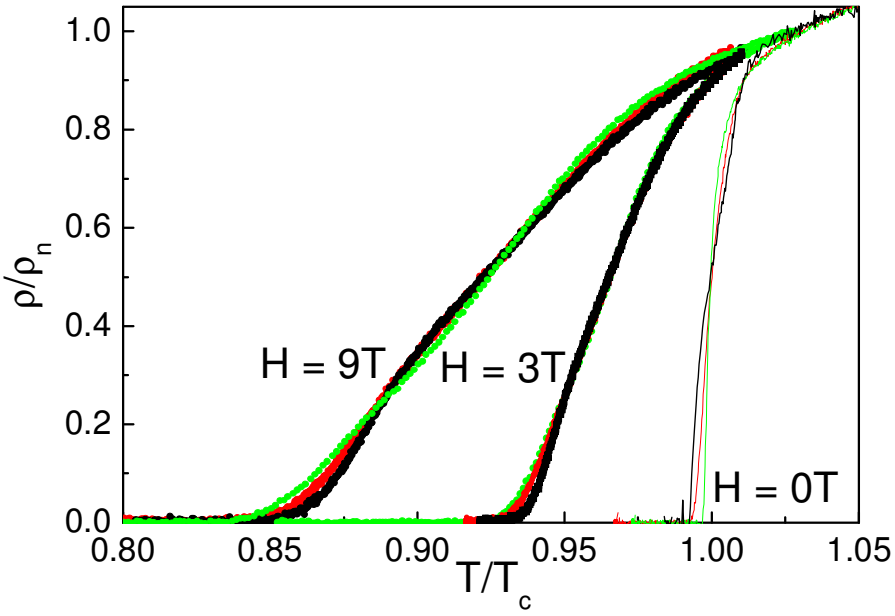

Figure 6.3: Temperature dependence of the resistivity for the samples with 20 (●),10 (●) and 0 (●)% wt of silver, for H=0,3 and 9T with H||c.

lated into the magnetic phase diagram, where an upwards shift of the irreversibility line is observed (see figure 6.4) as increasing the distance between microcracks.

For this particular direction of the magnetic field (H||c), however, the influence of twin boundaries may produce misleading effects. Moreover, the presence of silver particles has been shown to increase the density of twin boundaries. This, together with the fact that the temperature at which the dependence of the resistivity becomes different is similar to the onset of twin boundaries, suggest an strong influence of twin boundaries on these observations. Therefore, prior to attributing this upwards shift of the irreversibility line to microcracks, the influence of twin boundaries has to be extracted.

To extract the influence of twin boundaries, and following the procedure already used in the previous chapters, the angular dependence of the different R vs T curves has been analyzed and compared between the different samples. From this set of measurements, we are able to obtain the angular dependence of the irreversibility line, shown in figure 6.5. Here, it is observed that the previously mentioned upwards shift of the irreversibility line is obtained for all the directions of the magnetic field. Since a certain influence of twin boundaries on reducing vortex motion is only found at $\theta < \theta_{acc}(T)$ (which is similar for the three samples studied), the influence of twin boundaries has to be excluded as a possible origin and the shift of the irreversibility line has to be attributed to the decrease on the density of microcracks.

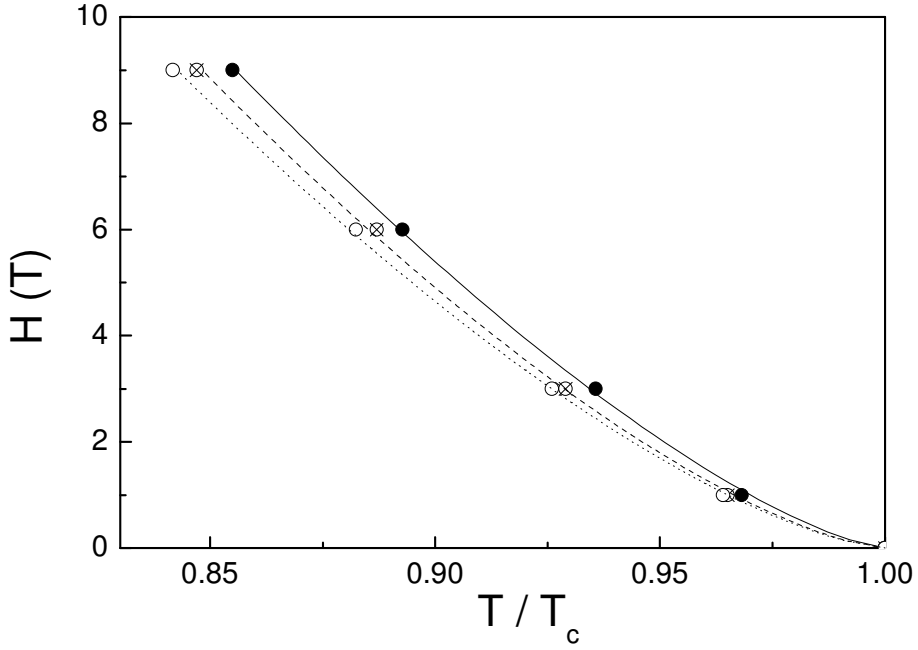

Figure 6.4: Irreversibility line for the samples with 0% (○), 10% (⊗) and 20% wt (●) of Ag_2O and H||c, i.e. distances between microcracks of 1.7, 3.7 and 6.7 μm.

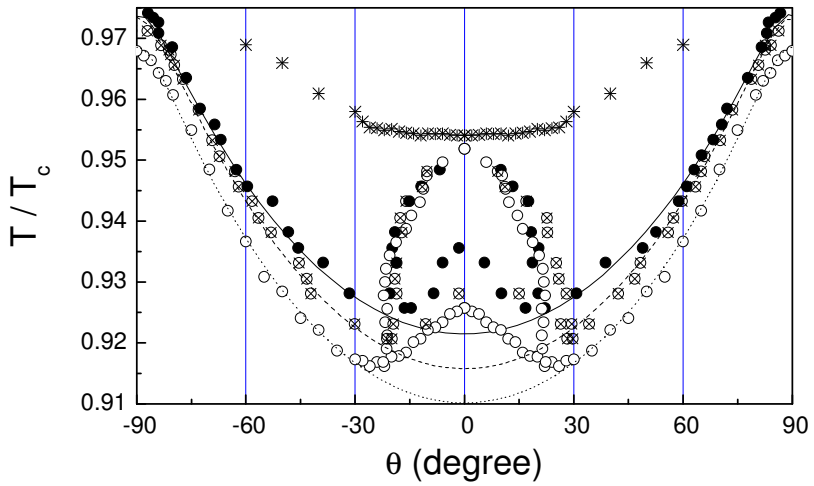

Figure 6.5: Angular dependent phase diagram for the samples with different distance between microcracks for H=3T. Shown are the irreversibility lines ($T_{irr}(\theta)$) and the limit of influence of twin boundaries (θ_{acc} (T)) for the samples with 0% (○), 10% (⊗) and 20%wt of silver (●). The limit of influence of microcracks on vortex motion,T^{onset}, (⋆) is also shown.

Together with this enhancement of the irreversibility line for all the directions of the magnetic field, the region of influence of microcracks is also worth of study. Certainly, the behavior of the temperature dependence (at high temperatures) of the resistivity (as seen in figure 6.3) is not exactly equal for the three samples, fact that could be related to the slight differences between the rest of microstructural characteristics. However, the temperature at which the temperature dependence of the resistivity starts clearly to deviate, may be estimated by considering the temperature at which, for instance, $\left|\frac{\frac{\rho(T)}{\rho n}\Big|_{20\%} - \frac{\rho(T)}{\rho n}\Big|_{0\%}}{\frac{\rho(T)}{\rho n}\Big|_{20\%}}\right| = 5\%$, for different directions of the magnetic field. This limit of influence of microcracks is represented in figure 6.5 for all the directions of the magnetic field. It is observed that this temperature (T^{onset}) increases as approaching the ab-plane, consistently with the anisotropy of the $YBa_2Cu_3O_{7-\delta}$ system. At large angles, however, the definition of this temperature becomes difficult to define. However, it appears clearly that there exists an important influence of microcracks that may not be related to twin boundaries since this region expands outside the region of influence of twin boundaries.

An interesting feature observed in the angular phase diagram is that, for H||c, the limit of influence of twin boundaries and microcracks coincides, strongly suggesting that this temperature may correspond with an intrinsic feature of vortex behaviour in the liquid state, as will be discussed in chapter 8.

The angular dependent phase diagram at different intensities of the magnetic field enables to determine the complete magnetic phase diagram for H||c (see figure 6.6). In this phase diagram, it is further reinforced the coincidence between the limit of influence of twin boundaries and microcracks and the upwards shift of the irreversibility even when the influence of twin boundaries is extracted.

The magnetic phase diagram for H||c, allows us to adjust the irreversibility line for the different samples to equation 3.6, and therefore to quantify the influence of the microcracks. The obtained values of H_0^{bg} and H_0^{TB} for these samples are shown in figure 6.7 as a function of the distance between microcracks. It is observed an enhancement of H_0^i (i=bg,TB) as increasing the distance between microcracks, thus, further reinforcing the detrimental influence of microcracks. Another issue observed in figure 6.7 is that the dependence of H_0^{TB} is stronger than that of H_0^{bg} (the slope of H_0^{TB} (d_{planar}) is a 50% larger than that of H_0^{bg} (d_{planar})). The analysis of this difference, related to the influence of twin boundaries will be performed on chapter 7.

6.2.2 Vortex Dynamics

Once studied the influence of microcracks on the magnetic phase diagram, we proceed to investigate whether the vortex activation energy is modified or not by the presence of microcracks. Therefore, we studied the angular dependence of the vortex activation energy for the three considered samples, which is shown in figure 6.8.

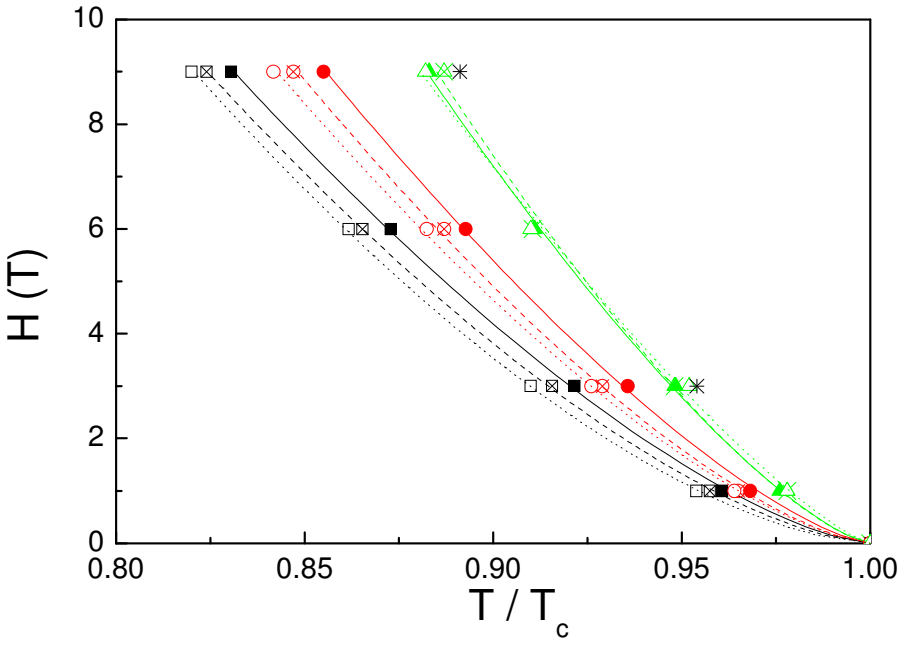

Figure 6.6: Magnetic phase diagram for the samples with 0% wt (empty symbols), 10%wt (crossed symbols) and 20%wt (solid symbols). Shown are T_{irr}^{TB} (○,⊗ and ●) and T_{irr}^{bg} (□, ⊠ and ■), T^* (△,⧋ and ▲) and the limit of influence of microcracks on vortex motion (∗). Solid lines are the fit of the experimental irreversibility line to equation 3.6.

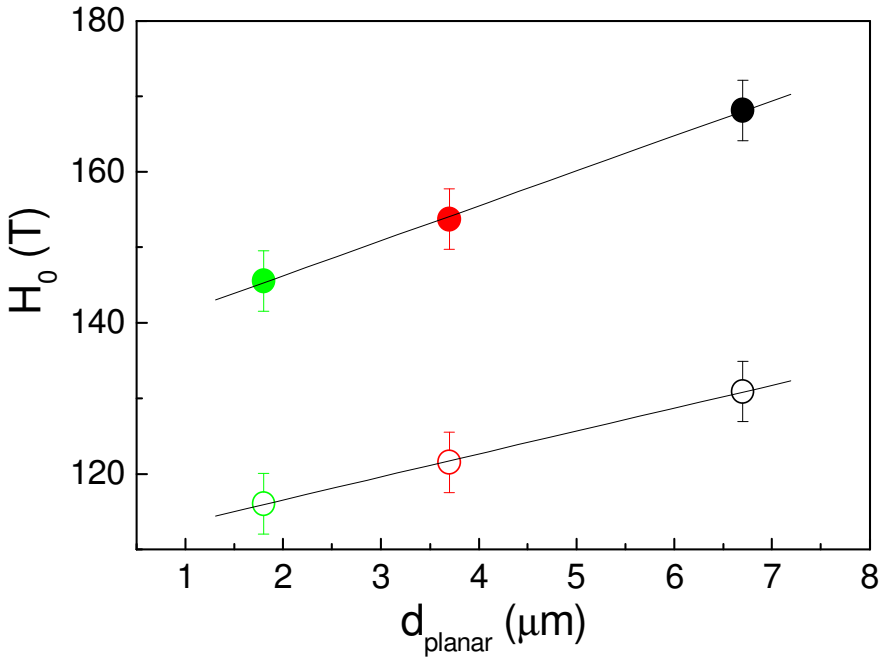

Figure 6.7: Dependence of the fitting parameter H_0^{bg} (open symbols) and H_0^{TB} (solid symbols) with the distance between microcracks.

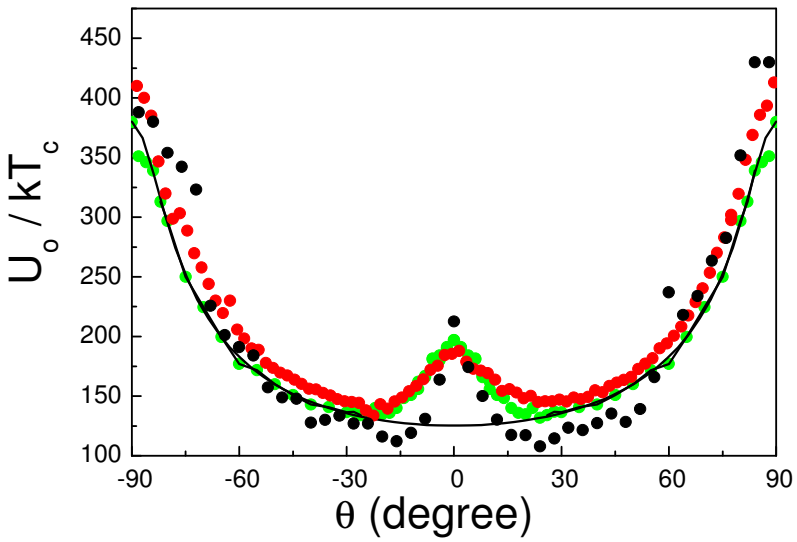

Figure 6.8: Angular dependent vortex activation energy for the sample with different distance between microcracks:1.7μm (●), 3.7 μm (●) and 6.7 μm (●).

Here, it is observed that, in spite of the upwards shift of the irreversibility line when the distance between microcracks is changed, the vortex activation energy is not modified within the experimental resolution. This behavior certainly contrasts with that obtained with Y_2BaCuO_5 particles and twin boundaries where an upwards shift of the irreversibility line is accompanied by an enhancement of the vortex activation energy. This distinct behavior is a direct consequence of the different origin of the modification of the superconducting properties: twin boundaries and Y_2BaCuO_5 particles increase vortex pinning and this promotes the reduction of dissipation, while microcracks are not modifying vortex pinning (the influence of pinning centers is not modified) but promotes by cutting the vortex or deforming the vortex line, depending on the energy cost.

A qualitative picture explaining the obtained results could be the following:

1. microcracks are not able to modify vortex pinning, which is reflected in the independence of either the vortex activation energy in the liquid state and the critical currents in the solid state.

2. microcracks may lead to a system of vortices only partially coupled across microcracks, requiring a lower thermal energy in order to produce thermal fluctuations strong enough to promote the transition from the solid to the liquid vortex state. However, as will be shown in *chapter* 8 by means of flux transformer measurements, full correlation of the vortex system may still be preserved, in spite of the presence of microcracks in the sample.

In order to further study the different behavior we proceed by considering the ratio between the thermal energy and the vortex activation energy at the irreversibility line, i.e., the relative thermal energy that vortex requires to overcome leading to the beginning of the vortex motion:

$$\left.\frac{k_B T}{U(T)}\right|_{T_{irr}} = \frac{k_B T_c}{U_0} \cdot \frac{t_{irr}}{1 - t_{irr}} \tag{6.1}$$

This ratio is represented in figure 6.9 where it is shown that this ratio is larger at a low density of microcracks (8% vs 14%). It is observed that a larger relative thermal energy (almost a factor 2) is then required in order to promote vortex motion by increasing the distance between microcracks from 1.7 to 6.7 μm.

The upwards shift of relative thermal energy required as the density of microcracks is reduced should be associated to a hardening of the vortex solid state. In the present case, however, the influence is not related to vortex pinning. Therefore, it has to be related to the larger distance between microcracks and thus, the larger vortex length to be thermally activated.

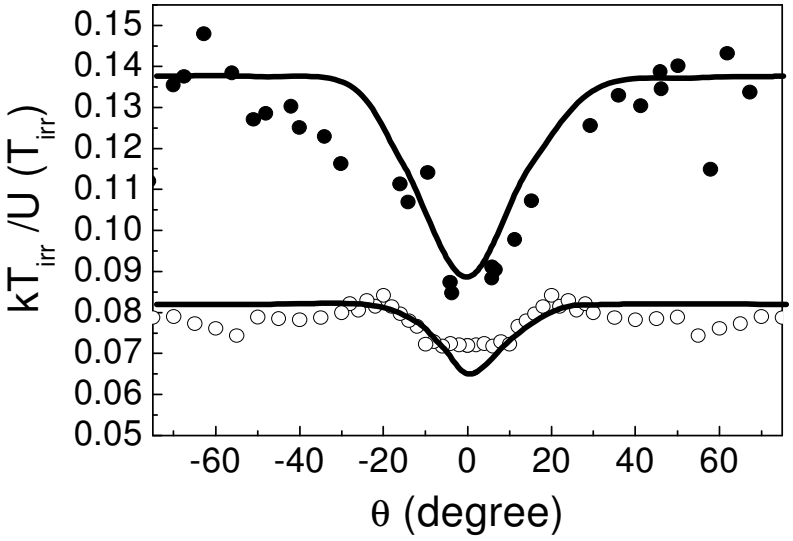

Figure 6.9: Angular dependence of the ratio between the vortex thermal energy and the vortex activation energy at the irreversibility line for the sample with 0% (○) and 20 % wt (●) of silver.

6.3 Influence of stacking faults

The influence of microcracks (having a typical distance of the order of several micrometers) on vortex motion in the liquid phase has been considered in the previous section. However, the study of another planar defect defining a much shorter distance between them is certainly worth of study in order to further analyze the vortex behavior. MTG-$YBa_2Cu_3O_{7-\delta}$ samples provide such a possibility since the increase of the density of stacking faults (down to distances $d \sim 40nm$) is obtained by submitting the sample to a thermal annealing under high pressure of oxygen. A sample thus obtained is studied in this section.

To study the influence of stacking faults, a high pressure of oxygen has been applied over a piece of a sample already studied (see section 3.3). The parameters of the oxygenation (P=1bar, T=600^{o}C and t=24h) were chosen in order to overcome the first stage where the increase in the density of dislocations is dominant over the generation of stacking faults. This treatment has been shown to promote a decrease of the critical currents and a strong downwards shift of the irreversibility line (when determined by magnetic measurements). The distance between stacking faults was estimated to be $d \sim 40nm$, thus leading to a typical distance (d_{planar}) much shorter than that considered when the influence of microcracks is studied.

The angular dependent phase diagram for this sample has been obtained by means of resistive measurements, and it is shown together in figure 6.10 with the phase diagram for a piece of the sample prior to the HOP treatment (see section 3.3). A point that arises when

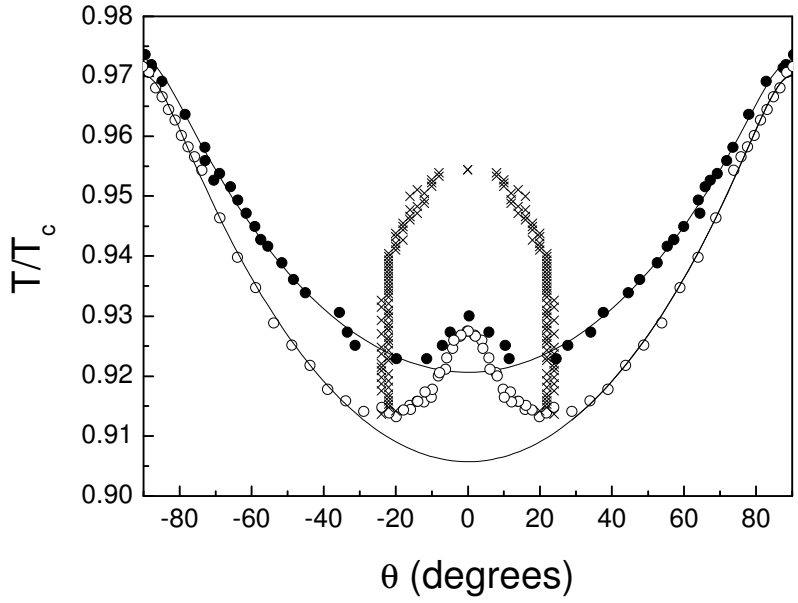

Figure 6.10: Angular dependent irreversibility line (H=3T) for the sample before (•) and after (○) the HOP. Also shown is the region of influence of twin boundaries for the sample after HOP.

comparing the irreversibility line between these two samples is that the irreversibility line is shifted downwards for all the directions of the magnetic field. This behavior is qualitatively similar to that obtained with the presence of microcracks, in spite of the strong differences existing between these two defects.

It has to be noted that, in spite of the strong density of the superconducting phase $YBa_2Cu_4O_8$ present in the sample, the overall sample anisotropy is not found to be modified by it since the angular dependence of the irreversibility line is consistent with $\gamma^{-1} \approx 7$, in agreement with the intrinsic anisotropy of $YBa_2Cu_3O_{7-\delta}$. Certainly, the anisotropy of $YBa_2Cu_4O_8$ ($\gamma^{-1} \sim 14$) is not expected to be found, since at these temperatures $YBa_2Cu_4O_8$ is already in its normal state (T_c =82K). For this reason, the $YBa_2Cu_4O_8$ unit cell inserted will behaves as planar vortex breaking defects. However, the layered structure could led to a modification in the anisotropy. As it appears from the fact that $\gamma^{-1} \sim 7$, the actual distance between stacking faults is not capable of modifying the intrinsic anisotropy of the sample. This behavior is consistent with that observed in $YBa_2Cu_3O_{7-\delta}/PrBa_2Cu_3O_{7-\delta}$ multilayers where angular dependent resistive measurements have shown that the intrinsic anisotropy is preserved even for layers of $YBa_2Cu_3O_{7-\delta}$ consisting of 8 unit cells[109].

These measurements enable also to obtain the angular dependence of the vortex activation energy. As it is observed in figure 6.11, the vortex activation energy is not modified by the presence of these stacking faults, similarly to what was previously observed when considering the influence of microcracks on vortex motion in the vortex liquid state.

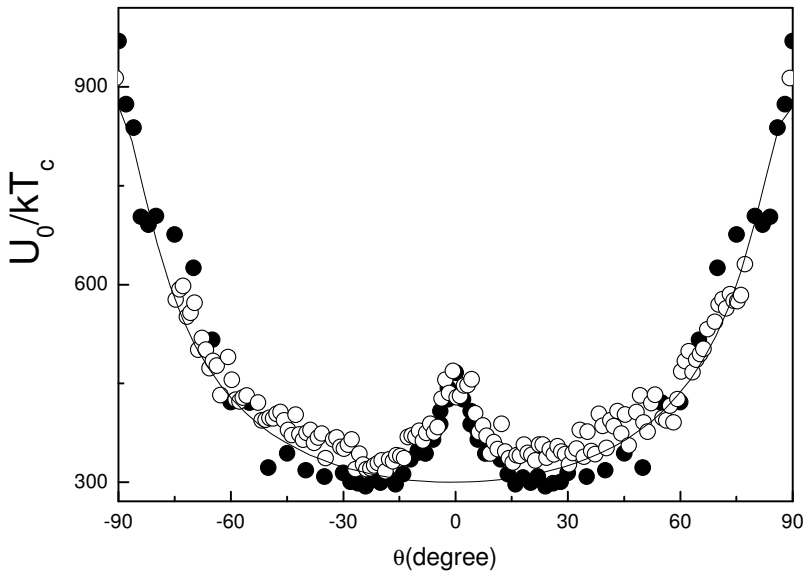

Figure 6.11: Angular dependent vortex activation energy (H=3T) for the sample before (•) and after (○) the HOP.

6.4 Comparison between both planar defects

From a qualitative point of view, a similar influence of microcracks and stacking faults has been reported, on the superconducting properties in the vortex liquid state. Arising from this qualitative agreement, one may wonder whether the behavior is similar also from a quantitative point of view.

In order to compare these defects, we proceed to study the dependence of H_0^{bg} obtained with the distance between planar defects, d_{planar}. It has to be considered, however, that the reference samples in both series of measurements are different:

- We used samples with 18%wt of Y_2BaCuO_5 particles for the samples where the density of microcracks has been strongly modified, and
- A sample with 31%wt of Y_2BaCuO_5 particles when considering the influence of stacking faults.

In order to perform such comparison, the influence of the main microstructural difference between these two samples has to be taken into account. To do so, the results of chapter 4 have been recalled, and the difference in the parameter H_0^{bg} between both reference samples has been subtracted from the sample submitted to HOP. The dependence of H_0^{bg} thus obtained is shown in figure 6.12.

From this figure, it becomes apparent that the values of d_{planar} corresponds to strongly different scales, and therefore, it is difficult to ensure from this figure the existence a common

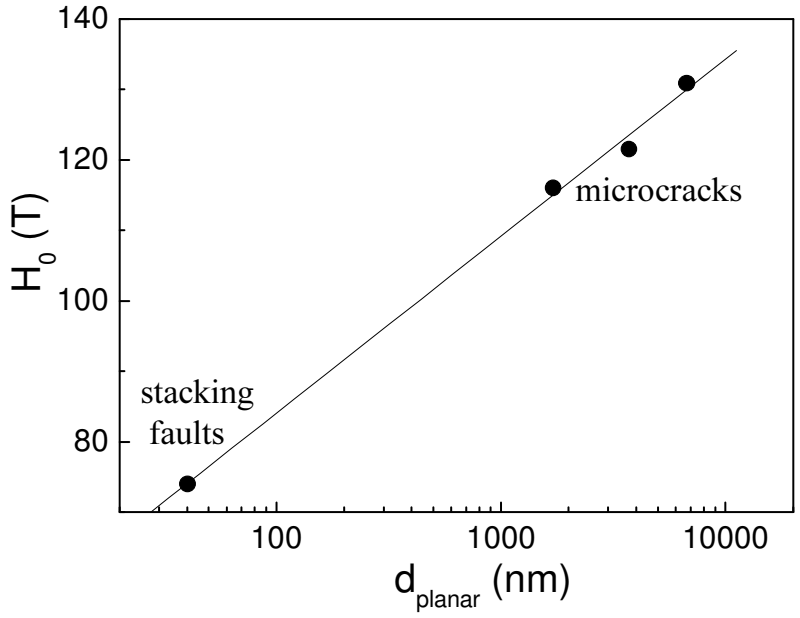

Figure 6.12: Thickness dependence of H_0^{bg} for the samples studied in this chapter.

behavior. However, the existence of a possible relation between the irreversibility line and the distance between the different defects arises as an interesting point worth of further study.

Although the strong influence of the distance between planar defects on the irreversibility line, both defects have demonstrated their lack of influence on the vortex activation energy. As it arise from figures 6.8 and 6.11, the introduction of these planar defects in MTG-$YBa_2Cu_3O_{7-\delta}$ do not modify the vortex activation energy. This lack of influence of the vortex activation energy has to be related to the fact that vortex pinning centers in these samples is not modified.

6.5 Conclusions

In the present chapter, the influence of planar defects such as microcracks and stacking faults, acting as vortex breaking defects has been studied, where they enable to study this influence as the distance between planar defects is reduced over two order of magnitude. Similarly to the previous chapters we have investigated their influence on the angular dependent phase diagram. We have observed that the presence of these defects promotes a downwards shift of the irreversibility line for all the directions of the magnetic field. This contrasts with the upwards shift of the irreversibility line obtained for $YBa_2Cu_3O_{7-\delta}/Y_2BaCuO_5$ interfaces, twin boundaries and dislocations (as linear pinning center). This different behaviour is related to the different geometry of the defects, since stacking faults and dislocations are not able to act as pinning centers. In this angular dependent phase diagram, it is also determined

the region of influence of twin boundaries,θ_{acc} (T), which is not modified. Furthermore, the region of influence of microcracks on vortex motion in the vortex liquid state (determined through the comparison of the temperature dependence of the resistivity for the different samples) has been shown to coincide, for H||c with the limit of influence of twin boundaries (T^*). This coincidence will be further analyzed in chapter 8.

The influence of these microcracks and stacking faults on the vortex activation has also been investigated. It has been observed that they do not modify the vortex activation energy even in samples where the distance between planar defects is reduced down to 40nm. This lack of influence has been attributed to the invariance of the density of pinning centers in these samples.

The downwards shift of the irreversibility line and the not modification of the vortex activation energy, produces that the relative thermal energy required to promote the solid-liquid transition is strongly increased when the distance between microcracks is enhanced. This strong enhancement (almost a factor of 2) has been related to the hardening of the vortex solid due to the reduction of finite size effects on vortex motion.

Chapter 7

Twin Boundaries

7.1 Introduction

The nature of vortices in HTSC and the large thermal energies involved in this system promotes that point-like pinning centers, such as dislocations or oxygen vacancies, have little impact on the superconducting properties at high temperatures. Therefore, in order to strongly modify the phase diagram, the introduction of strong, linear columnar defects, capable of acting over a large vortex length is required. In this sense, the study of vortex dynamics in clean samples with columnar tracks introduced in a controlled way has been shown to be essential in this investigation. The phase diagram of irradiated samples is characterized, as observed in figure 7.1 [110], by a kink in the magnetic field dependence of the irreversibility temperature, separating two different dependencies of the irreversibility line. At low fields, there is a weaker dependence of T_{irr} vs H which sharply increases at the kink, showing the existence of two different regimes: a strongly pinned phase at low fields and a weakly pinned phase at high fields.

The origin of this different behavior is found in the density of vortex pinned: at low fields, the density of columnar defects is larger than that of vortex and therefore, all vortices

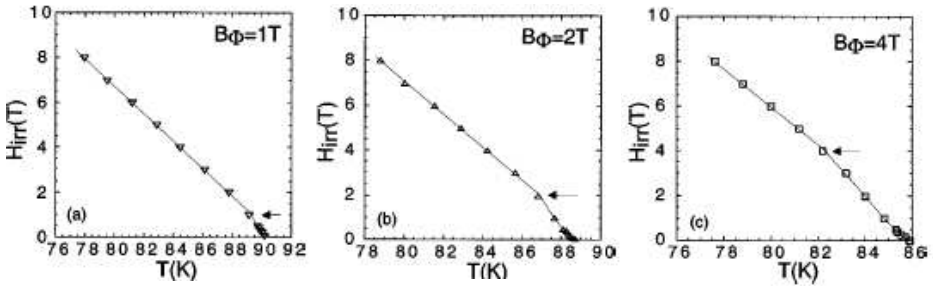

Figure 7.1: Magnetic phase diagram for a sample irradiated with columnar tracks [110].

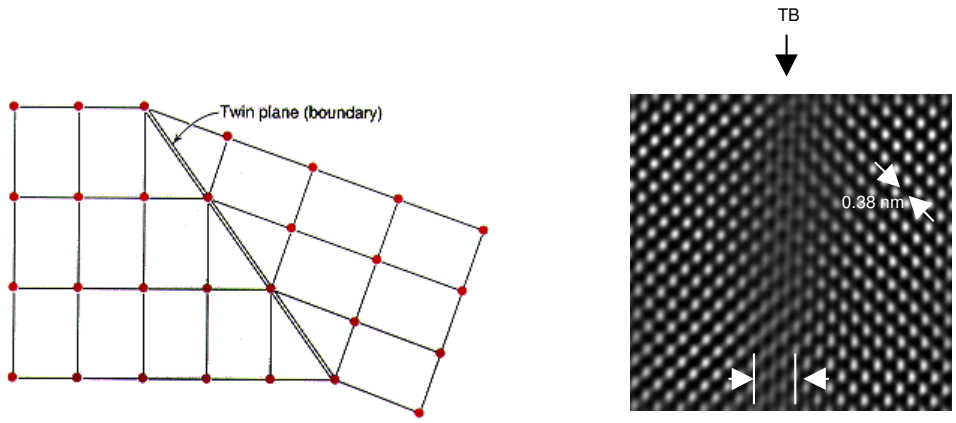

Figure 7.2: a)Atomic structure of a twin boundary. The scheme is not drawn to scale.b)HR-TEM [77].

may be strongly pinned. At magnetic fields larger than the matching field, B_Φ, i.e. for densities of vortices larger than the density of columnar tracks, there exists vortex which are not pinned to the columnar defects which easier dissipate. At magnetic fields much larger than $B_\Phi = \frac{\Phi_0}{\langle d \rangle^2}$, the solid-liquid transition after the irradiation approaches the one obtained prior to irradiation. This behavior, has been shown to be consistent with the nature of the solid-liquid transition in these samples: a Bose-glass transition.

$YBa_2Cu_3O_{7-\delta}$ samples, however, already present an intrinsic and extended defect capable of pinning the vortex over a finite length: twin boundaries. They form two different families of planes orthogonal between them. These twin boundaries are formed due to the similarity between the lengths of *a* and *b* axis which are interchanged (see figure 7.2a) at the tetragonal orthorhombic transition. However, in the structure shown in 7.2a, all the atoms are well located and a local destruction of the superconducting properties should not be expected. This expectations, certainly contrasts with the large number of works studying and demonstrating the influence of twin boundaries over superconducting properties [40, 48, 111, 112]. Furthermore, recent observations of the distribution of vortex by Scanning Tunneling Spectroscopy near the region of twin boundaries suggest that the superconducting properties actually vanishes at twin boundaries[113].

This apparent contradiction is clarified when the atomic positions in the proximities of twin boundaries are found by High Resolution-Transmission Electron Microscopy: a slight displacement of all the atoms along the twin boundary and within a width ~ 10Å is observed, as shown in figure 7.2b [77]. Therefore, in twin boundaries, the dimension of the defect is also similar to the coherence length, thus leading to the strong influence of these defects on vortex motion and pinning as experimentally observed.

Although the influence of twin boundaries has been widely studied and analyzed in single crystals [40, 111, 112], the effect of different densities of twin boundaries, to our knowledge, has not been yet investigated in the vortex liquid state. Certainly, a behavior different from that obtained with columnar defects is to be expected, since twin boundaries may enable to define a matching field as $B_\Phi = \frac{\Phi_0}{d_{TB}^2}$ ($B_\Phi \approx 0.2T$ for $d^{TB} \sim 1000$Å), but the number of vortex pinned at twin boundaries increases with the magnetic field even for $B > B_\Phi$, contrary to the behavior found in columnar tracks, where the number of vortex pinned is not modified at $B > B_\Phi$. Therefore, any existing kink in T_{irr} (H) is expected to be softened. Moreover, if we perform this analysis in MTG-$YBa_2Cu_3O_{7-\delta}$ samples, the existence of other sources of pinning and disorder on the sample should also contribute to soften the behavior across B_Φ.

In this thesis, several MTG-$YBa_2Cu_3O_{7-\delta}$ samples with strong microstructural differences have been measured, and the influence of these defects in the vortex liquid state has been quantified. But the strong differences existing between the microstructure of these samples are also capable to modify the density of twin boundaries, due to the change in the distribution of stresses when modifying, for instance, Y_2BaCuO_5 concentration or adding silver particles. In this chapter, the influence of twin boundaries and their density is explored, both in the phase diagram and in vortex dynamics. This study, has been performed on the samples analyzed in the previous chapters, and required the determination of the twin boundaries spacing for all the samples, which was described in section 2.3.2.

7.2 Phase diagram

Two important manifestations of the presence of twin boundaries arise in the angular dependent phase diagram: the upwards shift of the irreversibility line for magnetic fields (nearly) parallel to the c-axis and the reduction of vortex motion in a region of the angular dependent magnetic phase diagram limited by θ_{acc} (T). These two characteristics are further studied in the following.

7.2.1 Irreversibility line

As observed through the thesis, the presence of twin boundaries parallel to the c-axis produces an upwards shift of the irreversibility line for magnetic fields aligned with this direction. In the previous chapters, the influence of twin boundaries has been extracted by considering not the experimental irreversibility line but the extrapolation of the anisotropic behavior to H$\|$c, thus enabling to quantify the influence of the other microstructural modifications. In the present chapter, the procedure is reversed, since what is extracted is the background in order to obtain the contribution of twin boundaries as the shift between the values of the background and the experimental value.

The validity of the previous analysis was ensured if the angular dependence of the irreversibility line were given by the effective magnetic field. The present analysis, however, also

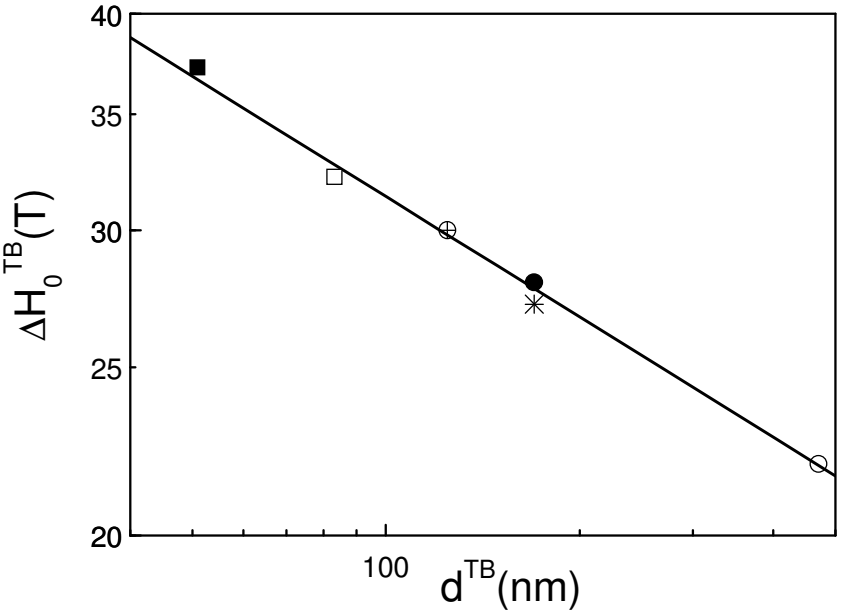

Figure 7.3: Dependence of the enhancement of the irreversibility line with the distance between twin boundaries. The samples considered are (see 2.1, pag 36 for a summary of their microstructural characteristics): 0%Y211 (○), 18%Y211 (⊕), 31% Y211 (●), 10%Ag_2O (□), 20% Ag_2O (■) and HOP(SF) (∗). Solid line is the fit of the experimental data to equation 7.2.

requires the effect to the different defects to be simply additive. Certainly, there exist such an important modification on twin boundaries density that we have to expect that the main contribution will come from this change in the density. Furthermore, any strong deviation from the observed dependence could enable to study the existence of combined effects.

In the course of this thesis, the curves of the irreversibility line (either including or excluding the influence of twin boundaries) for all the samples considered have been adjusted to,

$$H_{irr} = H_0^i \cdot (1-t)^{1.5} \tag{7.1}$$

with i=bg or TB. Therefore, these lines are fully described with the fitting parameter: H_0^i (H_0^{bg} or H_0^{TB}). Consequently, the upwards shift of the irreversibility line may be parameterized with the increase of H_0: $\Delta H_0 = H_0^{TB} - H_0^{bg}$.

In figure 7.3 it is shown the dependence of the ΔH_0^{TB} with the distance between twin boundaries in the samples previously studied. It is clearly observed that the enhancement of the distance between microcracks leads to a strong decrease on the influence of twin boundaries as might have been expect and similar (from the qualitative point of view) with

that obtained for columnar tracks [114]. Furthermore, it is observed the decrease of the ΔH_0^{TB} follows a power law dependence:

$$\Delta H_0^{TB} \propto d_{TB}^{-\sigma}, \tag{7.2}$$

with $\sigma \approx 0.23$, obtaining fairly good agreement with the experimental data. The good agreement between the experimental data and the fit, suggests that the contribution of twin boundaries as a pinning source is simply additive to the background, either when the background pinning is modified (by adding Y_2BaCuO_5 particles) and when vortex motion is promoted by reducing the distance between layers (increasing the density of microcracks or stacking faults).

In order to evaluate the increase in T_{irr} due to the presence of twin boundaries (and compare this result with that obtained theoretically and in irradiated samples), we proceed to relate ΔH_0 with the upwards shift of the irreversibility line (at a particular magnetic field). Using equation 7.1 that describes the irreversibility line, we obtain the shift of the irreversibility line at a fixed magnetic field (H_{irr}):

$$\Delta t \equiv \frac{T_{irr}^{TB}}{T_c} - \frac{T_{irr}^{bg}}{T_c} = H_{irr} \cdot \left[\left(\frac{1}{H_0^{bg}} \right)^{2/3} - \left(\frac{1}{H_0^{TB}} \right)^{2/3} \right], \tag{7.3}$$

and reintroducing equation 7.1 for the background to eliminate H_{irr}:

$$\Delta t = (1 - t^{bg}) \cdot \left[1 - \left(\frac{1}{1 + \frac{\Delta H_0}{H_0^{bg}}} \right)^{2/3} \right]. \tag{7.4}$$

And finally, developing up to first order in $\frac{\Delta H_0}{H_0^{bg}}$ ($\frac{\Delta H_0}{H_0^{bg}} \sim 15 - 25\%$), we obtain:

$$\Delta t \sim \frac{2}{3} \cdot (1 - t^{bg}) \cdot \frac{\Delta H_0}{H_0^{bg}}, \tag{7.5}$$

which shows that the enhancement of the temperature of irreversibility (Δt) linearly increases with ΔH_0 as it is indeed experimentally observed (see figure 7.3). If we combine this expression with the experimental result given by the expression 7.2 we obtain an empirical relationship between the enhancement of the temperature of irreversibility and the distance between twin boundaries:

$$\Delta t \propto \frac{(1 - t^{bg})}{H_0^{bg}} \cdot d_{TB}^{-0.23} \tag{7.6}$$

where the validity of this expression, is shown in figure 7.4.Up to our knowledge, there is any theoretical expression relating the upwards shift of the irreversibility line with the density of

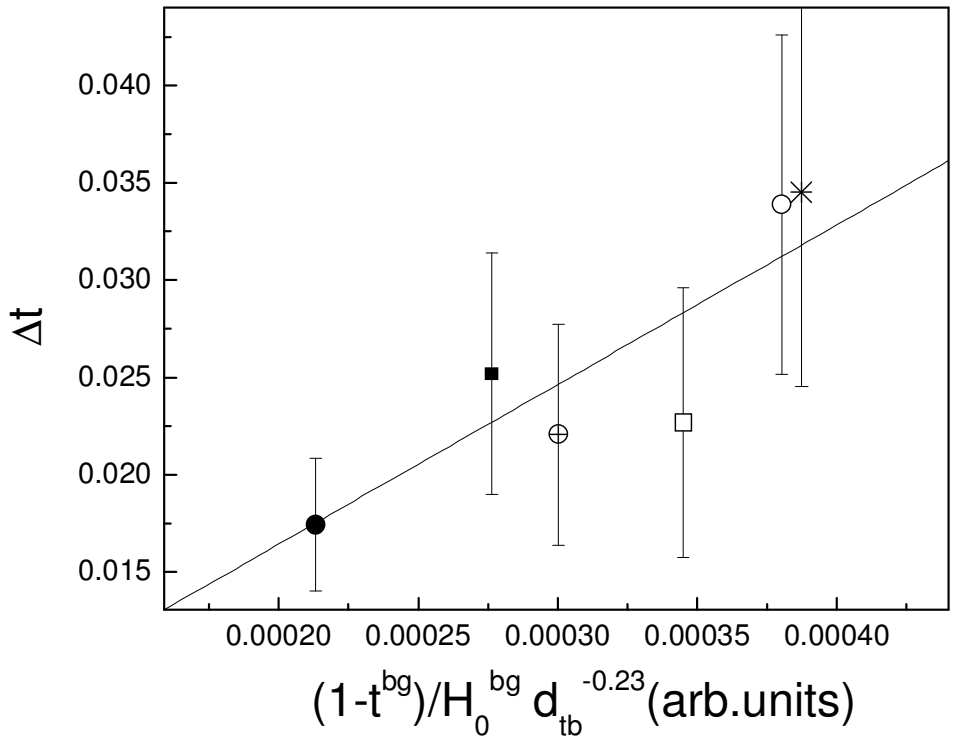

Figure 7.4: Dependence of the shift Δt with $\frac{1-t^{bg}}{H_0^{bg}} \cdot d_{TB}^{-0.23}$for the different samples: 0%Y211 (○), 18%Y211 (⊕), 31% Y211 (●), 10%Ag_2O (□), 20% Ag_2O (■) and HOP(SF) (∗).

twin boundaries. However, in the framework of the Bose-glass theory as applied to columnar defects, it has been shown [17] that:

$$\Delta t = \frac{T_{BG} - T_m}{T_c} = \frac{T_m}{T_c} \cdot \frac{a_0}{d} \cdot \left(\frac{T^*}{T_m} \right)^2, \tag{7.7}$$

with T_m the melting temperature, T_{BG} the Bose-glass temperature, a_0 the distance between vortices, d the distance between columnar defects and T^* a characteristic temperature of the system related to the strength of vortex pinning at the particular pinning center considered. Certainly, twin boundaries, due to their higher dimensionality, should have a different behavior than columnar defects. However, the upwards shift of the irreversibility line when increasing the density of twin boundaries is consistent with the initial upwards shift of the irreversibility line with the dose in ion irradiated samples.

From a quantitative point of view, however, the results are strongly different. The dependence is less pronounced when considering twin boundaries, since the enhancement of the irreversibility temperature is linear with the inverse of the distance between defects, in contrast with the power law dependence obtained for twin boundaries. This smoother dependence of the shift of the irreversibility line with the density of twin boundaries should be related to the different dimensionality of the defects.

7.2.2 Region of influence of twin boundaries in the vortex liquid state

The second feature observed in the angular dependent phase diagram is the presence of a certain region where a noticeable influence of twin boundaries on reducing vortex motion is observed. This region, defined by the accommodation angle θ_{acc} (T), has been already determined for the samples studied through this thesis. Here, the results obtained will be recovered in order to study the origin of the boundary of this region, and check whether its behavior is determined by the density of twin boundaries or not.

In figure 7.5, the temperature dependence of two different samples is shown, for all the applied magnetic fields. The same qualitative behavior is observed in this figure for both samples, and it has been observed for all the studied samples:

- For a fixed magnetic field, there is a monotonic decrease of the accommodation angle as the temperature is increased. This accommodation angle ends up at a certain temperature, which increases as the magnetic field is decreased.

- As the magnetic field is increased, the accommodation angle reduces.

The existence of a certain influence of twin boundaries even for fields not directly aligned with them, as it has already been shown in figure 7.5, has been attributed to the existence of a finite vortex elasticity that enables the vortex to distort itself in order to enable the alignment, over a finite length of the vortex on twin boundaries, therefore leading to a reduction of the

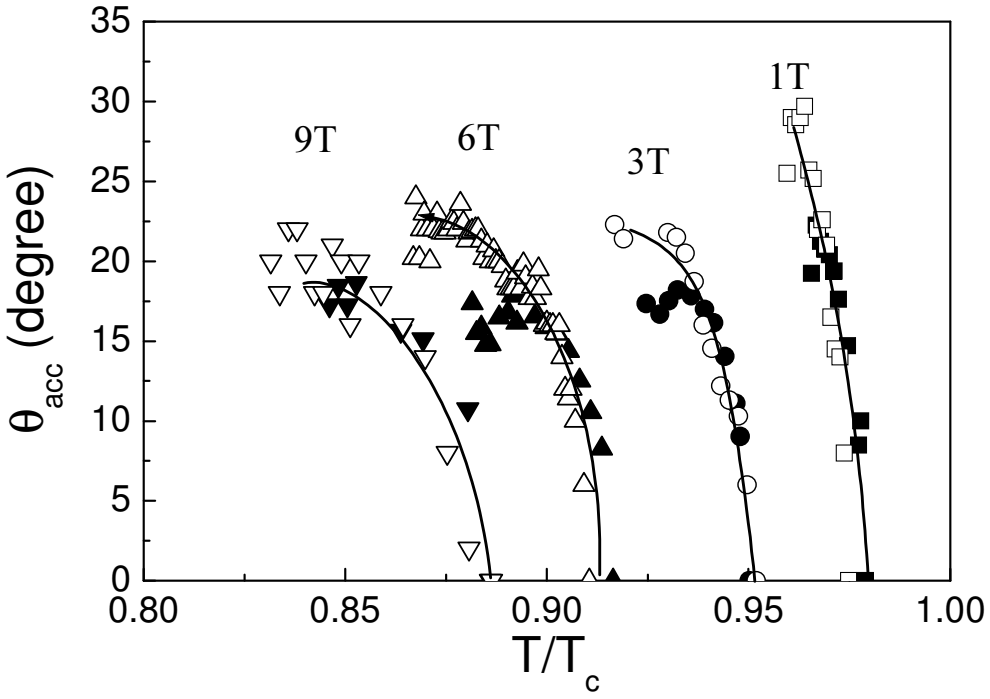

Figure 7.5: Temperature dependence of the accommodation angle for the sample with 31% of Y_2BaCuO_5 (solid symbols) and the sample with 18% of Y_2BaCuO_5 particles (open symbols).

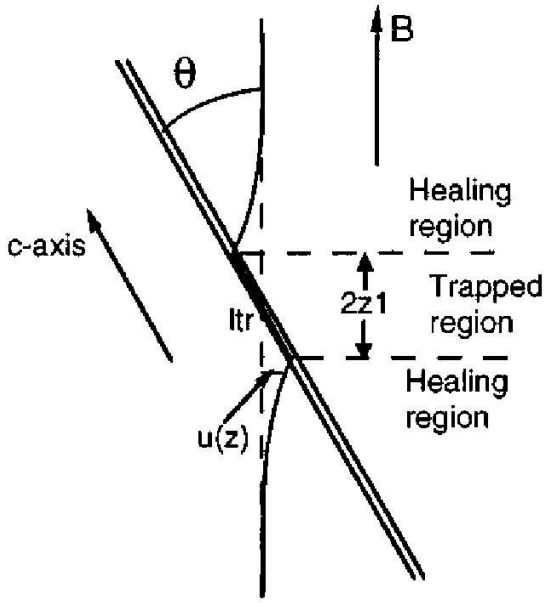

Figure 7.6: Scheme of the vortex[94].

total vortex energy for this configuration, and therefore, to a reduction of vortex motion. A simple scheme of the vortex distortion, for fields not aligned with twin boundaries is observed in figure 7.6. Within this model, the boundary of this region occurs when the vortex pinning energy of the trapped region is compensated by the increase of the elastic energy of the healed region. Thus, it has been obtained[94]:

$$E = \int \left[\underbrace{\frac{\varepsilon_1}{2}\left(\frac{du}{dz}\right)^2} + \underbrace{K/2 \cdot u^2} \right] dz - \underbrace{U_p \cdot l_{tr}} + \underbrace{2\int dz \cdot K\,(z_1\theta)^2\, exp(-2k_0 z)} \tag{7.8}$$

where $\varepsilon_1 = \frac{\Phi_0^2}{(4\pi\lambda_c)^2} \cdot \ln(\frac{a_0}{\xi})$ is the vortex line tension, $a_0 \approx 1.07\sqrt{\frac{\Phi_0}{B}}$ is the distance between vortices, K accounts for the vortex-vortex interaction, U_p is the vortex pinning energy per unit length and $k_0 = \sqrt{\frac{K}{\varepsilon_1}}$. In this equation, the first term gives the cost of energy of deforming the vortex in the healing region, the second terms accounts for the vortex-vortex repulsion and the third term gives the energy gain of pinning the vortex on the twin boundary. Finally, the fourth term gives the cost of deformation of the vortex outside the healing region. Thus E, gives the overall cost of deforming the vortex to pin it to twin boundaries for an arbitrary direction of the magnetic field.

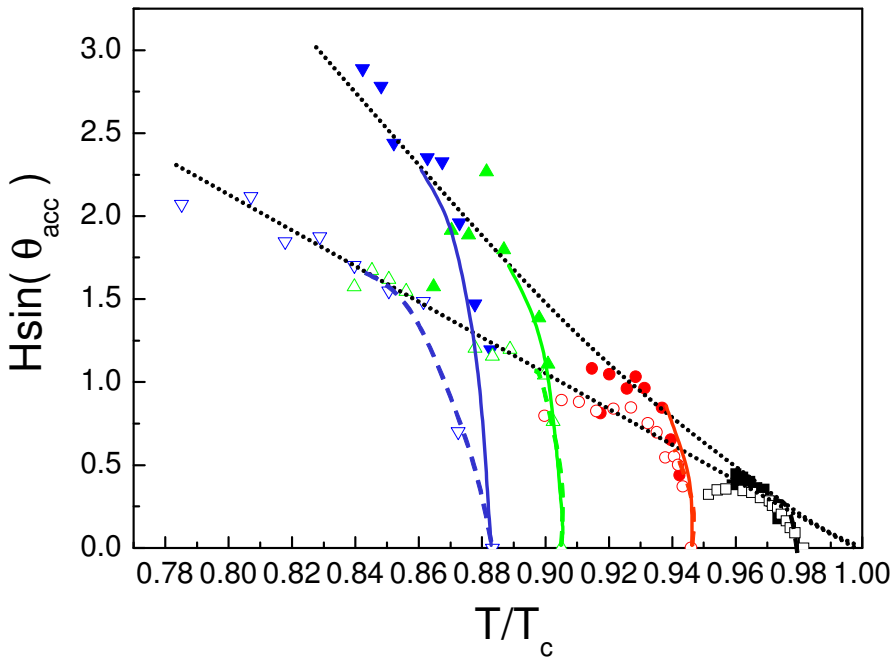

Figure 7.7: Temperature dependence of $H \cdot \sin\theta_{acc}$ for the sample with an initial content of $ZrBaO_3$ (open symbols) and the sample with 20% of silver (solid symbols).

Developing this equation, it has been obtained:

$$U_p' = \varepsilon_0 \left(\frac{2k_B T tan\theta_{acc}}{\varepsilon_0 a_0} \right)^{2/3}, \tag{7.9}$$

This expression, therefore, relates the accommodation angle with the vortex pinning energy per unit length at twin boundaries, U_p.

On the other hand, it has been suggested that columnar defects have a region of influence characterized by $H \cdot \sin\theta_{acc}(T)$, which gives the maximum torque that vortices may resist before being depinned. In figure 7.7, it is observed that, for twin boundary pinning, the data for different magnetic fields follow the same dependence at low temperature (slightly above the irreversibility line), i.e. a smooth, linear decay, extrapolating to zero at a temperature close to the T_c. This tendency, however, is modified as the temperature approaches T* (H) (the temperature at which θ_{acc} (T)=0) where a sudden drop to zero of the accommodation angle is observed.

These two different behaviors suggest that different phenomena are dominating at both regimes. This suggestion, is further reinforced when this behavior is analyzed for the different samples studied in this work, since:

- the low temperature regime, (having a weak temperature dependence), is found to be strongly dependent on the particular sample studied. The parameter $H \sin\theta_{acc}$ is the

highest for the sample having the largest density of twin boundaries, and the smallest for the sample with the lowest density of twin boundaries. Thus, it suggests that the actual value of $\sin\theta_{acc}$ depends on the density of defects, contrary to that expected from equation 7.9. In the derivation of this equation, the influence of the density of columnar defects is not considered, and thus, the existence of interstitial vortices at large magnetic fields was neither introduced. Although the rest of samples seem to follow the same tendency (i.e. $H\sin\theta_{acc}$ increasing with the density of twin boundaries), the experimental error ascribed to the determination of $\sin\theta_{acc}$ disables to fully conclude in this sense.

- In spite of the strong sample dependence with ΔH_0 and θ_{acc} (T), being the former directly related to the density of twin boundaries, the temperature $T^*(H)$ where twin boundaries are not longer effective for H$\|$c, has been found to be sample independent. Two main possibilities arise to explain this independence. Firstly, it is possible that the vortex pinning energy at twin boundaries vanishes at T^*. Secondly, it is also possible a complete lost of the line tension[115], strongly modifying the structure of the phase diagram, since at temperatures $T > T^*$ vortex could not be considered as a line. The existence of a transition or crossover in the vortex liquid state where vortex losses their line tension has been already argued from the theoretical point of view [115, 116] and from numerical simulations [117] and would easily explain the coincidence of the limit of influence of twin boundaries for all the studied $YBa_2Cu_3O_{7-\delta}$ samples. Such a possibility will be further discussed and analyzed in chapter 8, where different results obtained through the theses will be compared.

7.3 Vortex dynamics

Vortex dynamics has been explored through the investigation of the ratio between the thermal energy required to overcome these the pinning barriers (kT) and the vortex activation energy (U(T)) and therefore, produce the solid-liquid transition. This value has been seen to be independent of the intensity of the magnetic field and its direction. However, a dip is observed for directions of the magnetic fields where the influence of twin boundaries is present.

The rest of microstructural defects have also been seen to have a certain experimental influence over this value: microcracks and stacking faults, while reducing the length of vortices, contribute to reduce this value. On the other hand, the introduction of a certain density of Y_2BaCuO_5 particles as strong pinning centers lead to an enhancement of this value. This behavior of $\frac{kT_{irr}}{U(T_{irr})}$ has been qualitatively explained by relating this value to the influence of the defects on vortex *entanglement*: shortening vortex length promotes a reduction of vortex wandering, and therefore, a decrease of vortex entanglement. The introduction of Y_2BaCuO_5 particles promotes an important distortion of vortices from the expected *straight* behavior, which may end up in an enhancement of vortex wandering and entanglement.

The observed modification on the ratio $\frac{kT_{irr}}{U(T_{irr})}$ for directions of the magnetic field where the influence of twin boundaries is present, could be also accounted to the degree of vortex entanglement. Twin boundaries are straight, linearly correlated pinning centers. The first influence of twin boundaries is to promote an enhancement of vortex pinning as already observed in the last section, with an upward shift of the irreversibility line, which is also dependent on the density of pinning centers. But these defects, being straight pinning centers, certainly promote a reduction of vortex wandering [17]. If this enhanced vortex localization is also present in the solid-liquid transition, it should promote a reduction of vortex entanglement, and therefore, to the observed dip in the ratio between the vortex pinning energy and the thermal energy.

Another item that has been considered while studying vortex dynamics is the vortex activation energy. It has been shown that it slightly increases for magnetic fields parallels to twin boundaries. Therefore, it seems worth of study the vortex activation energy related to twin boundaries. To do so, the contribution of the rest of the microstructural defects has to be eliminated. This can be done by assuming a two fluid model like, where each pinning center contributes to a vortex viscosity and the resulting vortex viscosity is the addition of all the individual defects viscosities:

$$\eta = 1/\rho = \eta_{bg} + \eta_{TB} = 1/\rho_{bg} + 1/\rho_{TB}, \tag{7.10}$$

where η_{bg} is the viscosity ascribed to non-aligned defects and η_{TB} is the viscosity related to twin boundaries. By considering that vortices may be thermally activated from all different effects we obtain:

$$\frac{1}{\rho_0^{exp} e^{-\frac{U^{exp}(T)}{kT}}} = \frac{1}{\rho_0^{bg} e^{-\frac{U^{bg}(T)}{kT}}} + \frac{1}{\rho_0^{TB} e^{-\frac{U^{TB}(T)}{kT}}} \tag{7.11}$$

Assuming a linear dependence of the vortex activation energy with the temperature ($U^i(T) = U_0^i \cdot (1 - T/T_c)$), and developing, we finally obtain that:

$$U^{TB} = -Tln(\rho_0^{exp} \cdot \rho_0^{bg}/\rho_0^{TB}) + (U_0^{exp} \cdot (1 - T/T_c) + U_0^{bg} \cdot (1 - T/T_c)) + Tln(\rho^{bg} - \rho^{exp}), \tag{7.12}$$

from where the vortex activation energy may be extracted. Although this expression is rather complicated, it has been shown [118] that, slightly above the irreversibility line, the first and the third term of the equations are similar and of opposite sign. Therefore, with a good correctness (7% of error), it is obtained that:

$$U^{TB}(T) \approx U^{exp}(T) + U_0^{bg}(T), \tag{7.13}$$

which gives an easy relation between the vortex activation energy at twin boundaries and the vortex activation energy due to the background and the overall vortex activation energy. Using this equation, we may compute the vortex activation energy at twin boundaries for all

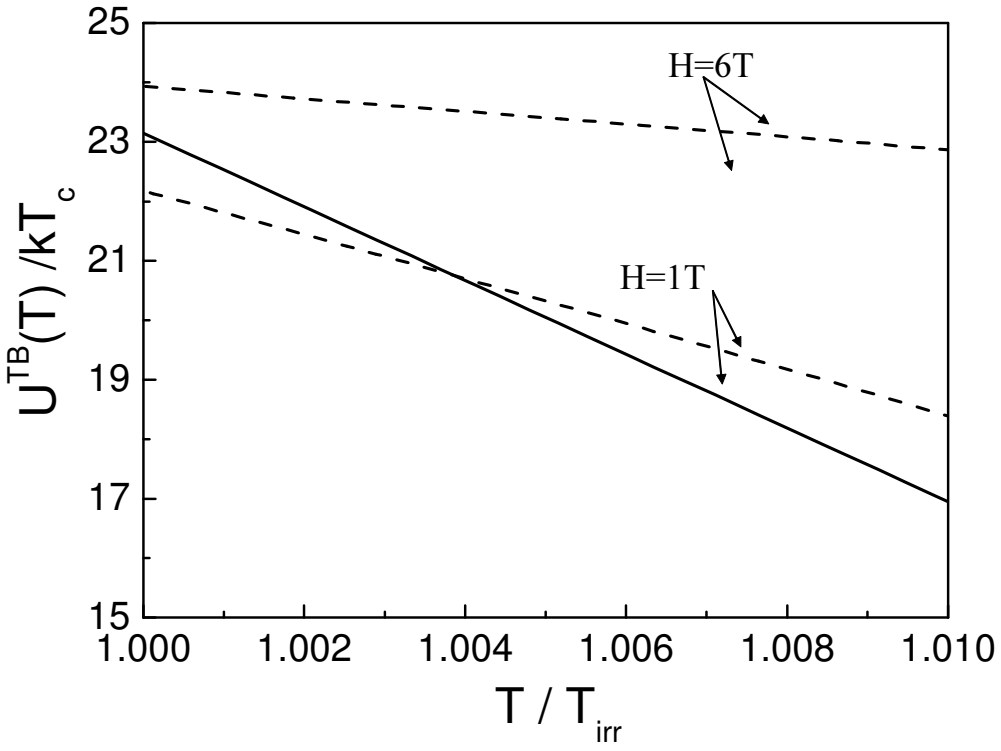

Figure 7.8: Vortex activation energy related to twin boundaries as obtained from equation 7.12 (dashed lines) and 7.13 (continuous line).

the samples considered in this work for a particular magnetic field. In figure 7.8 is shown for comparison the temperature dependence of the vortex activation energy related to twin boundaries obtained from equations 7.12 and 7.13.

In particular, in figure 7.9 it is shown the dependence of the vortex activation energy at twin boundaries on the twin boundary separation in samples with different content of Y_2BaCuO_5. Although the contribution of the rest of the microstructural defects to the vortex pinning energy has been extracted, it is clearly observed in figure 7.9 that U_0^{TB} is not determined by the distance between twin boundaries, but strongly modified by the content of Y_2BaCuO_5 particles. This fact may be understood when it is considered that this quantity is not the vortex pinning energy at twin boundaries, but the energetic cost of depinning the vortex from twin boundaries in a system where other strong pinning centers such as Y_2BaCuO_5 particles exist. As the content of Y_2BaCuO_5 particles is enhanced, vortex pinning is strongly increases, and thus, the energetic cost of depinning vortices from twin boundaries is also increased. The observed behavior reflects, therefore, the complexity of vortex dynamics in the liquid phase in samples with coexistance of strong pinning centers.

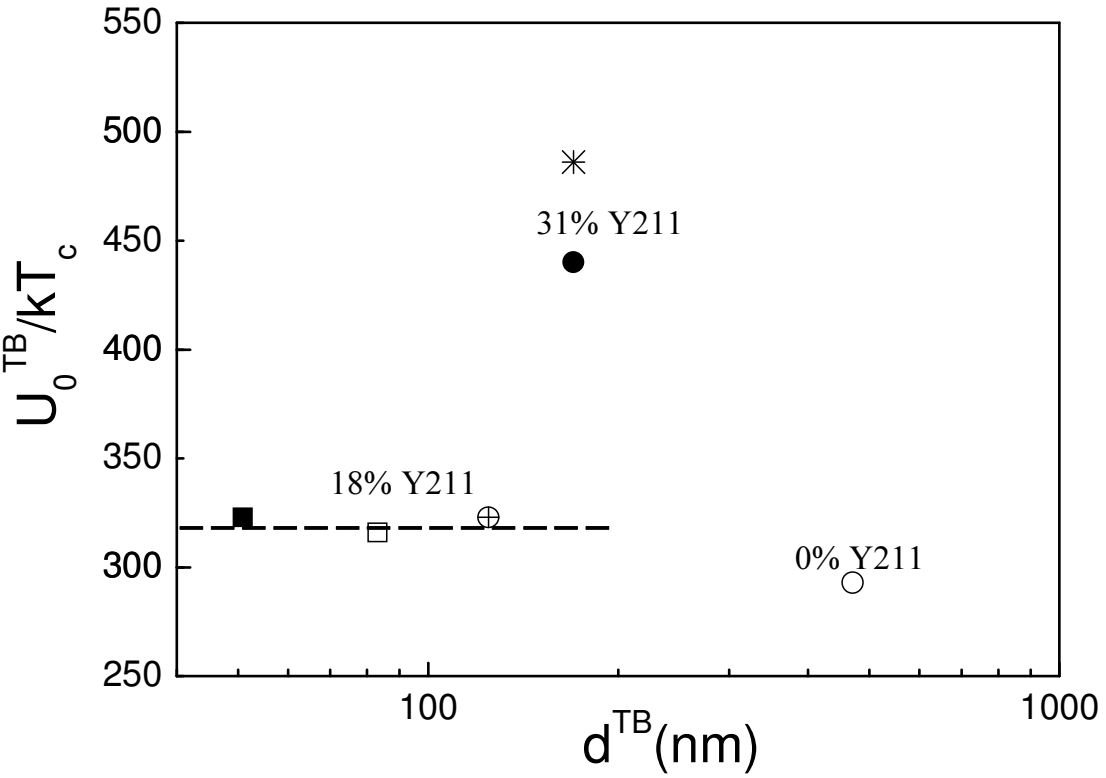

Figure 7.9: Dependence of the vortex activation energy related to twin boundaries (U_0^{TB}) at H=3T with the distance between twin boundaries for the samples: 0%Y211 (○), 18%Y211 (⊕), 31% Y211 (●), 10%Ag_2O (□), 20% Ag_2O (■) and HOP(SF) (∗).

7.4 Conclusions

In this chapter, the influence of twin boundaries in the vortex liquid state has been analyzed. We have shown in the previous chapters that twin boundaries promote a reduction of vortex motion for $\theta < \theta_{acc}(T)$, and thus, leads to an upwards shift of the irreversibility line for H||c. In the present chapter, the upwards shift of the irreversibility line related to twin boundaries has been determined for all the samples studied. We have shown that the upwards shift of the irreversibility line follow a power law dependence on the density of twin boundaries. On the other hand, the temperature dependence of the region of the vortex liquid state influenced by twin boundaries has also been investigated. We have found that the temperature at which θ_{acc}(T)=0 (i.e, the influence of twin boundaries for H||c vanishes), T^*, is similar, within the experimental error for all the samples studied, while the value of θ_{acc} (T) is strongly sample dependent and seems to be related, also, to the density of twin boundaries.

The influence of twin boundaries on the vortex activation energy has also been studied. It has been shown that the vortex activation energy increases for H||c, consistently with an enhancement of vortex pinning at twin boundaries. The angular behaviour of the vortex activation energy has enabled to deconvolute the vortex activation energy related to twin boundaries from that related to the background. It has been observed, that the vortex activation energy related to twin boundaries is, actually, determined by the particular content of Y_2BaCuO_5 particles.

Finally, we have observed that twin boundaries leads to a dip in the ratio between the thermal energy and the vortex activation energy for H||c at the irreversibility line. This behavior contrasts to that observed for $YBa_2Cu_3O_{7-\delta}/Y_2BaCuO_5$ interface that, acting also as strong pinning centers lead to an upwards shift of this ratio, thus hardening the vortex solid state. For $YBa_2Cu_3O_{7-\delta}/Y_2BaCuO_5$ interfaces, we suggested that the observed behavior is related to an enhanced vortex wandering and increasing vortex entanglement. In the present case, twin boundaries are linearly aligned correlated pinning centers and thus, a reduction of vortex entanglement is to be expected. This decrease of vortex entanglement, should, therefore, produce the observed reduction of the relative thermal energy required in order to promote the solid-liquid transition.

Chapter 8

Vortex liquid phase diagram

8.1 Introduction

Up to now, the influence of the different microstructural defects present on MTG-$YBa_2Cu_3O_{7-\delta}$ samples on vortex motion has been studied. Their action on the vortex liquid has been thoroughly analyzed as a function of the applied magnetic field, its direction and temperature. In this sense, we have studied the influence of Y_2BaCuO_5 particles, twin boundaries, dislocations (either acting as point-like or line-like pinning centers), microcracks and stacking faults.

The defects present in MTG-$YBa_2Cu_3O_{7-\delta}$ samples have demonstrated to have strongly different consequences on the angular dependent phase diagram, depending on their geometry and structural characteristics of the particular defects. Comparison between the different features of the phase diagram reveals two important points:

- The irreversibility line is determined by the action of the existing defects. However, in spite of the observed strong influence of the microstructure, the same angular dependence has been obtained for all the samples when the magnetic field is rotated from H$\|$c to H$\|$ab. This angular dependence is characterized by an angular dependent background irreversibility temperature (where the influence of aligned defects has been extracted), $T_{irr}^{bg}(\theta)$. This angular dependent irreversibility line follows the intrinsic anisotropy of a three dimensional system.

- The limit of effectiveness of the considered defects in the angular dependent phase diagram has also been determined by comparing the temperature dependence of the resistivity for different directions, in samples with different microstructure.

  In particular, it has been observed that the onset of influence of twin boundaries, T*(θ), and that of microcracks coincide for H$\|$c. The coincidence of these temperatures, may suggest the possibility of a common origin.

The present chapter pretends to study up to which extension the above considered common features observed in $YBa_2Cu_3O_{7-\delta}$ hold. Namely the scaling of the magnetic field with the effective magnetic field will be analyzed and a possible transition/crossover in the vortex liquid that could be responsible for the coincidence in the limit of influence of defects acting differently over vortices will be considered.

The first feature has been analyzed by comparing the results obtained (on the same sample) in the two different geometries employed through the thesis: the magnetic field applied within the ab-plane and from the c-axis to the ab-plane in order to check whether a relation exist. On the other hand, a crossover/transition in the liquid has been tested by performing flux transformer experiments on one of the samples already studied, allowing us to determine if full vortex correlation exists. All these results will be contrasted with the experimental data found in the literature for $YBa_2Cu_3O_{7-\delta}$ and other layered cuprates.

8.2 Scaling of the measurements

In this section, the results that we have previously obtained for one sample in two different geometries (with I‖ab and H‖c (see section 3.3) and for I‖c and H‖ab (studied in section 5.3)) are used in order to check whether the phase diagram is similar in both geometries from a qualitative point of view. Thus, comparison between the obtained phase diagrams in the different geometries has been performed.

In figure 8.1, the phase diagram in both geometries is shown. It appears clearly that the same regions are found for H‖ab and H‖c, thus demonstrating the 3-D character of $YBa_2Cu_3O_{7-\delta}$. However, and following the anisotropic character of these samples, all the curves corresponding to H‖ab are situated at much higher temperatures than their equivalent for H‖c. This difference on the position of the transitions, may be analyzed quantitatively by considering the magnetic field dependence of the several different irreversibility lines appearing in this figure. As it has been shown previously, the irreversibility line follows the dependency given by:

$$H_{irr} = H_0^i \left(1 - \frac{T}{T_c}\right)^{1.5}, \tag{8.1}$$

and, therefore, the values obtained for H_0^i serve as a parameter to quantify the different influence of an c-axis or a within-plane magnetic field. The obtained values have been $H_0^{bg} = 1020T$ and $H_0^{TB} = 1153T$ for in plane magnetic fields and $H_0^{bg} = 138.2T$ and $H_0^{bg} = 165.8T$ for H‖c.We have shown through the thesis that the magnetic field the physical magnitudes scale when the effective magnetic field ($\varepsilon_\theta \cdot H = \sqrt{\gamma^2 \cdot \sin^2(\theta) + \cos^2(\theta)} \cdot$ H) is considered, which includes the anisotropy of the sample. Following this scaling for magnetic

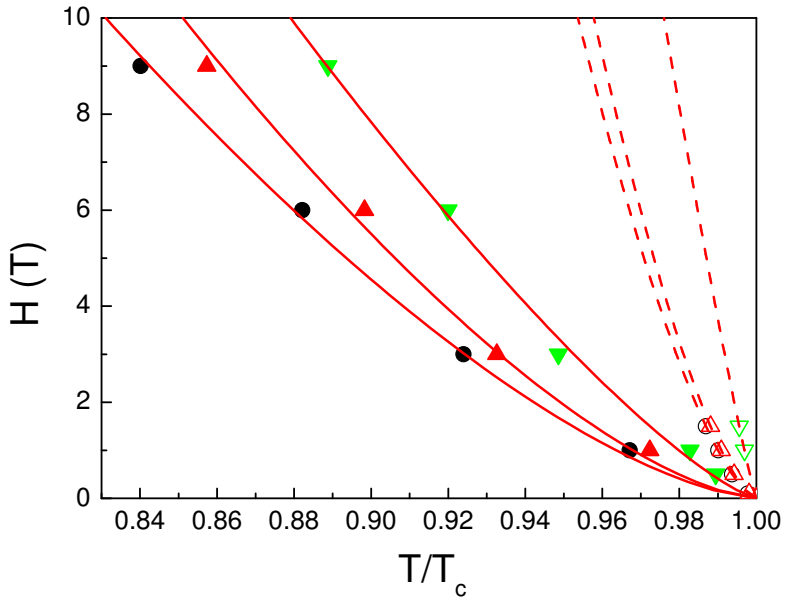

Figure 8.1: Magnetic phase diagram for H‖c (solid symbols, continuous lines) and H‖ab (open symbols, dashed lines). Shown are T_{irr}^{bg} (○, ●), T_{irr}^{TB} (▲,△) and T^* (▼,▽).

fields applied parallel to the ab-plane and the c-axis, one should obtain:

$$\frac{H_{irr}^{i,ab}}{H_{irr}^{i,c}} = \frac{\varepsilon_{90}}{\varepsilon_0} \approx \gamma^{-1}, \tag{8.2}$$

and from the experimental values we obtain $\frac{H_0^{TB,c}}{H_0^{TB,ab}} \approx 7$ and $\frac{H_0^{bg,c}}{H_0^{bg,ab}} \approx 7.3$, in close agreement with the value $\gamma^{-1} \approx 7$ that has been obtained from the angular dependent irreversibility lines for the different samples studied in the previous chapters.

Together with the scaling of in-plane and out-of-plane measurements when the effective magnetic field is considered, these in-plane measurements also allow to compare the influence of twin boundaries for H‖c and H‖ab. To do so, several factors have to be considered:

1. For H‖ab‖ [110], the family of twin boundaries parallel to $[1\bar{1}0]$ is not enhancing vortex pinning, while for H‖c all twin boundaries may act as linear-like pinning center.

   Therefore, we may consider, assuming an equal distribution of both families of twin boundaries, that the effective density of twin boundaries has been halved for in-plane magnetic fields: $d_{eff}^{TB,ab} = 1/2 \cdot d_{eff}^{TB,c}$.

2. In plane magnetic fields produce a stretched triangular vortex lattice, since vortex-vortex interaction between vortex laying in the same ab-plane or in different layers are

strongly different. This distortion produces a higher number of vortices in the c-axis direction, and therefore an enhanced effective density of vortices at twin boundaries. The distortion of the cell parameters of the vortex lattice for in-plane magnetic fields has been shown to be given by $\sqrt{\gamma}$ [119], and gives a vortex density at twin boundaries enhanced by a factor $\sqrt{\gamma^{-1}} \approx 2.65$.

Therefore, this stretching leads to an effective density of twin boundaries $d_{eff}^{TB,ab} = d_{eff}^{TB,c} \cdot \sqrt{\gamma^{-1}}$.

3. Apart from these geometric considerations that may modify the apparent density of twin boundaries, a third effect appears: i.e. the distortion of the core of the vortices themselves. The vortices lying in the ab-plane have the coherence length along the c-axis reduced by a factor γ^{-1}, i.e. in the direction parallel to twin boundaries($\xi_c = {}^{1}\!/\!_{\gamma^{-1}} \cdot \xi_{ab}$). This effect reduces the 'volume' of vortex that may be pinned.

If we take into account the three factors mentioned above (represented in figure 8.2), we obtain that the pinned volume (v_{pin}) at twin boundaries for H$\|$ab is related to that for H$\|$c in the following way:

$$v_{pin}^{ab} = \underbrace{{}^{1}\!/\!_{2}}_{1} \cdot \underbrace{\sqrt{\gamma^{-1}}}_{2} \cdot \underbrace{{}^{1}\!/\!_{\gamma^{-1}}}_{3} \cdot v_{pin}^{c} = \frac{1}{2\sqrt{\gamma^{-1}}} \cdot v_{pin}^{c} \tag{8.3}$$

Therefore, the pinning 'volume' is found to be smaller by a factor ~ 5 for the same sample when the magnetic field is parallel to the ab-plane than that for H$\|$c. Thus, it should lead to a much lower influence corresponding to a density of twin boundaries 5 times smaller. In figure 8.3, the effective enhancement of H_0 due to twin boundaries is represented as a function of the effective density of twin boundaries. There, it is observed that the value obtained from measurements within the ab-plane (once the effects, and the effective magnetic field have been taken into account) follows the same curve than the samples measured with out-of-plane magnetic fields:

$$\Delta H_0^{eff} \propto d_{TB}^{-0.23}, \tag{8.4}$$

consistently with the arguments exposed above.

Although the influence of twin boundaries for H$\|$ab is found to be lower than that of H$\|$c, the obtained irreversibility line scales with a good approximation with the anisotropic factor, and therefore, in order to analyze if the same physical mechanisms are responsible for the behavior observed when H$\|$c and H$\|$ab, we proceed to represent the phase diagram considering the effective magnetic field, as shown in figure 8.4. In this figure, it appears clearly that the different phases existing for H$\|$c appear also for H$\|$ab, as it has been already shown in figure 8.1. However, further information is obtained when considering the effective magnetic field, since it is observed that the different transitions obtained collapse with that of

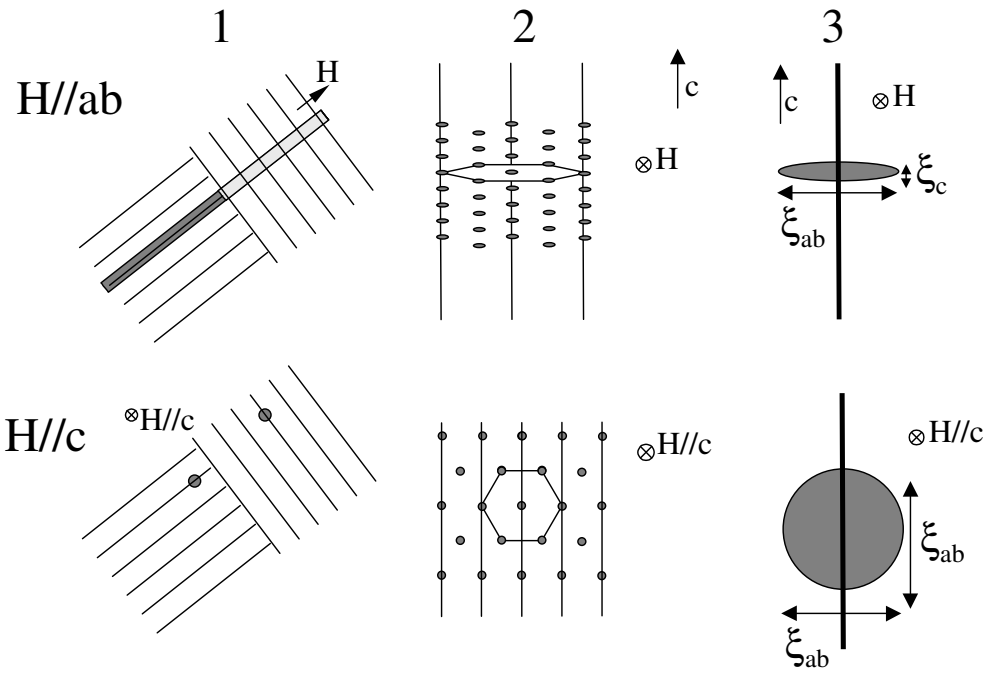

Figure 8.2: Scheme of the different influences of twin boundaries on vortex pinning for magnetic fields in plane or parallel to the c-axis.

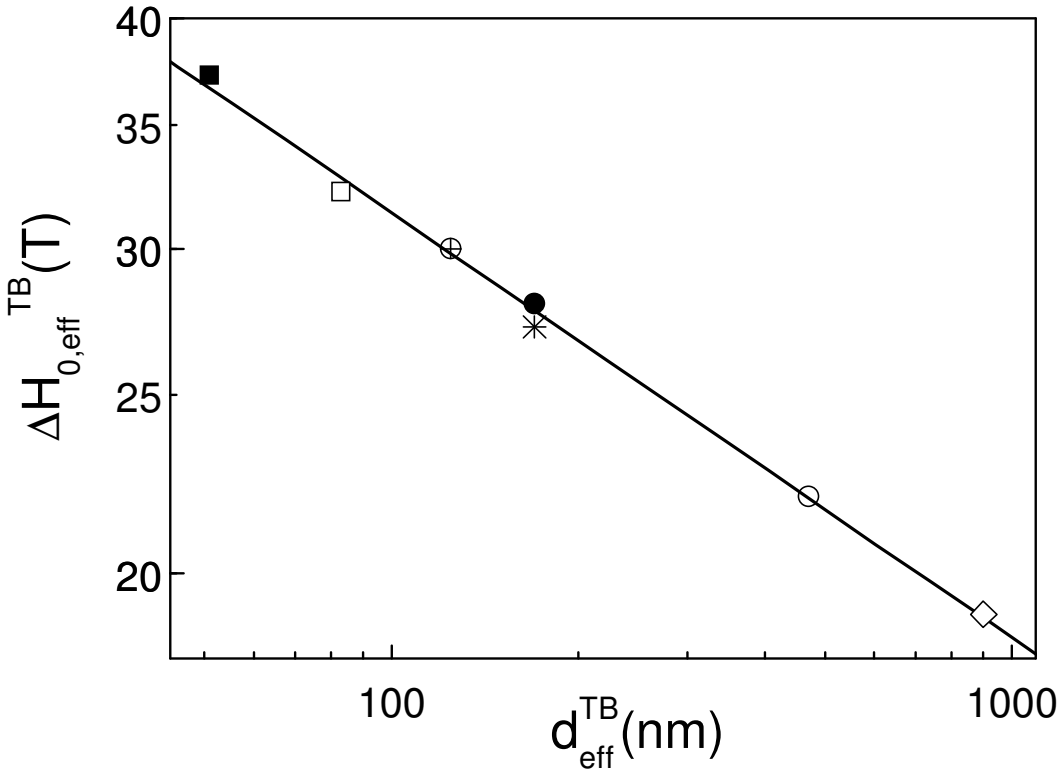

Figure 8.3: Dependence of ΔH_0^{eff} with the effective distance between twin boundaries. Shown is the experimental data obtained for H$\|$c for the samples : 0%Y211 ($\circ$), 18%Y211 ($\oplus$), 31% Y211 ($\bullet$), 10%Ag_2O ($\square$), 20% Ag_2O ($\blacksquare$) and HOP(SF) ($\star$). Also shown is the data for H$\|$ab for the sample 31% Y211 ($\diamond$).

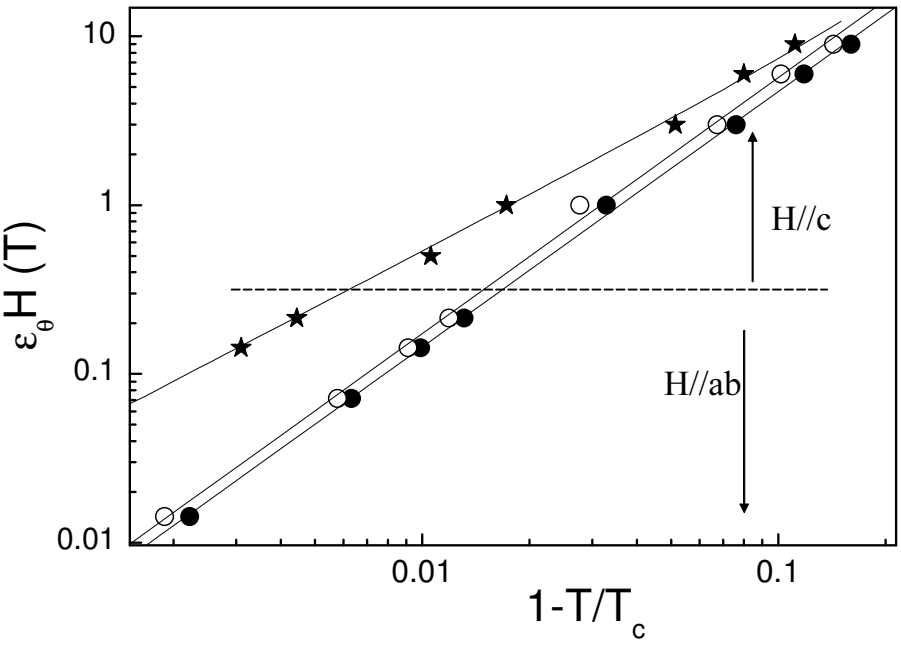

Figure 8.4: Magnetic phase diagram, shown in a log-log scale. Shown is T_{irr}^{bg}, T_{irr}^{TB} and the limit of effectivity of twin boundaries.

H‖c (in particular the irreversibility line follow the same power with the same exponent for H‖ab and H‖c), thus suggesting that the mechanisms responsible for the different transitions for H‖ab are the same than those for H‖c. Thus, from these results, we suggest that the anisotropic scaling proposed by G.Blatter [12] holds for $YBa_2Cu_3O_{7-\delta}$ even for magnetic fields applied within the ab-plane, where any deviation to this anisotropic scaling should be strongly enhanced. This scaling is observed not only for the irreversibility line, but also for the limit of effectivity of twin boundaries. The importance of this scaling will be stressed in the next section.

8.3 Vortex correlation

8.3.1 Flux Transformer measurements

The coincidence of the limit of influence of twin boundaries and microcracks (for H‖c) strongly suggests that these features may be, actually, different manifestations of the same physical phenomena. An interesting possibility that has to be considered is the existence of two different phases in the vortex liquid state. In this sense, two different scenarios have been proposed from the theoretical point of view that could promote the observed behavior:

- the first, related to strongly anisotropic superconductors, suggested the possibility of a

vortex decoupling between superconducting layers, at high temperatures. However, in $YBa_2Cu_3O_{7-\delta}$ the condition of extremely anisotropic system, $\xi_c << s$ is not fulfilled ($\xi_c > s$ at T>0.75T_c), and this origin seems implausible. Furthermore, the scaling of the superconducting properties with H_{eff} also suggests further discards this possibility.

- the second one involves the existence of strong thermal fluctuations on vortex positions that have been interpreted as the creation of thermal vortex lines.[115] At high enough temperatures, the relative importance of thermal fluctuations becomes infinity, and therefore, the sample reaches the normal state even below the upper critical field. This transition may also be seen as a vanishing *effective* vortex line tension along the direction of the magnetic field. Similar arguments have been used also by other authors in order to investigate the influence of thermal fluctuations [116, 120].

Certainly, these two different arguments promotes the observed behaviors, namely, the coincidence of the limit of influence of linear defects for H$\|$c and the limit of influence of microcracks on promoting vortex motion at high temperatures within the liquid state. However, one strong difference between these theoretical predictions is to be expected: its angular dependence. Vortex decoupling should not exist for H$\|$ab since vortex would be parallel to the superconducting layers. On the other hand, the lost of vortex tension recently suggested related to thermal fluctuations is independent of the existence of these *layers*, and therefore, one may expect the influence of the direction of the magnetic field to be related to the modification of the effective magnetic field as it is rotated away from the c-axis.

The existence of vortex correlation has been extensively checked in $YBa_2Cu_3O_{7-\delta}$ single crystals, while there are only a few works studying the vortex correlation in MTG-$YBa_2Cu_3O_{7-\delta}$ samples. Furthermore, most of these works where performed only for magnetic fields parallel to the c-axis and consequently, the study of the vortex correlation for different directions of the magnetic field appears to be worth of investigation.

Therefore, we proceed by measuring a MTG-$YBa_2Cu_3O_{7-\delta}$ sample in a geometry of flux transformer. First, and in order to check whether the data is similar to that obtained in single crystals, we proceed by determining the temperature dependence of the voltage at the top and bottom of the sample at different intensities of the magnetic field and H$\|$c. As it is observed in figure 8.5, the obtained data collapse at temperatures above the irreversibility line up to a certain temperature, defined as $T_{thermal}$.

This behavior is similar to that observed in single crystals, but is in contrast with previous results obtained in MTG-$YBa_2Cu_3O_{7-\delta}$ samples, where the voltage at the top of the sample is observed to be proportional to the voltage at the bottom[53]. The existence of this proportionality factor was attributed to Y_2BaCuO_5 particles promoting vortex cutting. However, recent studies performed in MTG-(Nd,Eu,Gd)$Ba_2Cu_3O_{7-\delta}$ showed that complete coherence between vortex motion in the top and the bottom of the sample may also be achieved in Melt-Textured samples with a high degree of disorder [54].

These measurements allow us to obtain the magnetic field dependence of the upper temperature where full vortex correlation across the sample is still present (shown in figure 8.6).

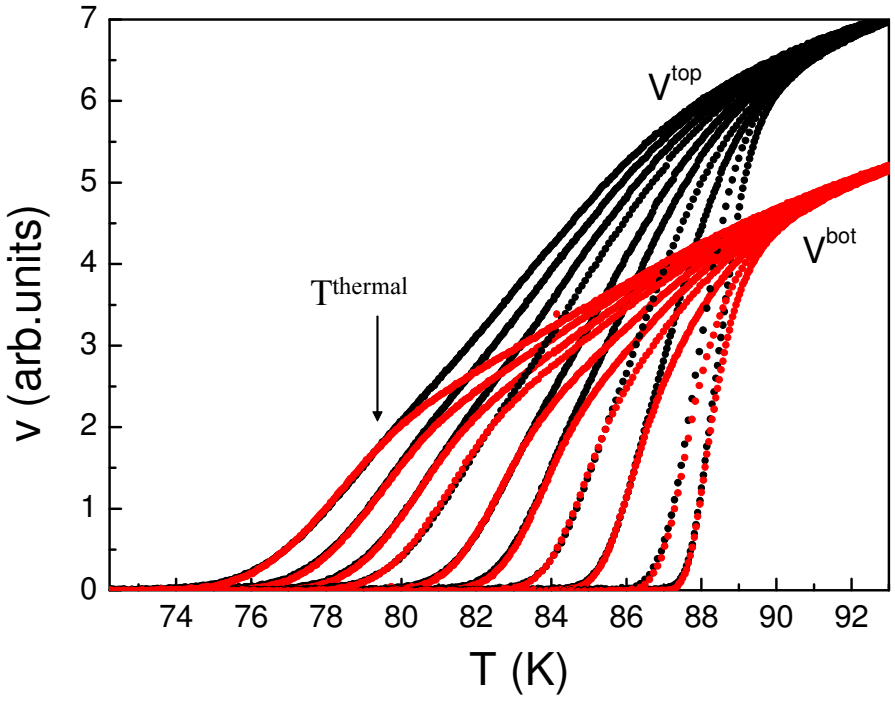

Figure 8.5: Resistivity measurements in a geometry of flux transformer for the sample submitted to HOP up to a high density of stacking faults for H||c and different intensities of the magnetic field (H=0.5,1,2,...,9T). Arrow signal the end of correlation along the direction of the magnetic field ($T_{thermal}$).

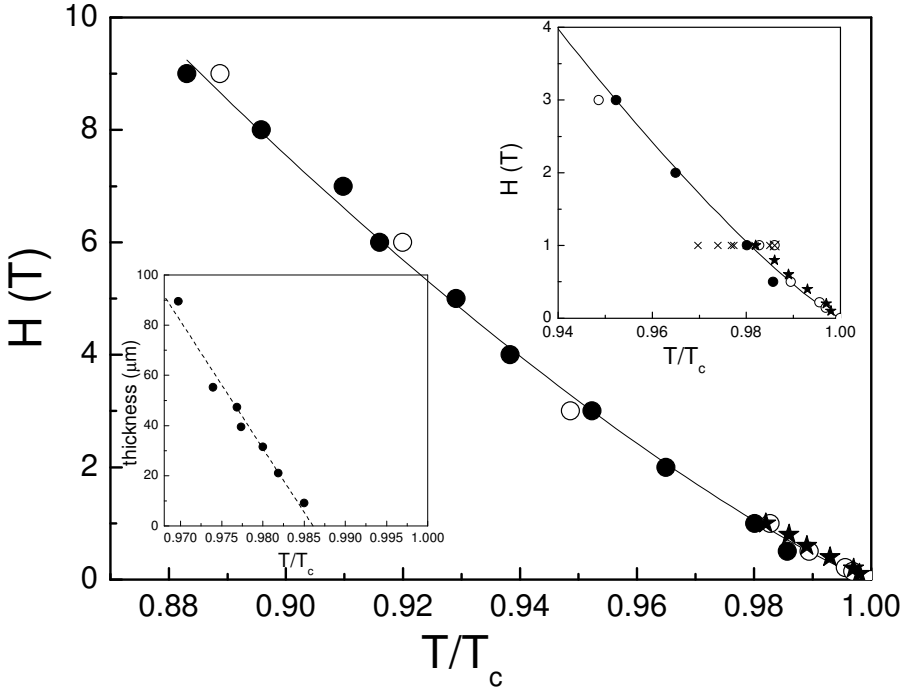

Figure 8.6: Magnetic field dependence of the $T_{thermal}$ for a MTG-$YBa_2Cu_3O_{7-\delta}$ sample (•). Also shown for comparison is the limit of influence of twin boundaries (○) and $T_{thermal}$ for a single crystal (⋆) [121]. Lower inset, thickness dependence of $T_{thermal}$ for different single crystals [41]. Upper inset: curves of the main figure together with $T_{thermal}$ for single crystals with different thickness (×) [41]. Also shown for comparison is the extrapolation to 0μm of $T_{thermal}$ (⊗).

In this figure, it is also shown, for comparison, the limit of effectivity of twin boundary pinning and $T_{thermal}$ for a single crystal. As it should be expected from a scenario where the vortex correlation is lost, they all coincide in the same H-T line. In the inset of figure 8.6 $T_{thermal}$ measured in single crystalline samples of different thickness (ranging from $10\mu m$ to $90\mu m$ is shown. As it can be observed, the dependence of $T_{thermal}$ spon a certain temperature range below T^* of $T_{thermal}$ for a MTG-$YBa_2Cu_3O_{7-\delta}$. Actually, the thickness dependence of $T_{thermal}$ reported in [41] shows that there is indeed a temperature region where the vortex correlation disappears, even in the presence of twin boundaries, thus suggesting that there is a loss of the vortex line tension. Thus, the thickness dependence of $T_{thermal}$ does not preclude the possibility of a complete loss of vortex correlation at this liquid-liquid transition in $YBa_2Cu_3O_{7-\delta}$. At large enough thickness, the loss of full vortex correlation across the sample, as determined by flux transformer measurements, may start at low temperatures, although a certain vortex line tension is still preserved.

Once determined that the experimental results around T* are consistent with losing the vortex correlation, we continued by analyzing the influence of rotation of the magnetic field. Therefore, we performed sets of $V_{top/bot}$-T curves for different directions of the magnetic field. These measurements, are shown in figure 8.7, and reveals the same behavior, i.e. a coincidence between the measurements at the top and the bottom of the sample for all the directions of the magnetic field, which enables to define $T_{thermal}(\theta)$.

The temperature dependence of $T_{thermal}$ is shown in figure 8.8, together with the region of the angular dependent phase diagram where vortex dynamics is influenced by twin boundaries. It appears from the figure that, although twin boundaries are not able to modify vortex dynamics for angles higher than $\sim 30^o$, vortex correlation is preserved up to angles close to $\theta = 90^o$. However, at high angles, the superconducting transition become sharper and $T_{thermal}$ is ill defined. In spite of the bad definition of $T_{thermal}$ at high angles, it appears clear that it follows the anisotropic scaling. We should stress, however, that a conclusive evidence of the existence of vortex correlation not promoted by twin boundaries at high angles ($\theta > 30^o$) would only we reached if untwinned samples are also investigated.

The anisotropic scaling of this transition/crossover is in close agreement with the coincidence of the limit of influence of twin boundaries for H$\|$c and H$\|$ab when the effective magnetic field is considered and it follows the intrinsic anisotropy scaling. In our opinion, the scaling of this transition discards vortex decoupling between the superconducting layers as the origin of this transition in $YBa_2Cu_3O_{7-\delta}$. Therefore, we suggest that these different phenomena arise as a consequence of the introduction of thermal induced vortices, which induce a modification of the effective vortex line tension as has been suggested [115]. As the temperature is increased, this effective line tension vanishes, and thus, determines the limit of influence of twin boundaries, microcracks and the end of a complete vortex correlation across the sample, as experimentally determined.

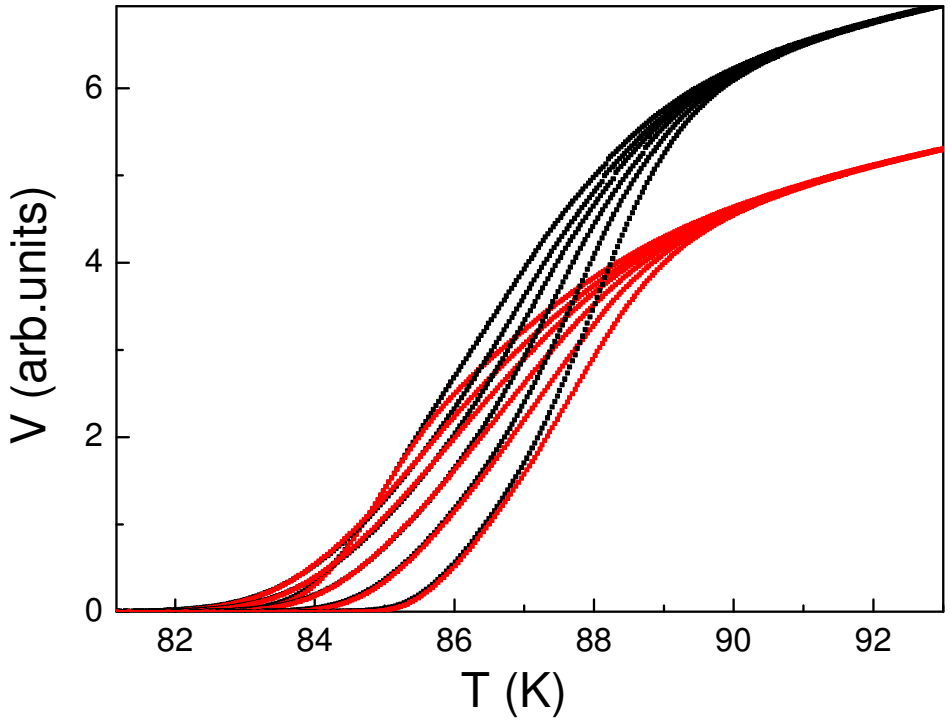

Figure 8.7: V_i versus Temperature (i=top,bot) data for $\theta = 0, 20, 30, 40, 50$ and 60^o at H=3T.

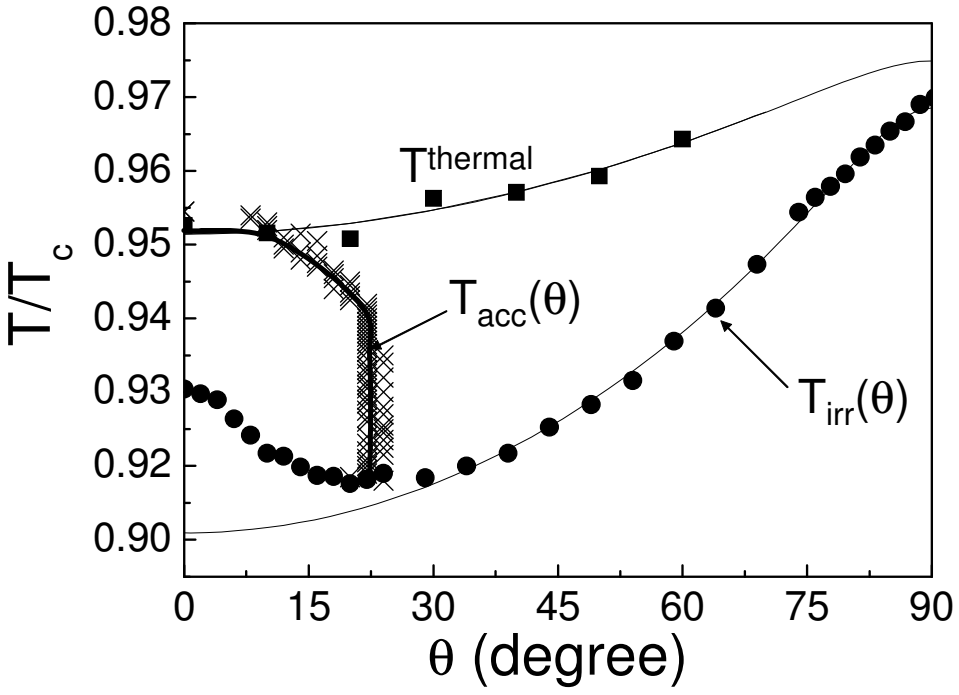

Figure 8.8: Angular dependent phase diagram. Shown are the irreversibility line, the limit of influence of twin boundaries and the $T_{thermal}(\theta)$.

8.3.2 Discussion

In this section, we have analyzed the possible existence of a lost of vortex correlation along the direction of the magnetic field. We have first observed by flux transformer measurements that full vortex correlation exists in the samples even if they have a very complex microstructure. On the other hand, we have observed that there is a temperature at which the full correlation disappears and which coincides with the limit of influence of twin boundaries, in agreement with that expected if vortex correlation is completely destroyed. But losing completely the vortex correlation should also have other important consequences:

- The influence of microstructural extended defects behaving as linear pinning centers should be considerably reduced and even vanish at this transition. This phenomenon has already been observed for twin boundaries, but it should also influence other linearly correlated defects such as columnar tracks created through irradiation. Therefore, any influence of columnar tracks should also vanish at the same temperature. Certainly, a strong upwards shift of the irreversibility line is produced as the dose increases, mainly below the matching field. However, measurements in the literature have reported that this upward shift tends to saturate at high matching fields [122], below the kink in the irreversibility line (shown in figure 7.1). Certainly, loosing the line tension impedes columnar tracks to further shift the irreversibility line and thus, it saturates.

- Any strong influence of the finite size of the sample should disappear when the effective line tension has vanished, and thus defects such as microcracks parallel to the ab-planes should not have a significative influence above the transition.

- If pinning is absent above this transition, a regime very similar to flux flow is expected to be found. In chapter 3, the dynamic behavior at high temperatures was shown to be consistent with *flux flow*.

- The disappearance of the vortex line tension at this transition avoids the possibility of having in the flux transformer measurements $V_{bot} = V_{top}$ above it, as it is indeed found experimentally.

Further support to our proposal for the existence of a new transition line in the vortex liquid state is gained by observing the results reported in figure 8.9, where the temperature dependence of the above mentioned curves is shown. Although the (apparent) strong differences existing between the origin of these different curves, they all coincide in the magnetic phase diagram. From our point of view, this coincidence can only we explained if vortices lose their line tension.

From these experimental results, therefore, we may suggest that the liquid region of the magnetic phase diagram of $YBa_2Cu_3O_{7-\delta}$ has the following regions (as shown schematically in figure 8.10):

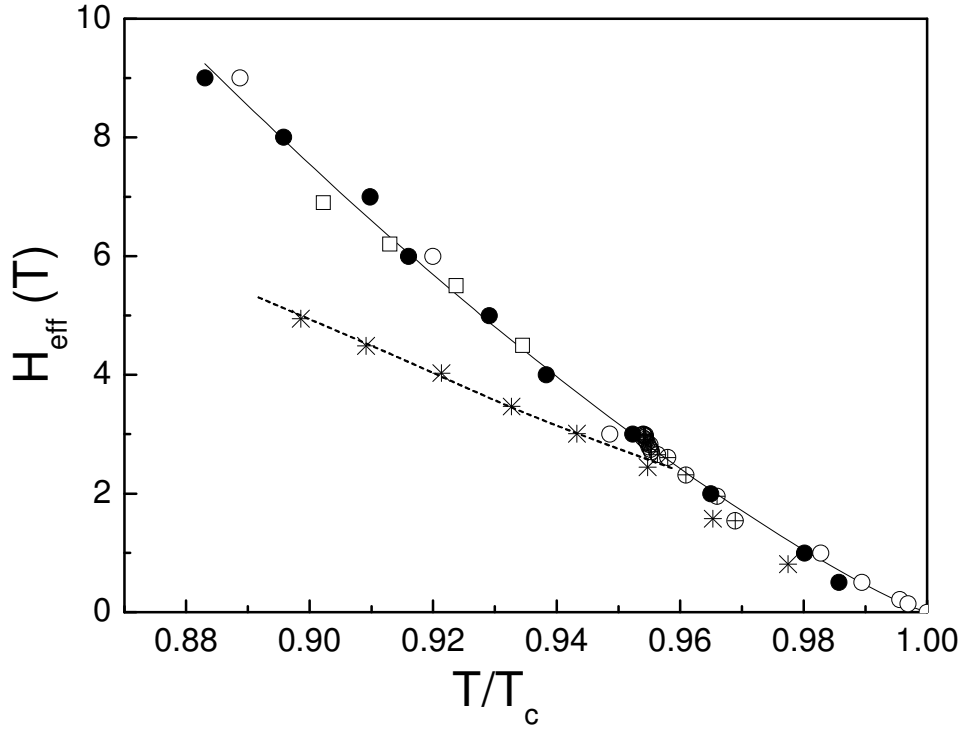

Figure 8.9: Magnetic phase diagram. Shown is the limit of influence of microcracks ($\oplus$), the irreversibility line for a sample with a high density of columnar defects [122] ($*$), $T^{thermal}$ for an MTG-$YBa_2Cu_3O_{7-\delta}$ sample ($\bullet$), the lower limit of the flux flow region ($\square$) and the limit of influence of twin boundaries ($\circ$).

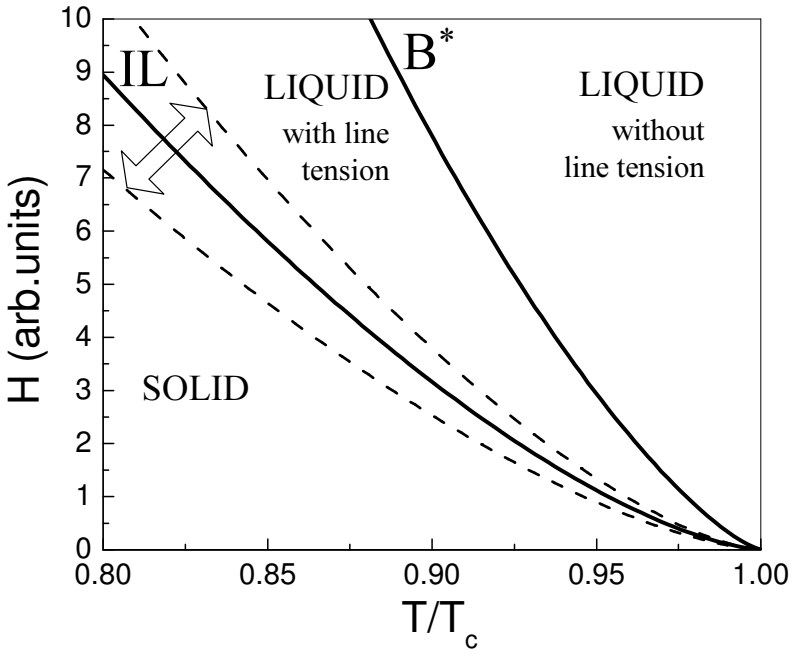

Figure 8.10: Schematic representation of our concept of the magnetic phase diagram. Shown are the dependence of the solid-liquid transition and the liquid with/without vortex lines.

- A solid of vortices, as determined by the zero-resistivity of the samples below the irreversibility line. This region can be actually formed by several different phases depending on the strength and dimensionality of the defects.

- A liquid of vortices with a certain effective line tension. The existence of this effective line tension enables linear-like pinning centers such as twin boundaries to act as linearly correlated pinning centers and modify vortex dynamics.

- A liquid of vortices, above $T_{thermal}$, without an effective vortex line tension, and therefore with hardly any effect of defects on vortex pinning.

These different phases also appear in the angular dependent phase diagram, schematically shown in figure 8.11. In this figure, the different boundaries that have appeared in this thesis are shown:

- An angular dependent irreversibility line. Its position has been seen to be strongly determined by the microstructure. For H$\|$c, an upwards shift is observed related to the influence of twin boundaries. The angular dependence of the irreversibility line (for $\theta > \theta_{acc}$, i.e. outside the influence of twin boundaries) follows the intrinsic anisotropy of $YBa_2Cu_3O_{7-\delta}$.

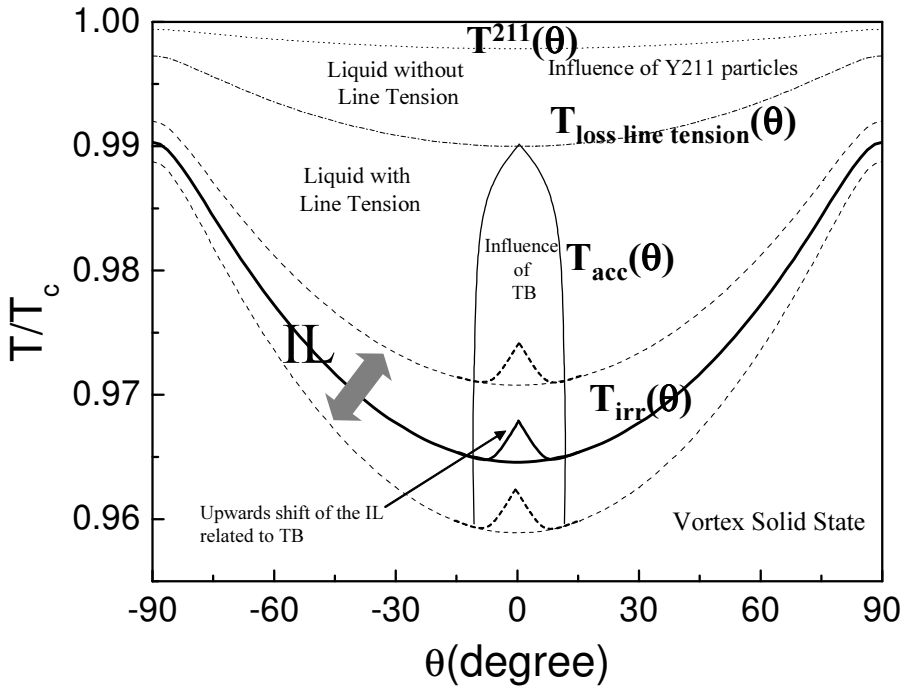

Figure 8.11: Scheme of the angular dependent phase diagram. Shown is the angular dependent irreversibility line ($T_{irr}(\theta)$), the limit of the region influenced by twin boundaries ($T_{acc}(\theta)$), the limit of the region with vortex line tension ($T_{loss\ line\ tension}$) and the limit of influence of $YBa_2Cu_3O_{7-\delta}/Y_2BaCuO_5$ particles ($T^{211}(\theta)$).

- The upper limit of a finite vortex line tension. It also follows the intrinsic anisotropy of the sample. Further analysis is required from the theoretical point of view to observe if this is the expected behaviour within this model.
- The limit of the region influenced by twin boundaries. Although the value of θ_{acc} (T) is sample dependent, the temperature at which θ_{acc} (T)=0, i.e. T^*, has been shown to be sample independent. Furthermore it coincides with the loss of line tension, strongly suggesting that linear pinning centers are not effective above this upper limit where a finite vortex line tension is lost.
- The upper limit of influence of $YBa_2Cu_3O_{7-\delta}/Y_2BaCuO_5$ particles on the viscosity of the vortex liquid. $YBa_2Cu_3O_{7-\delta}/Y_2BaCuO_5$ interfaces have been shown to be unique defects to modify the properties of the vortex liquid to extremely high temperatures (up to $\frac{T}{T_c} > 0.95$ at H=9T).

We have concluded that in $YBa_2Cu_3O_{7-\delta}$ a transition exists between a liquid of vortex lines with effective line tension to a liquid of vortex lines with vanishing effective line tension, we may now wonder if other compounds with modified intrinsic anisotropy also display

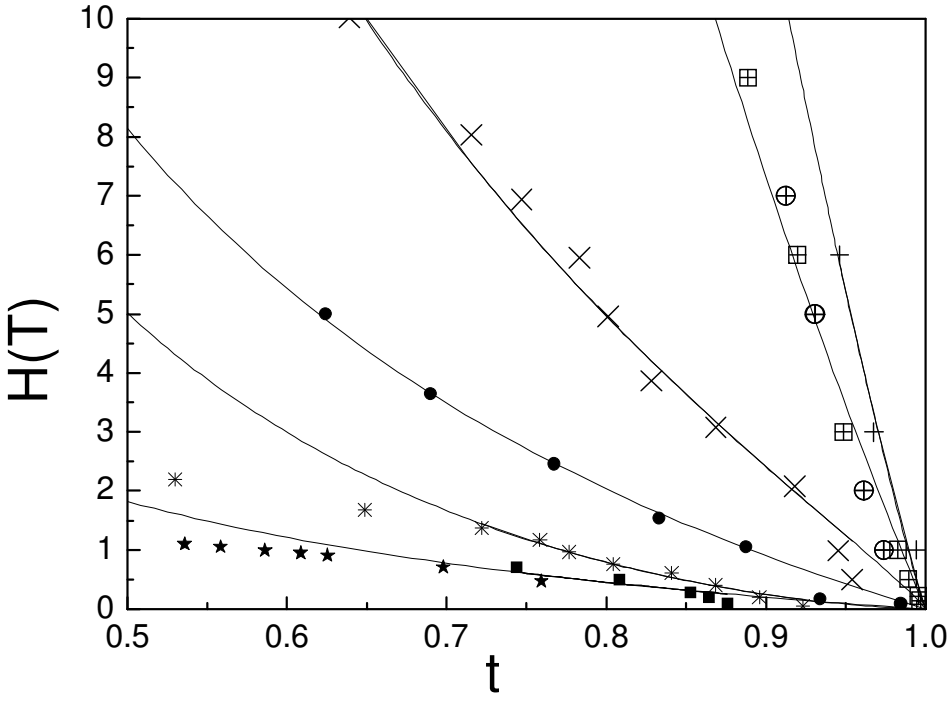

Figure 8.12: Position of the loss of vortex line tension transition for different compounds with different methods: $NdBa_2Cu_3O_{7-\delta}$ (+), resistivity measurements, present work, chapter 3; $(Nd,Eu,Gd)Ba_2Cu_3O_{7-\delta}$ ($\oplus$), flux transformer measurements [54]; $YBa_2Cu_3O_{7-\delta}$ ($\boxplus$), resistivity measurements, present work, chapter 3; $Bi_{1.8}Pob_{0.33}Sr_{1.87}Ca_2Cu_3O_y$ ($\bullet$), resistivity measurements[123]; magnetic relaxation $Hg_{0.8}Cu_{0.2}Ba_2CuO_4$ ($*$), [124];$Bi_2Sr_2CaCuO_8$, Josephson plasma resonance ($\star$) [125] and flux transformer ($\blacksquare$) [126].

this transition in the H-T phase diagram. To do so, we have extracted from the literature the position of several H-T lines where a certain signature of loss of the line tension has been reported. Although a wide diversity of experimental techniques have been used to determine a loss of the line tension in the liquid, most of the authors employed magnetoresistance measurements, either in a flux transformer configuration or analyzing specific anomalies in the temperature dependence of the resistivity. Irradiation with heavy ions have been often used in highly anisotropic compounds.

The position of these transition lines for different layered cuprates is shown in figure 8.12. It appears clearly that in low anisotropy compounds (H^*) lay at much higher temperatures than in more anisotropic compounds.

It is worth to note that the position of the transition for these several compounds strongly displaces on the phase diagram. These compounds cover a wide range of anisotropies: from the low anisotropic (where thermal fluctuations produce the lose of the effective line tension [115]) to the highly anisotropic $Bi_2Sr_2CaCu_2O_8$ (where vortex decoupling is most likely to

produce the observed results), and thus, we could expect to observe two clearly differentiated behaviors, corresponding to the introduction of thermal vortices (for 3D systems) and vortex decoupling (for 2D systems). In figure 8.12, we observe a gradual displacement of the transition as the anisotropy of the considered compound increases.

In highly anisotropic compounds, this loss of line tension is given by vortex decoupling and have been shown to follow[127]:

$$B_{cr}(T) = \frac{\Phi_0^3}{16 \cdot \pi^3 \cdot k_B T \cdot s \cdot e\lambda_{ab}(T)^2 \gamma^{-2}}, \tag{8.5}$$

with $B_{cr}(T)$ the magnetic field where the decoupling is observed, and s the interlayer spacing . For less anisotropic compounds, such as $YBa_2Cu_3O_{7-\delta}$, the possibility of vortex decoupling is not possible. Up to our knowledge, the position of this transition where vortex line tension is lost, and its dependence on the intrinsic parameters of each systems has not been yet obtained. However, it is worth to note that similarly to that predicted from equation 8.5, this transition is shifted downwards as the anisotropy of the compound increases from that of $NdBa_2Cu_3O_{7-\delta}$ ($^{-1} \sim 5$)$tothatofYBa_2Cu_4O_8$ ($\gamma^{-1} \sim 14$). Certainly, the derivation of a theoretical expression in the frame exposed by [115] is worth of further study.

The existence of this transition in the vortex liquid state, certainly should have an important consequence over the optimization of the superconducting properties above this transition, since, linearly correlated pinning centers could not have an influence on vortex dynamics. In particular, the irreversibility line should be restricted to temperatures below this transition. However, an interesting possibility arises that can enable to improve the superconducting properties: the existence of defects such as splayed defects or $YBa_2Cu_3O_{7-\delta}/Y_2BaCuO_5$ interface that, due to their particular geometry, promotes entanglement and thus, modifies vortex viscosity even at temperatures above this transition.

8.4 Conclusions

In this chapter, the main properties of the vortex liquid state have been investigated and analyzed. Firstly, we have demonstrated that the phase diagram for H||c and for H||ab are similar. In particular, we have seen that a solid-liquid transition and a transition above which twin boundaries are not longer effectives to modify vortex pinning exist for both directions. Furthermore, we have demonstrated that the position of these curves (T_{irr}^{TB}, T_{irr}^{TB} and T^*) scale with the effective magnetic field. This scaling of the superconducting properties with the effective magnetic field further confirms that $YBa_2Cu_3O_{7-\delta}$ has a 3-D behaviour even for magnetic fields very close to the ab-plane. This 3-D behaviour was actualy to be expected since $\xi_c(T) > s$ in the temperature range investigated in this thesis.

In the previous chapters, we observed that the limit of influence of twin boundaries (acting as pinning centers) and the limit of influence of microcracks (acting as detrimental defects) coincide for H||c. An interesting possibility arose in order to explain this coincidence:

an intrinsic transition within the vortex liquid state where the vortex line tension is lost. In order to further study this possibility, flux transformer measurements in MTG-$YBa_2Cu_3O_{7-\delta}$ samples have been performed. We have observed that the temperature where full correlation is lost coincides with the limit of influence of twin boundaries and microcracks, and follows the intrinsic anisotropy of the system, strongly suggesting the existence of such a transition in the liquid vortex state. Furthermore, different phenomena have been observed to coincide in this curve: the limit of influence of twin boundaries, the upper limit of the irreversibility line in $YBa_2Cu_3O_{7-\delta}$ single crystals irradiated with heavy ions, the limit of influence of microcracks, the appearance of flux flow just above this transition and the lost of full vortex correlation as determined from flux transformer measurements. In our point of view, the coincidence of these phenomena in the same H-T line is consistent with the loss of the vortex line tension in this transition.

Thus, the magnetic phase diagram for $YBa_2Cu_3O_{7-\delta}$ samples is obtained. In this phase diagram it has been found:

- An angular dependent irreversibility line. Although it has been demonstrated to be strongly dependent on the microstructure of the sample, it follows the anisotropy of the system. In this angular dependent irreversibility line, an upwards shift is obtained for H||c, determined by the density of twin boundaries.

- A liquid-liquid transition where the vortex line tension is lost. Similarly to the irreversibility line, it follows the intrinsic anisotropy of the system. However, it is an intrinsic transition and thus is sample independent.

- A region of influence of twin boundaries and Y_2BaCuO_5 particles.

Finally, further insight into this liquid-liquid transition has been done by considering different cuprates with anisotropies ranging from 3-D systems to 2-D systems. Although the strong different characteristics of these systems, it is observed that they follow a similar temperature dependence and is shifted downwards as the anisotropy of the system is increased. This dependence has been compared with the predictions for 2-D (related to vortex decoupling) and 3-D systems (related to the existence of thermal fluctuations).

Chapter 9

Conclusions

The goal of this thesis has been to investigate the influence of the microstructure on the superconducting properties of the vortex liquid state in Melt Textured Grown $YBa_2Cu_3O_{7-\delta}$ samples. Melt Textured Grown $YBa_2Cu_3O_{7-\delta}$ samples, due to their rich microstructure are an interesting material in order to investigate the impact of defects over vortex dynamics under the presence of different kinds of defects.

We have explored the capability of different treatments and post-processes to strongly modify the density of the naturally grown microstructural defects in Melt Textured single domains while keeping the density of the rest of the defects almost constant. On one hand, the microstructure has also been modified through the preparation process of the sample, which has been modified by changing the initial content of Y_2BaCuO_5 particles, or adding $ZrBaO_3$ (enabling to obtain a Melt Textured samples without Y_2BaCuO_5 particles) or adding AgO_2 (thus increasing the separation between microcracks). On the other hand, the action of different post-processing treatments such as the Cold Isostatic Pressing (enhancing the density of in-plane dislocations parallels to <110>) and High Oxygen Pressure (increasing the density of dislocations aligned parallel to <100> and, at latter stages increasing the density of stacking faults) has been used to modify the microstructural characteristics and therefore, the superconducting properties.

The existence of this large variety of defects in MTG-$YBa_2Cu_3O_{7-\delta}$ samples requires also a methodology capable of distinguish and deconvolute the influence of each one of the defects present in the sample. To do so, the angular dependence of magnetoresistance in the different samples has been used. We have mainly analyzed the angular dependence of the magnetoresistance while rotating the magnetic filed from the c-axis to the ab-plane. This angular dependent magnetoresistance is governed by the intrinsic anisotropy of the system, and thus, a c-axis magnetic field has a stronger influence than an ab-plane magnetic field. To this anisotropic background, the influence of aligned defects such as twin boundaries or dislocations is superposed, which can be detected for certain directions of the magnetic field. Thus, the contribution of aligned defects may be evaluated and extracted through the study of the angular dependence of the superconducting properties.

The dimensionality of the different defects reveals itself as a main subject since it determines its angular dependence. In this sense, we have classified the defects present in MTG-$YBa_2Cu_3O_{7-\delta}$ samples in the following categories:

- In-plane dislocations, when the magnetic field is rotated from the c-axis to the ab-plane, behave as point-like pinning centers. We have experimentally demonstrated that in samples with strong pinning centers such as twin boundaries or $YBa_2Cu_3O_{7-\delta}/Y_2BaCuO_5$ interfaces, the influence of point-like pinning centers vanishes in the vortex liquid state.

- In-plane dislocations, for in-plane magnetic fields behave as linear-like pinning centers. It has been shown that these pinning centers promote an enhancement of the vortex activation energy and an upwards shift of the irreversibility line.

- The influence of twin boundaries in the vortex liquid state has been investigated. For magnetic fields parallel to twin boundaries, the upwards shift of the irreversibility line has been determined and shown to be dependent on the density of twin boundaries. The upper limit of influence of twin boundaries (T^*), however, has been found to be sample independent. The vortex activation energy also increases but this enhancement depends on the density of Y_2BaCuO_5 particles, thus demonstrating the complexity of vortex dynamics in MTG-$YBa_2Cu_3O_{7-\delta}$ samples.

- The interfaces of $Y_2BaCuO_5/YBa_2Cu_3O_{7-\delta}$ interfaces have been seen to decrease vortex motion in a wide region of the vortex liquid state (up to temperatures higher than the limit of influence of twin boundaries and dislocations). In particular, the strong action of $Y_2BaCuO_5/YBa_2Cu_3O_{7-\delta}$ interfaces in the vortex liquid state has been also shown to lead to a linear shift of the irreversibility line with the interface density of Y_2BaCuO_5 particles. The shift of the irreversibility line has been shown to be active for all the directions of the magnetic field, in agreement with their quasi-spherical geometry. On the other hand, the vortex activation energy has been shown to increase only at high contents of Y_2BaCuO_5 particles.

- Microcracks and stacking faults have been seen to be able to promote a downwards shift of the irreversibility line. This detrimental influence has been attributed to an increased vortex mobility due to the shortening of the vortex length. The limit of influence of microcracks in the angular dependent phase diagram has also been determined. We have observed that the limit of influence of microcracks coincides with that of twin boundaries for H$\|$c.

The coincidence of the limit of influence of twin boundaries and microcracks (for H$\|$c), while being very strongly different defects with different actions over vortices revealed worth of further study. The coincidence of these two phenomena could be related to a loss of the vortex line tension, and therefore, angular dependent flux transformer measurements where

performed in order to investigate the possible existence of such transition in the vortex liquid state. Our measurements confirm the existence of such a transition. Furthermore, the angular scaling of this transition with the effective magnetic field strongly suggests an intrinsic nature of this transition, determined by the anisotropy of the material.

In addition to the fundamental relevance of this new transition, its existence of a new transition within the liquid vortex state characterized by the loss of the vortex line tension may have important consequences from the point of view of technological applications for these compounds. The linear pinning centers are not longer effective above this transition and, therefore, this transition could be regarded as an upper limit of the irreversibility line of $YBa_2Cu_3O_{7-\delta}$. We envisage that it would be practically impossible to define a defect nanostructure that can become effective to pin vortices at such high temperatures if they do not keep any line tension. Eventhough, defects such as $Y_2BaCuO_5/YBa_2Cu_3O_{7-\delta}$ interfaces or splayed defects have been shown to still modify the vortex viscosity above this liquid-liquid transition.

To conclude, the influence of the main defects present in MTG-$YBa_2Cu_3O_{7-\delta}$ samples on the superconducting properties of the vortex liquid state has been investigated. The particular action of each kind of defect has been analyzed and explored in terms of their geometry and dimensionality. The common features of their influence lead to the determination of an intrinsic transition in the vortex liquid state where the vortex line tension may be lost.

Bibliography

[1] H. Onnes, Leiden Comm. **120b, 122b, 124c** (1911).

[2] A.A.Abrikosov, Soviet Phys. JETP **5**, 1174 (1957).

[3] J. Bardeen, L. N. Cooper, and J. R. Schrieffer, Phys.Rev. **108**, 1175 (1957).

[4] J. Bednorz and K.A.Müller, Z.Phyz. **64**, 189 (1986).

[5] N.-C. Yeh, Association of Asia Pacific Physical Societies Bulletin **12**, 2 (2002).

[6] I. K. Schuller, A.Bansi, D.N.Basov, M.R.Beasley, J.C.Campuzano, J.P.Carbotte, R.J.Cava, G.Crabtree, R.C.Dynes, D.Finnemore, et al., *A snapshot view of high temperature superconductivity 2002*, http://physics.ucsd.edu/ iksgrp/HTReport.pdf.

[7] F.Beech, S.Miraglia, A.Santoro, and R.S.Roth, Phys.Rev.B **35**, 8778 (1987).

[8] J.Nagamatsu, N.Nakagawa, T.Murakana, Y.Zenitani, and J.Akimitsu, Nature **410**, 63 (2001).

[9] O.Gunnarsson, Rev.Mod.Phys. **69**, 575 (1997).

[10] G. Blatter, M.V.Feigel'man, V.B.Geshkenbein, A.I.Larkin, and V.M.Vinokur, Rev.Mod.Phys. **66**, 1125 (1994).

[11] T.Ito, H.Takagi, S.Ishibashi, T.Ido, and S.Uchida, Nature **350**, 596 (1991).

[12] G. Blatter, V.M.Geshkenbein, and A.I.Larkin, Phys.Rev.Lett. **68**, 875 (1992).

[13] J.C.Davis, http://www.ccmr.cornell.edu/ jcdavis/stm/results/nbse2/index.htm.

[14] T. Giamarchi and P. Doussal, Phys.Rev.B **52**, 1242 (1995).

[15] H.Fangohr, A.E.Koshelev, and M.J.W.Dogson, cond-mat p. 0210580 (2002).

[16] D. Fisher, M.P.A.Fisher, and D.M.Huse, Phys.Rev.B **43**, 130 (1991).

[17] D.R.Nelson and V.M.Vinokur, Phys.Rev.B **48**, 13060 (1993).

[18] D.R.Nelson and P. Doussal, Phys.Rev.B **42**, 10113 (1990).

[19] H.Hilgenkamp and J.Mannhart, Rev.Mod.Phys. **74**, 485 (2002).

[20] T.T.M.Palstra, B.Batlogg, L.F.Schneemeyer, and J.V.Waszczak, Phys.Rev.Lett. **61**, 1662 (1988).

[21] T.T.M.Palstra, B.Batlogg, R. Dover, L.F.Schneemeyer, and J.V.Waszczak, Phys.Rev.B **41**, 6621 (1990).

[22] W. Kwok, S.Fleshler, U.Welp, V.M.Vinokur, S.Downey, and G.W.Crabtree, Phys.Rev.Lett. **76**, 3370 (1992).

[23] H.Safar, P.L.Gammel, D.A.Huse, D.J.Bishop, J.P.Price, and D.M.Ginzberg, Phys.Rev.Lett. **69**, 824 (1992).

[24] E. Zeldov, D.Majer, M.Konczykowski, V.B.Geshkenbein, V.M.Vinokur, and H.Shtrikman, Nature **375**, 373 (1995).

[25] A.Schilling, R.A.Fisher, N.E.Philips, U.Welp, D.Dasgupta, K.W.Kwok, and G.W.Crabtree, Nature **382**, 791 (1996).

[26] J. Fendrich, W.K.Kwok, J.Giaputzakis, C. der Beek, V.M.Vinokur, S.Fleshler, U.Welp, H.K.Viswanath, and G.W.Crabtree, Phys.Rev.Lett. **74**, 1210 (1995).

[27] M. Konczykowski, F.Rillier-Alberque, A.Shaulov, Y.Yeshurin, and P.Lejay, Phys.Rev.B **44**, 7167 (1991).

[28] L. Civale, A.D.Marwick, T.K.Worthington, M.A.Kirk, J.R.Thompson, L.Krusin-Elbaum, Y.Sim, J.R.Clem, and F.Holtzberg, Phys.Rev.Lett. **67**, 648 (1991).

[29] T.K.Worthington, M.P.A.Fisher, D.A.Huse, J.Toner, A.D.Marwick, T. C.A.Feild, and F.Holtzberg, Phys.Rev.B **46**, 11854 (1992).

[30] W. Jiang, N.-C.Yeh, D.S.Pmeed, U.Kriplani, D.A.Bem, M.Konczykowsky, T.A.Tombrella, and R.Holtzberg, Phys.Rev.Lett. **72**, 550 (1994).

[31] W. Kwok, R.J.Olson, G.Karapetrov, L.M.Paulius, W.G.Moulton, D.J.Hofman, and G.W.Crabtree, Physical Review Letters **84**, 3706 (2000).

[32] J. Figueras, T.Puig, X.Obradors, A.Erb, and E.Walter, Phys.Rev.B **65**, 092505 (2002).

[33] T.Sasagawa, K.Kishio, Y.Togawa, J.Shimoyama, and K.Kitazawa, Phys.Rev.Lett. **80**, 4297 (1998).

[34] A. Koshelev and V.M.Vinokur, Phys.Rev.B **57**, 8026 (1998).

[35] T.Nattermann and S.Scheidl, Adv. in Phys. p. 607 (2000).

[36] P.W.Anderson and Y.B.Kim, Rev.Mod.Phys. **36**, 39 (1964).

[37] P.H.Kes, J.Aarts, J. den Berg, C. van der Beek, and J.A.Mydosh, Supercond.Sci.Technol. **1**, 242 (1989).

[38] A. Schilling, R.A.Fisher, N.E.Phillips, U.Welp, W.K.Kwok, and G.W.Crabtree, Phys.Rev.Lett. **78**, 4833 (1997).

[39] S. Fleshler, W.K.Kwok, U.Welp, V.M.Vinokur, M.K.Smith, J.Downey, and G.W.Crabtree, Phys.Rev.B **47**, 14448 (1993).

[40] W. Kwok, U.Welp, G.W.Crabtree, K.G.Vandervoot, R.Hulsher, and J.Z.Liu, Phys.Rev.Lett. **64**, 966 (1990).

[41] D.López, E.F.Rigui, G.Nieva, F. la Cruz, et al., Phys.Rev.B **53**, 8895 (1996).

[42] M.Murakami, M.Morita, and N.Koyama, Jap.J.Appl.Phys. **28**, L1125 (1989).

[43] H.Suematsu, H.Okamura, S.Nagaya, and H.Yamauchi, Adv. Supercond. X **2**, 661 (1998).

[44] F.Sandiumenge, S.Piñol, X.Obradors, E.Snoeck, and C.Roucou, Phys.Rev.B **50**, 7032 (1994).

[45] F.Sandiumenge, T.Puig, J.Rabier, J.Plain, and X.Obradors, Adv.Mat **12**, 375 (2000).

[46] C.-J. Kim and G. Hong, Supercond.Sci.Technol. **12**, R27 (1999).

[47] B.Martínez, X.Obradors, A.Gou, V.Gomis, S.Piñol, J.Fontcuberta, and H. Tool, Phys.Rev.B **53**, 2797 (1996).

[48] S.Sanfilipo, A.Sulpice, O.Laborde, D.Bourgault, and Th.Fournier, Phys.Rev.B **58**, 15189 (1998).

[49] M.Murakami, *Processing and Properties of High T_c superconductors* (S.Jin (world Scientifics), Singapure, 1993), vol. 1, pp. 215–268.

[50] V.M.Pan, *Physics and materials science of vortex states, flux pinning and vortex dynamics* (1999), ed.R.Kossowsky, S.Bose, V.Pan and Z.Durusoy, NATO Science Series, p.1.

[51] J.Plain, Ph.D. thesis, Institut de Ciència de Materials de Barcelona (2001).

[52] J.Plain, F.Sandiumenge, T.Puig, X.Obradors, and J.Rabier, Phys.Rev.B **65**, 104526 (2002).

[53] F. Galante, E.Rodriguez, J.Fontcuberta, and X.Obradors, Physica C **296**, 96 (1998).

[54] A.K.Pradhan, M.Muralidhar, Y.Feng, M.Murakami, K.Nakao, and N.Koshizuka, Phys.Rev.B **64**, 172505 (2001).

[55] A.E.Carrillo, Master's thesis, Institut de Ciència de Materials de Barcelona (2003).

[56] E.Mendoza, Ph.D. thesis, Institut de Ciència de Materials de Barcelona (2002).

[57] A. Carrillo, T. Puig, J. Plain, J. Figueras, and X. Obradors, Physica C **336**, 213 (2000).

[58] B.Martínez, F.Sandiumenge, T.Puig, X.Obradors, L.Richard, and J.Rabier, Appl.Phys.Lett. **74**, 73 (1999).

[59] J.Figueras, T.Puig, X.Obradors, and J.Rabier, Appl.Superconductivity IOP Conf.Series **167**, 763 (2000).

[60] T. Puig, J.Plain, F.Sandiumenge, X.Obradors, J.Rabier, and J.A.Alonso, Appl.Phys.Lett. **75**, 1952 (1999).

[61] E.Mendoza, T.Puig, E.Varesi, A.E.Carrillo, J.Plain, and X.Obradors, Physica C **334**, 7 (2000).

[62] F.Sandiumenge, B.Martínez, and X.Obradors, Supercond.Sci.Technol. **10**, pA93 (1997).

[63] A.Erb, E.Walker, J.Y.Genoud, and R.Flukiger, Physica C **282**, 89 (1997).

[64] J. Figueras, T.Puig, X.Obradors, A.Erb, and E.Walter, Physica C **369**, 209 (2002).

[65] G.W.Crabtree et al., *Vortex melting and the liquid state in* $YBa_2Cu_3O_{7-\delta}$ (1998), proceedings of the NATO Advanced Study Institute on the Physics and Materials Science of Vortex States, Flux Pinning and Dinamics.

[66] F.Lindemann, Phys.Z. **11**, 69 (1910).

[67] R.M.Langan, S.N.Gordeev, P. de Groot, A.G.M.Jansen, R.Gagnon, and L.Taillefer, Phys.Rev.B **58**, 14548 (1998).

[68] G. Crabtree, W.K.Kwok, L.M.Paulius, A.M.Petrean, R.J.Olsson, G.Karapetrov, V.Tobos, and W.G.Moulton, Physica C **332**, 71 (2000).

[69] U.C.Täuber and D.R.Nelson, Phys.Rep. **289**, 157 (1997).

[70] R.M.Langan, S.N.Gordeev, M.Oussena, P. Groot, A.G.M.Jansen, R.Gagnon, and L.Taillefer, Physica C **313**, 294 (1999).

[71] U.Welp, S.Fleshler, W.K.Kwok, J.Downey, G.W.Crabtree, H.Claus, A.Erb, and G.Muller-Vogt, Phys.Rev.B **47**, 12369 (1993).

[72] T. R. Chien, Z. Z. Wang, and N. P. Ong, Phys.Rev.Lett. **67**, 2088 (1991).

[73] E.W.Hudson, S.H.Pan, A.K.Gupta, K.W.Ng, and J.C.Davis, Science **285**, 88 (1999).

[74] J. Figueras, T.Puig, A.E.Carrillo, and X.Obradors, Supercond.Sci.Technol. **13**, 1067 (2000).

[75] J.Figueras, A.E.Carrillo, T.Puig, and X.Obradors, J.Low Temp.Phys. **117**, 873 (1999).

[76] X.Obradors, T.Puig, E.Mendoza, J.Plain, J.Figueras, X.Granados, A.E.Carrillo, E.Varesi, F.Sandiumenge, and P.Tixador, Supercond.Sci.Technol. **13**, 879 (2000).

[77] F.Sandiumenge, private Comunication.

[78] C.Panagopoulos, J.R.Cooper, N.Athanassopoulou, and J.Chrosch, Phys.Rev.B **54**, R12721 (1996).

[79] J.Axnäs, W.Holm, Y.Eltsev, and Ö.Rapp, Phys.Rev.B **53**, R3003 (1996).

[80] K.Semba, A.Matsuda, and T.Ishii, Phys.Rev.B **49**, 10043 (1994).

[81] K.Tomimoto, I.Terasaki, A.I.Rykov, T.Mimura, and S.Tajima, Phys.Rev.B **60**, 114 (1999).

[82] Ö.Rapp, M.Andersson, J.Axnäs, Y.Eltsev, B.Lundqvist, and A.Rydh (Kluwer Academic Publishers, 1999), p. 289, M. Ausloos and S. Kruchinin ed.

[83] Th.Wolf, A.-C.Bornarel, H.Kupfer, R.Meier-Hirmer, and B.Obst, Phys.Rev.B **59**, 6308 (1997).

[84] K.Takita, H.Akinaga, H.Katoh, H.Asano, and K.Masuda, Jap.J.Appl.Phys. **2**, L67 (1988).

[85] J.G.Lin, C.Y.Huan, Y.Y.Xue, C.W.Chu, X.W.Cao, and J.C.Ho, Phys.Rev.B **51**, 12900 (1995).

[86] N.H.Babu, W.Lo, D.A.Cardwell, and A.M.Campbell, Appl.Phys.Lett. **75**, 2981 (1999).

[87] J.M.Tarascon, W.R.McKinnon, L.H.Greene, G.W.Hull, and E.M.Vogel, Phys.Rev.B **36**, 226 (1989).

[88] P. Diko, W.Gawalek, T.Habisreuthere, T.Klupsch, and P.Görnet, Phys.Rev.B **52**, 13658 (1995).

[89] T.Puig, F.Galante, E. M. González, J. L. Vicent, B.Martínez, and X.Obradors, Phys.Rev.B **60**, 13099 (1999).

[90] T.Puig and X.Obradors, Phys.Rev.Lett. **84**, 1571 (2000).

[91] T. Puig, J.Figueras, and X.Obradors, Physica C **341-348**, 2301 (2000).

[92] V. Geshkenbein, A.Larkin, M.Feigel'man, and V.Vinokur, Physica C **162-164**, 239 (1989).

[93] M.A.Moore and N.K.Wilkin, Phys.Rev.B **50**, 10294 (1994).

[94] L. M. Paulius, J.A.Fendrich, W.K.Kwok, A.E.Koshelev, V.M.Vinokur, G.W.Crabtree, and B.G.Glagola, Phys.Rev.B **56**, 913 (1997).

[95] W. Kwok, L.M.Paulius, V.M.Vinokur, A.M.Petrean, R.M.Rommingen, and G.W.Crabtree, Phys.Rev.B **58**, 14594 (1998).

[96] Y.Abulafia, A.Shaulov, Y.Wolfus, R.Prozorov, L.Burlachkov, Y.Yeshurun, D.Majer, E.Zeldov, H.Wühl, V.B.Geshkenbein, et al., Phys.Rev.Lett. **77**, 1596 (1996).

[97] J. Kierfeld and V. M. Vinokur, Phys.Rev.B **61**, R14928 (2000).

[98] W. Jiang, N.-C.Yeh, T.A.Tombrello, A.P.Rice, and F.Holtzberg, J.Phys.Condens.Matter **9**, 8085 (1997).

[99] L. Civale, A.D.Marvic, M.W.MacElfresh, T.K.Worthington, A.P.Malezemof, F.H.Holtzberg, J.R.Thompson, and M.A.Kirk, Phys.Rev.Lett. **65**, 1164 (1990).

[100] D.López, L.Krusin-Elbaum, H.Safar, E.Righi, F. la Cruz, S.Grigera, C.Field, W.K.Kwok, L.M.Paulius, and G.W.Crabtree, Phys.Rev.Lett. **80**, 1070 (1998).

[101] E.F.Rigui, S.A.Grigera, G.Nieva, D.López, and F. la Cruz, Phys.Rev.B **55**, 14156 (1997).

[102] Y.Zhang, M.Mironov, J.F.Lee, and K.Salama, Jap. J.Appl.Phys. **34**, 3077 (1995).

[103] P.X.Zhang, L.Zhou, P.Ji, W.M.Bian, X.Z.Wu, and Z.H.Lai, Supercond.Sci.Technol. **8**, 15 (1995).

[104] D. Bourgault, L.Porcar, A. Sulpice, D. Isfort, F. Giovannelli, R. Tournier, and G. Desgardin, Physica C **372**, 1843 (2002).

[105] T.Bjornangen, A.Rydh, and O.Rapp, Phys.Rev.B **64**, 224510 (2001).

[106] L.Civale, T.K.Worthington, and A.Gupta, Phys.Rev.B **43**, 5425 (1991).

[107] H.Obara, A.Sawa, and S.Kosaka, Phys.Rev.B **49**, 1224 (1994).

[108] E.S.Sadki, Z.H.Barber, S.J.Lloyd, M.G.Blamire, and A.M.Campbell, Phys.Rev.Lett. **85**, 4168 (2000).

[109] J. Villegas, E. M. Gonzalez, J. L. Vicent, M. Varela, Z. Sefrioui, and J. Santamaria, Mat.Res.Proc.Symp **659,II**, 10.4.1 (2001).

[110] R.J.Olsson, Ph.D. thesis, Michigan State University (2000).

[111] H.Suematsu, H.Okamura, S.Nagaya, and H.Yamauchi, Supercond.Sci.Technol. **12**, 274 (1999).

[112] S.Sanfilippo, Ph.D. thesis, Joseph Fourier Grenoble I (1997).

[113] Ø.Fisher, private communication (2001).

[114] A.V.Samoilov, M.V.Feigelman, M.Konczykowski, and F.Holtzberg, Phys.Rev.Lett. **76**, 2798 (1996).

[115] Z.Tesanovic, Phys.Rev.B **59**, 6449 (1999).

[116] P.Benetatos and M.C.Marchetti, Phys.Rev.B **64**, 54518 (2001).

[117] A. K. Nguyen and A.Sudbø, Europhys.Lett. **46**, 780 (1999).

[118] J.Figueras, T.Puig, and X.Obradors, Phys.Rev.B **67**, 014503 (2003).

[119] M.P.Delamare, G.Poullain, C. Simon, S. Sanfilippo, X. Chaud, and A.Brûlet, Eur.Phys.J.B **6**, 33 (1998).

[120] H.Nordborg and G.Blatter, Phys.Rev.B **58**, 14556 (1998).

[121] D.López, G.Nieva, and F. la Cruz, Phys.Rev.B **50**, 9684 (1994).

[122] M. Konczykowski and A.V.Samoilov, Phys.Rev.Lett. **78**, 1830 (1997).

[123] E. Mezzetti, R.Gerbaldo, G.Ghigo, L.Gozzelino, and L.Gherardi, Phys.Rev.B **59**, 3890 (1999).

[124] A. Daignere, A.Maignan, V.Hardy, and Ch.Simon, Supercond.Sci.Technol. **14**, 659 (2001).

[125] M.Kosugi, Y.Matsuda, M.B.Gaifullin, L.N.Bulaevskii, N.Chikumoto, M.Konczykowski, J.Shimoyama, K.Kishio, K.Hirata, and K.Kumagai, Phys.Rev.Lett. **79**, 3763 (1997).

[126] M. Sato, T.Shibauchi, S.Ooi, T.Tamegai, and M.Konczykowski, Phys.Rev.Lett. **79**, 3759 (1997).

[127] X.G.Qiu, V.V.Moshcalkov, Y.Bruynseraede, and J.Karpinski, Phys.Rev.B **58**, 8826 (1998).

List of articles

- "Solubility limit and anisotropy analysis of Mg doping in Melt Textured $YBa_2Cu_3O_{7-\delta}$", J.Figueras, A.E.Carrillo, T.Puig and X.Obradors.
  Journal of Low Temperature Physics,**117**, 873 (1999).

- "Effects of Cold Isostatic Pressing in pinning in Melt Textured Grown YBCO", J.Figueras, T.Puig, F.Sandiumenge, X.Obradors and J.Rabier.
  Applied Superconductivity: I.O.P. Conference Series number **167**, vol 1, 763 (1999).

- "In-plane Mg doping in $YBa_2Cu_3O_{7-\delta}$:Influence on superconducting properties", J.Figueras, T.Puig, A.E.Carrillo and X.Obradors.
  Superconducting Science and Technology, **13**,1067 (2000).

- "Tunninig the critical currents in bulk MTG-YBCO for current limiting devices", X.Obradors, T.Puig, E.Mendoza, J.Plain, J.Figueras, X.Granados, A.E.Carrillo, E.Varesi, F.Sandiumenge and P.Tixador.
  Superconducting Science and Technology, **13**,839 (2000).

- "Zr-oxide additions in MTG-YBCO: $YBa_2Cu_3O_{7-\delta}$ free composites", A.E.Carrillo, T.Puig, J.Plain, J.Figueras and X.Obradors.
  Physica C, **336**, 213 (2000).

- "Competition effects between random quenched and linearly correlated disorders in MTG-YBCO", T.Puig, J.Figueras and X.Obradors.
  Physica C, **341-348**, 2301 (2000).

- "Anisotropic behaviour of the melting line and the low critical field in YBCO". J.Figueras, T.Puig, X.Obradors, A.Erb and E.Walker.
  Physica C, **369**, 209 (2002) .

- "Anisotropy of the low-field critical point of the melting line of twinned $YBa_2Cu_3O_{7-\delta}$ single crystals". J.Figueras, T.Puig, X.Obradors, A.Erb and E.Walker.
  Physical Review B, **65**, 092505 (2002).

- "Influence of quenched disorder on liquid vortex plasticity of $YBa_2Cu_3O_{7-\delta}$", J.Figueras, T.Puig and X.Obradors.
  Physical Review B**67** , 014503 (2003).